Brandenburgische
Technische Universität
Cottbus - Senftenberg

# A Simulation Analysis to Improve the Dielectric Strength Inside High Voltage Vacuum Interrupters

Von der Fakultät für Maschinenbau, Elektrotechnik und
Wirtschaftsingenieurwesen der Brandenburgischen Technischen Universität
Cottbus-Senftenberg zur Erlangung des akademischen Grades eines
Doktors der Ingenieurwissenschaften
genehmigte Dissertation

vorgelegt von

M.Sc

**Karthik Reddy Venna**

geboren am 24. Oktober 1988 in Nellore, Indien

Vorsitzender: Prof. Dr. Harald Fien

Gutachter 1: Prof. Dr.-Ing. Harald Schwarz

Gutachter 2: Prof. Dr.-Ing. Dr. h. c. Heinz-Helmut Schramm

Tag der mündlichen Prüfung: 20. Januar 2015

© Karthik Reddy Venna 2014
ALL RIGHTS RESERVED

# Abstract

Vacuum circuit breakers are expected to be one of the possible alternatives for $SF_6$ circuit breakers in transmission voltages up to 230kV because of the excellent insulation as well as environmental friendly characteristics of vacuum. But for higher voltages, maintaining the electrical insulation inside and outside the interrupter tube is very important and becoming a challenge for the design engineers. Normally a vacuum interrupter consists of metal shields sandwiched between the ceramic insulator blocks inside the tube. The primary purpose of these metal shields is to protect the insulator walls by avoiding metal vapor deposition during the arcing process. On the other hand, these metal shields also influence the electric field distribution inside the interrupter tube. The presence of the metal shields may reduce the dielectric strength of the interrupter tube if proper measures are not taken.

This research is devoted to provide the information about the possible areas inside and outside the interrupter tube that are considered as critical in terms of dielectric strength because of the presence of metal shields. Possible solutions are also given in this thesis to overcome the high field stress in these critical areas with the help of 2D simulations that are simulated in ANSYS Maxwell.

The critical areas and their respective solutions presented in this work are (1) unidentified edges outside the interrupter tube which are formed by the metal shields that are inserted between the ceramic blocks. These edges, at high field stress, may act as a source of discharges between the interrupter tube and the outer insulator. This problem can be reduced by the combination of using a pressurized insulating gas (which is in this case $N_2$) between interrupter tube and outer insulator and by extending the unidentified edges and covering them with field grading rings which are conductive in nature. (2) Triple junctions (Vacuum-Ceramic-Metal shield) are the sources of high field stress inside the interrupter tube and are considered as a primary source of Secondary Electron Emission Avalanche that takes place on the (3) ceramic surface. The triple junction emissions can be avoided by properly designing the insulator geometry at point of contact with the metal shield. In addition, inserting metal parts of certain depth at the both ends of the ceramic insulators can also reduce the field stress at the triple junctions and avoid surface flashovers on the ceramic surface. (4) The gap between the metal shield and the contact rod is also considered to be a critical area which can be highly stressed (field) if the geometry of metal shield curvature is not properly designed. Various metal shield curvatures are proposed and simulated and an optimum geometry is suggested that reduces the electric field stress between the metal shield and contact rod. Using this optimized metal shield curvature, the diameter of the interrupter tube can be reduced considerably which in turn reduces the size of the interrupter tube.

**Key Words:**

High voltage vacuum interrupter, triple junctions, field grading rings, metal shields, ANSYS Maxwell, electric field, metal inserts, dielectric strength, electric field stress.

# Zusammenfassung

Vakuum-Leistungsschalter sind eine der möglichen Alternativen zum $SF_6$-Leistungsschalter in den Übertragungsspannungen bis 230kV auf Grund der ausgezeichneten Isolierung sowie umweltfreundlichen Eigenschaften des Vakuums sein. Aber für höhere Spannungen ist das Aufrechterhalten der elektrischen Festigkeit innerhalb und außerhalb der Schaltröhre sehr wichtig und immer eine Herausforderung für die Entwicklungsingenieure. Normalerweise enthält eine Vakuumschaltröhre Metallabschirmungen, die zwischen den Keramikisolatoren im Inneren der Röhre angeordnet sind. Der Hauptzweck dieser Metallabschirmungen ist, die inneren Wände des Isolators vor Metalldampf-Ablagerungen zu schützen, die während des Löschprozess auftreten. Diese Metallabschirmungen beeinflussen die elektrische Feldverteilung im Inneren der Schaltröhre und können daher die dielektrische Festigkeit der Schaltröhre reduzieren, wenn keine entsprechenden Maßnahmen getroffen werden.

Ziel der vorliegenden Untersuchung ist es, Informationen über die möglichen Bereiche innerhalb und außerhalb der Schaltröhre zu sammeln, die aufgrund der Anwesenheit von Metallabschirmungen als kritisch hinsichtlich der dielektrischen Festigkeit angesehen werden. Mögliche Lösungen werden in dieser Arbeit genannt, um die hohe Feldstärke in diesen kritischen Bereichen mit Hilfe von 2D-Simulationen in ANSYS Maxwell zu reduzieren.

Die kritischen Bereiche und ihre jeweiligen Lösungen in dieser Arbeit sind (1) undefinierte Kanten der Metallabschirmung außerhalb der Schaltröhre, die zwischen den Keramikteilen auftreten. Diese Kanten können bei hoher Feldstärke als Quelle von Entladungen zwischen der Schaltröhre und dem äußeren Isolator wirken. Dieses Problem kann durch die Kombination eines unter Druck stehenden Isoliergases (in diesem Fall $N_2$) zwischen der Schaltröhre und dem äußeren Isolator und durch die Verlängerung der undefinierten Kanten in leitfähige Feldsteuerringe hinein vermieden werden, die als Abdeckung wirken. (2) Triple-Punkte (Vakuum-Keramik-Metall Abschirmung) sind die Ursache einer hohen Feldstärke in der Schaltröhre und werden als primäre Quellen der Sekundärelektronenemission gesehen, die als Stoßentladung auf der Keramikoberfläche (3) auftreten. Die Triple-Punkte-Emissionen können durch die richtige Gestaltung der Isolatoren am Kontaktpunkt mit dem Metallschirm vermieden werden. Zusätzlich werden durch Einsetzen von Metallteilen bestimmter Tiefe an den beiden Enden der Keramikisolatoren auch die Feldstärke im Triple-Punkte Bereich reduziert und Überschläge auf der Keramikoberfläche vermieden. (4) Der Abstand zwischen der Metallabschirmung und dem Kontaktbolzen wird ebenfalls als kritischer Bereich durch das hoch belastete Feld betrachtet, wenn die Krümmung der Metallabschirmung nicht richtig ausgebildet ist. Verschiedene Krümmungen für die Metallabschirmung werden durch Simulation untersucht, Eine optimaler Geometrie der Krümmungen wird vorgeschlagen, die die elektrische Feldstärke zwischen der Metallabschirmung und dem Kontaktbolzen reduziert. Mit dieser optimierten Krümmung der Metallabschirmung kann der Durchmesser der Schaltröhre und damit das Volumen der Schaltröhre erheblich reduziert werden.

# Acknowledgements

At first, I extend my sincere thanks to Dr. Harald Fien (SIEMENS AG) for initiating the program "Siemens Graduierte Kollegen" at BTU and to Prof. Harald Schwarz for selecting me as a part of the program. This work has been carried out at the "Lehrstuhl Energieverteilung und Hochspannungstechnik" at Brandenburgischen Technischen Universität, Cottbus and at Schaltwerk-SIEMENS AG, Berlin, Germany. The financial support provided by SIEMENS AG and CEBra-Research is gratefully acknowledged.

I would like to convey my special thanks to my supervisor Prof. Heinz. H. Schramm for the wisdom he has shared with me and for his patient guidance, excellent advice and unfailing support at all possible times without which this document would not be possible.

My sincere thanks to R&D engineers, Dr. Stefan Giere (SIEMENS AG), Frank Richter (SIEMENS AG) and Dr. Stephan Wethekam (SIEMENS AG) for many interesting discussions and valued critical opinions throughout my research.

I wish to thank Dr. Iryna Shalaginova for being my wonderful coworker during these three years and for her regular suggestions about organizing a PhD work. I would also like to express my appreciation to my supervisor Prof. Schramm & my friend Krishna Kumar for their help in proof reading this dissertation and giving suggestions to improve its readability.

I would like to thank the fellow colleagues of this research group for their support and very nice discussions. Many thanks my best friends, spread far and wide around the globe for their continuous moral support. I am always in debt to you guys.

I wish to thank to my inspiration Mr. Pawan Kalyan Konidela for his inspirational speeches which helped me in boosting my confidence and courage all these years.

Last, and most significantly, I would like to thank my parents and my sister for their unconditional love and support. It has been a wonderful opportunity to live in Germany, work with SIEMENS AG and study at BTU. I hope that this thesis, at least in a small possible way will prove worthy of all the wonderful support you have given.

# TABLE OF CONTENTS

Abstract ..... I
Zusammenfassung ..... II
Acknowledgements ..... III
List of figures ..... VII
List of tables ..... XII

**1 INTRODUCTION ..... 1**

**1.1 $SF_6$ Vs Vacuum for High Voltage Circuit Breakers ..... 2**

**1.2 History & Development of High Voltage Vacuum Circuit Breakers ..... 4**

**1.3 Motivations for Research into High Voltage Vacuum Insulation ..... 7**

**1.4 Thesis Structure ..... 9**

**2 FUNDAMENTALS OF VACUUM CIRCUIT BREAKERS ..... 10**

**2.1 Basic operation of the vacuum interrupter ..... 10**

**2.2 Arc Behavior ..... 11**

**2.3 Different types of contacts & contact material ..... 13**

2.3.1 Radial Magnetic Field (RMF) ..... 13
2.3.2 Axial Magnetic Field (AMF) ..... 14
2.3.3 Contact Materials ..... 15

**2.4 Concept of shielding inside the interrupter tube ..... 17**

**3 HIGH VOLTAGE VACUUM INSULATION ..... 19**

**3.1 Basic Principle of Insulation Design ..... 19**

**3.2 Breakdown Mechanisms in Gases ..... 20**

**3.3 Breakdown Mechanisms in Vacuum ..... 23**

3.3.1 Particle Exchange Mechanism ..... 24
3.3.2 Field Emission Theory ..... 25
3.3.2.1 Anode heating mechanism ..... 25
3.3.2.2 Cathode Heating Mechanism ..... 25
3.3.3 Clump Mechanism ..... 26

**3.4 Surface Flashover Mechanism ..... 28**

**4 MODELING & SIMULATION OF A BASIC INTERRUPTER MODEL ..... 31**

**4.1 Maxwell´s Equations and the Types of Fields ..... 31**

**4.2 Introduction to ANSYS Maxwell ..... 32**

4.2.1 Solution Types ..... 33
4.2.2 Finite Element Method ..... 34

**4.3 Modeling and Simulation ..... 38**

4.3.1 Geometry modeling and assigning the materials ..... 38
4.3.2 Meshing and Excitations ..... 41
4.3.3 Setting up Boundary Conditions ..... 42
4.3.4 Solution Setup and Analyzing ..... 44
4.3.5 Post Processing ..... 45

**4.4 Concept of Field Grading ..... 49**

**5 PARAMETERS INFLUENCING THE WITHSTAND VOLTAGE OF THE INTERRUPTER & THEIR SIMULATIONS ..... 50**

**5.1 Field Grading Rings ..... 51**

**5.2 Conductivity of the Grading Rings ..... 59**

**5.3 Shape of the Insulator ..... 61**

**5.4 Metal Inserts ..... 67**

**5.5 Height of the Metal Shields ..... 70**

**5.6 Distance Between the Metal Shield and the Insulator ..... 73**

**6 SIMULATIONS WITH CONDITIONS CLOSE TO A REAL INTERRUPTER TUBE ..... 76**

**6.1 Threshold Values of the Influencing Parameters ..... 78**

6.1.1 Nitrogen Gas (Outside) ..... 78
6.1.2 Triple junctions & Ceramic Insulator ..... 80
6.1.2.1 Insulator Shape: ..... 80
6.1.2.2 Metal Inserts: ..... 83
6.1.3 Copper/ Stainless Steel Shields ..... 86
6.1.3.1 Diameter of the interrupter tube: ..... 87
6.1.3.2 Metal shield curvatures: ..... 89
6.1.3.2.1 Original Structure: ..... 89
6.1.3.2.2 Variation 1: ..... 91
6.1.3.2.3 Variation 2: ..... 93
6.1.3.2.4 Variation 3: ..... 95
6.1.3.2.5 Variation 4: ..... 98
6.1.3.2.6 Variation 5: ..... 100
6.1.3.3 Summary ..... 105

**7 CONCLUSIONS & FUTURE WORK.....106**

**7.1 Conclusions.....106**

**7.2 Future Work.....109**

**REFERENCES.....110**

**LIST OF PUBLICATIONS.....114**

# LIST OF FIGURES

**Figure1. 1** Relation between breakdown voltage and the gap distance for single-gap and double-gap units ..... 2

**Figure1. 2** Comparison of different insulating mediums regarding the relationship between breakdown voltage (KV) and contact gap (mm) ..... 4

**Figure1. 3** VCB with 4 vacuum interrupters in each arm, giving 8 vacuum interrupters in series per phase ..... 4

**Figure1. 4** 168kV, 31.5kA double break VCB in 1979 ..... 5

**Figure1. 5** Double break dead tank type VCB for 168kV (left) and single break VCB for 145kV (right) ..... 5

**Figure1. 6** 126kV two break VCB (left) and 126kV single break VCB prototype (right) ..... 6

**Figure1. 7** Comparison of 252kV, 126kV and 12kV vacuum interrupters ..... 6

**Figure1. 8** Critical points in the view of dielectric strength inside the interrupter tube 1- Contacts, 2- metal shield ends, 3- unidentified edges of metal shield (outside) and 4- triple points (including surface insulation) ..... 7

**Figure 2.1** Interrupter rated at 12kV 25kA 1250A ..... 11

**Figure 2.2** Arcing and interruption phenomena in vacuum ..... 12

**Figure 2.3** Natural Diffuse Mode on plain butt contact 200A@12kV ..... 12

**Figure 2.4** Natural Constricted Mode on plain butt contact at 5KA@12kV ..... 13

**Figure 2.5** Principle of operation of RMF contacts with B-Magnetic flux density, F- Azimuthal electromagnetic force and I-Current ..... 14

**Figure 2.6** Principle of operation of AMF contacts and the contact geometry ..... 15

**Figure 2.7** Breakdown voltages of Cu-Cr and Cu-Bi contacts in relation to the gap length ..... 16

**Figure 2.8** SEM photo of CuCr40 where the black particles are Cr and gray flat part is Cu ..... 16

**Figure 2.9** Possible multiple shield configurations for high voltage vacuum interrupters ..... 17

**Figure 3.1** Critical zones inside the interrupter in terms of insulation ..... 19

**Figure 3.2** (a) Dead Tank vacuum interrupter, (b) Vacuum interrupter with porcelain housing ..... 21

**Figure 3.3** An electron avalanche in front of a positive point electrode (a) field in the gap, (b) field in the region of ionization ..... 22

**Figure 3.4** Particle exchange mechanism of vacuum breakdown ..... 24

**Figure 3.5** Electron beam anode heating mechanism of vacuum breakdown ..... 25

**Figure 3.6** Heating of a micro- projection on the cathode that causes breakdown in vacuum ..... 26

**Figure 3.7** Clump mechanism of vacuum breakdown with stages of (a), (b), (c) ..... 27

**Figure 3.8** Secondary Electron Emission Avalanche (SEEA) ..... 29

**Figure 3.9** Electron cascade inside the insulator ..... 29

**Figure 3.10** Process of gas desorption assisting SEEA ..... 30

**Figure 4.1** Different methods of electromagnetic analysis ..... 33

**Figure 4.2** Finite elements (a) Tetrahedron for 3D and (b) Triangle for 2D ..... 35

**Figure 4.3** Adaptive meshing with respect to energy error ..... 36

**Figure 4.4** Flow chart of complete process in ANSYS Maxwell ..... 37

**Figure 4.5** Geometrical representation of a 72.5 kV Vacuum Interrupter in 2D with the following parts. A: Fixed contact, B: Movable contact with bellows, C: Insulator, D: Metal Shield, E: Triple Junction, F: Center Shield 39

**Figure 4.6** 2D geometry when swept with 360° around Z-axis turns into 3D model ..... 40

**Figure 4.7** Inside Selection mesh refinement ..... 41

**Figure 4.8** Mesh near the metal shield curvatures with surface approximation operation ..... 41

**Figure 4.9** Simulation region that is covering the interrupter geometry completely ..... 42

**Figure 4.10** Solution data showing the number of passes and percentage error ..... 44

**Figure 4.11** Potential field plot of the interrupter model ..... 45

**Figure 4.12** Potential distributions on each metal shield when one contact is at 0% and other at 100% potential ..... 46

**Figure 4.13** Electric field plot of the interrupter model ..... 47

**Figure 4.14** Electric field stresses of a metal shield at 50% potential: (A) Triple Junctions, (B) Metal shield curvatures, (C) metal shield edge ..... 48

**Figure 4.15** Triple Junction (A) without fine mesh and (B) with very fine mesh ..... 48

**Figure 5.1** Critical zones inside the interrupter in terms of insulation ..... 50

**Figure 5.2** Geometry of ceramic blocks, metal shield and shield edge ..... 52

**Figure 5.3** (A) Potential distribution, (B) Field distribution, and (C) Electric field stress at one of the shield edges . 52

**Figure 5.4** (A) Interrupter unit with field grading rings, (B) Electric field distribution, (C) Field stress near the edge of the metal shield ..... 53

**Figure 5.5** (1) Grading ring with the radius of 8mm and a distance of 6.5mm. (2) Grading ring with the radius of 10mm and a distance of 4.5mm. (3) Grading ring with the radius of 14mm and a distance of 0.5mm. (4) Grading ring with the radius of 8mm and a distance of 2mm(5) Grading ring with the radius of 10mm and a distance of 2mm. (6) Grading ring with the radius of 14mm and a distance of 2mm ..... 54

**Figure 5.6** Change in equipotential lines or potential distribution based on the distance from the insulator and radius of the rings ..... 55

**Figure 5.7** Electric field values along the outer surface of the ceramic showing the effect of change in distance to the insulator ..... 56

**Figure 5.8** Electric field values along the outer surface of the ceramic showing the effect of change in radius ..... 57

**Figure 5.9** Grading rings of elliptical shapes with constant distance of 2mm from the insulator ..... 57

**Figure 5.10** Electric field values along the outer surface of the ceramic showing the effect of elliptical shaped rings ..... 58

**Figure 5.11** Electric field plots inside and around the grading ring with respect to their conductivities ..... 59

**Figure 5.12** Electric field values around the grading rings of different conductivity ..... 60

**Figure 5.13** Mechanism of primary electron emission and its propagation along the insulator surface ..... 61

**Figure 5.14** Surface flashover fields with respect to insulator angle, PMMA insulator, d=6mm [48] [49] ..... 62

**Figure 5.15** Different shapes of insulators (1) Flat end with 90° angle of contact, (2) hemispheric shape with 2.5mm radius, (3) 45° angle of contact, (4) 135° angle of contact ..... 63

**Figure 5.16** Electric field plots of (1) Flat end insulator, (2) Hemispheric end, (3) 45° end insulator, (4) 135° end insulator ..... 64

**Figure 5.17** Direction of the electric field lines with respect to insulator surface ..... 65

**Figure 5.18** (a) Electron hopping mechanism that may leads to SEEA, (b) assumed hopping mechanism for 45° arrangement, (c) assumed hopping mechanism for 135°arrangment ..... 66

**Figure 5.19** 45° ceramic insulator with metal inserts of (a) 0.5mm deep, (b) 1mm deep, (c) 1.5mm deep and (d) 2mm deep ..... 67

**Figure 5.20** 135° ceramic insulator with metal inserts of (a) 0.5mm deep, (b) 1mm deep, (c) 1.5mm deep and (d) 2mm deep ..... 68

**Figure 5.21** Electric field values across the surface of the insulator of 45° with different metal inserts ..... 68

**Figure 5.22** Electric field values across the surface of the insulator of 45° with different metal inserts ..... 69

**Figure 5.23** Different distances between metal shields (a) 53mm, (b) 43mm, (c) 33mm and (d) 23mm ..... 70

**Figure 5.24** Electric field plots of models with different distances between the metal shields ..... 71

**Figure 5.25** Electric field values across the surface of the insulator with different distances between metal shields . 72

**Figure 5.26** Different distances between the metal shield and the insulator (a) 5mm, (b) 4mm, (c) 3mm and (d) 2mm ..... 73

**Figure 5.27** Electric field values across the surface of the insulator with different distances between the metal shield and the insulator ..... 74

**Figure 5.28** Electric field values across the surface of the insulator with different distances between the metal shield and the insulator ..... 74

**Figure 6.1** Prototype of a simulation arrangement of two models with different excitation voltages ..... 77

**Figure 6.2** Field grading rings of elliptical shape with different vertical and horizontal radius ..... 79

**Figure 6.3** Field stresses near the cathode triple junction with a default mesh ..... 81

**Figure 6.4** Field stresses near the cathode triple junction with a refined mesh ..... 82

**Figure 6.5** Electric field plots of the insulators with 45° and 135° angles of contact with shields ..... 82

**Figure 6.6** Electric field values along the surface of the insulator from CTJ to ATJ ..... 83

**Figure 6.7** Electric fields across the surface of the insulator of 45° shape with metal inserts of different depths ..... 84

**Figure 6.8** Electric fields across the surface of the insulator of 135° shape with metal inserts of different depths ... 85

**Figure 6.9** Different distances from the insulator to the contact rod ..... 87

**Figure 6.10** Electric field distribution near the surface of the Cu shield for Model A and B with 19mm distance ... 88

**Figure 6.11** Geometrical arrangement of original shield structure with changeable parameters a, b, c, d and e ..... 89

**Figure 6.12** Electric field plot and electric field values across the insulator starting from cathode triple junction to anode triple junction ..... 90

**Figure 6.13** Geometrical arrangement of variation 1 with taking the parameters a, b, c, d and e into consideration 91

**Figure 6.14** Electric field plot and electric field values on the surface of the shield curvature ..... 92

**Figure 6.15** Electric field values across the insulator starting from cathode triple junction to anode triple junction for variation 1 ..... 93

**Figure 6.16** Change in parameter (e) and the electric field plot of variation 2 ..... 94

**Figure 6.17** Electric field values on the surface of the shield curvature ..... 95

**Figure 6.18** Geometry of design variation 3 and its electric field plot ..... 96

**Figure 6.19** Electric field values (1) across the shield curvature and (2) along the surface of the ceramic insulator 97

**Figure 6.20** Design variations of parameters (a), (b), (c) and electric field plot of variation 5 ..... 98

**Figure 6.21** Electric field values along the surface of the curvature of the shield ..... 99

**Figure 6.22** Electric field values along the surface of the insulator ..... 100

**Figure 6.2**3 Design variations of parameters (a), (b), (c) and electric field plot of variation 5 ..... 101

**Figure 6.24** Electric field values (1) along the surface of the shield curvature, (2) along the surface of the insulator ..... 102

**Figure 6.25** Geometrical arrangement showing 21mm distance between the two metal shield with variation 4 and variation 5 ..... 103

**Figure 6.26** Electric field plot and the field values across the surface of the shield curvatures of variations 4 and 5 with 21mm distance between them ..... 104

**Figure 6.27** Field values across the surface of the insulator with 21mm distance between the shields ..... 105

**Figure 7.1** A possible design of an optimized 72.5kV vacuum interrupter in both 2D and 3D models ..... 108

# LIST OF TABLES

**Table 1.1** Differences between SF6 circuit breakers and Vacuum circuit breakers in the context of high voltage system applications ..... 3

**Table 4.1** Differential and Integral forms of Maxwell´s equations ..... 32

**Table 4.2** Boundary condition for electrostatics problem ..... 43

**Table 5.1** Comparison of electric field at the Cathode Triple Junction (CTJ) with respect to the depth of metal inserts ..... 69

**Table 5.2** Dependence of surface field stress and maximum field strength in the model on the distance between the metal shields ..... 72

**Table 5.3** Dependence of surface field stress and maximum field stress in the model on the distance between the metal shield and the insulator ..... 75

**Table 6.1** Different parameters that are simulated with Model A and Model B ..... 77

**Table 6.2** Relative breakdown voltages of insulating gases at 1atm ..... 78

**Table 6.3** Break down voltages of N2 in relation with SF6 at different pressure levels (10mm gap) ..... 78

**Table 6.4** E-field at CTJ and around the grading ring with different elliptical shapes ..... 80

**Table 6.5** Electric field stress near cathode triple junctions of two insulator shapes ..... 82

**Table 6.6** E-field values at cathode triple junction and at the corner of metal insert. ..... 85

**Table 6.7** E-field on the surface of the Cu shield and contact rod with respect to the changes in distance between the insulator and the contact rod. ..... 88

**Table 6.8** Summary of the design variations with maximum electric field on the shield and the insulator surface 105

# Chapter 1

# INTRODUCTION

Over the last four decades, vacuum switchgear has gained an immense applaud and has been extensively used in the distribution networks for making and breaking of fault currents and for switching all possible types of loads. Because of its outstanding performance and high reliability, the vacuum switching technology is continuously dominating in distribution systems. The basic simple idea behind this vacuum technology is that vacuum is considered as the best known insulating medium and contributes nothing to instigate conduction. The process of current interruption and dielectric recovery after the current interruption are accomplished inherently in vacuum thanks to its natural arc diffusion property. This is contrasting to other technologies like gas circuit breakers where the performance and design of the interrupter unit are highly dependent on the flow of gas inside the unit through mechanical support which is energized externally.

Witnessing the great success in distribution systems, it is obvious that a lot of researchers delved into the possibilities of implementing the vacuum technology for transmission voltage levels (>52kV). In the early decades, the reason behind this research might be the excellent switching capabilities of vacuum but since 2008, the main driver is to reduce the $SF_6$ gas (insulating medium of gas circuit breakers) which is recognized as a very strong greenhouse gas [1].

In order to implement the vacuum technology for high voltages, technically there are two possibilities to increase the dielectric strength of the switching gap to the values required for the insulation at transmission voltage levels. One is to stick with the traditional single-break interrupter concept of medium voltage vacuum interrupter by increasing the gap between the contacts. But the challenge in realizing this possibility is the nonlinear proportionality between the breakdown voltage ($U_b$) of the vacuum gaps and the gap length ($d$) which is following the relationship like $U_b=Ad^{\alpha}$ with $U_b$ being the breakdown voltage, $\alpha$ being a constant smaller than 1 and A is another constant. It is because that the breakdown in vacuum is a surface effect and completely determined by the contact surface condition [2]. The other solution is having two or more gaps in series which will help to share the voltage at each gap (equally in ideal cases) resulting the increase in breakdown voltage when compared to the breakdown voltage of a single gap length as shown in figure 1.1 [3]. In this case, operating all the contacts synchronously without any time delay between them is quite a challenge which is pushing the researchers to come up with the ideas of increasing the dielectric strength of a single break interrupter unit.

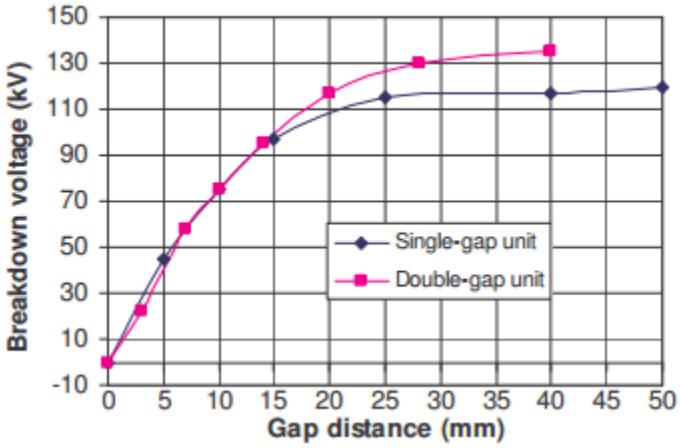


**Figure1. 1** Relation between breakdown voltage and the gap distance for single-gap and double-gap units [3]

## 1.1 $SF_6$ Vs Vacuum for High Voltage Circuit Breakers

Both $SF_6$ circuit breakers and vacuum circuit breakers are proved to be very successful in switchgear industry. When it comes to the medium voltage range, vacuum circuit breakers are dominating, whereas for the high voltage range $SF_6$ circuit breakers rule the market. From the success of their technologies in their respective voltage ranges, the following are their main competences that are acknowledged by the specialists of both switching technologies.

For vacuum circuit breaker:

- ✓ A large number of switching operations (approximately up to 100 000) and high level of short circuit capacity ( up to 100 full short circuits) [4]
- ✓ capable of interrupting ta very high rate of rise of current (di/dt)
- ✓ because of its fast dielectric recovery, the breaker can withstand a very high rate of rise of voltage (du/dt)
- ✓ vacuum breakers are able to clear the fault currents in open position, in case of contact gap breakdown
- ✓ and they need lower arc energy as well as drive energy

For $SF_6$ circuit breaker:

- ✓ Has a very high dielectric strength which increases proportional to the contact distance
- ✓ combination of very good switching capability, high dielectric strength and better heat transfer capability
- ✓ has the highest rated voltage and rated short-circuit current of all technologies

| Characteristic | SF6 | Vacuum | Remarks |
|---|---|---|---|
| Global warming potential | 24,900 | 0 | This makes VCBs as more environmental friendly than $SF_6$ breakers |
| Nominal Current above 2500 A | Easy to realize | Challenging to realize | At such a high nominal currents, the heat generation by VCB contact surface is very high and the interrupter has a limited heat transfer capability. |
| Monitoring of insulating medium | It is easier to check the quality of interruption medium | It is not practical to monitor the degree of vacuum in service | Because of VCB´s "seal for life" characteristic |
| No of Switching operations | Lower in comparison with vacuum | Higher | The higher endurance of VCB contact system to arcing makes it suitable for applications requiring very frequent switching operations. |
| Drive energy at a typical 72.5kV rating breaker | More than VCBs | As low as 20% of the $SF_6$ circuit breaker | |
| No of Interrupters | Single break circuit breakers up to 550kV have been put in service | May need more than one interrupter series above 145kV. | |
| Arc Voltage | Several hundreds of Volts | Several tens of Volts | |
| Duration of arc for fault current breaking (Arcing Time) | The minimum arcing time is typically $\geq$ 10ms | The minimum arcing time is typically $\leq$ 5ms | This is one of the reasons behind the higher number of switching operations for VCBs. |
| Spontaneous late breakdown | The case of late breakdown of a $SF_6$ gap is extremely rare. But once it occurs, the gap generally cannot recover. | Up to some hundreds of ms after the current interruption, vacuum gaps are known to show spontaneous late breakdown. | But the consequences of this late breakdown in vacuum are more limited than in $SF_6$ because the vacuum gap restores its insulation immediately. |
| Inductive load switching | The number of repeated re-ignitions are comparatively small in $SF_6$ CBs during inductive load switching | The repeated re-ignitions are significantly higher in Vacuum than $SF_6$. | Vacuum has the capability to interrupt high frequency currents which leads to re-ignitions. |
| Rate of rise of transient recovery voltage | Lower when compared with VCBs | Higher in VCBs because of their very fast dielectric recovery | |

**Table 1.1** Differences between SF6 circuit breakers and Vacuum circuit breakers in the context of high voltage system applications [3], [6]

Figure 1.2 shows that, for a certain contact gap and under normally used pressures, vacuum offers the highest dielectric strength but with a drawback of having a nonlinear relationship between withstand voltage and contact gap. On the other hand the withstand voltage of $SF_6$ is linearly proportional to the gap length and pressure [5].

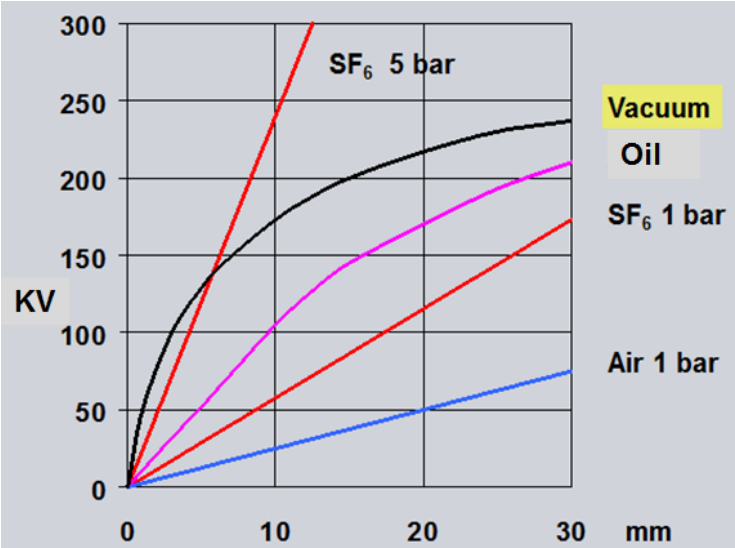


**Figure1. 2** Comparison of different insulating mediums regarding the relationship between breakdown voltage (KV) and contact gap (mm)

In general, both $SF_6$ and Vacuum Circuit Breakers (VCB) are equally good in handling their regular duties of fault and load current switching. However, by considering their different current interruption principles, there exist certain differences in the situation of high voltage applications. The table1.1 gives a brief explanation about the differences between $SF_6$ and vacuum.

## 1.2 History & Development of High Voltage Vacuum Circuit Breakers

The commercial developments of vacuum circuit breakers for transmission voltage levels were first testified in UK in 1968. It was for 132kV with 8 vacuum interrupters connected in series as shown in the figure 1.3

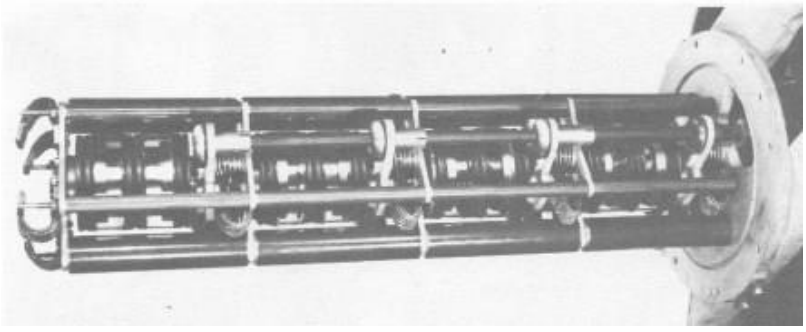

**Figure1. 3** VCB with 4 vacuum interrupters in each arm, giving 8 vacuum interrupters in series per phase [7]

In 1970´s, USA and Japan had simultaneously developed vacuum circuit breakers for transmission voltages [8] [9]. The USA had installed a breaker with four vacuum interrupters per phase up to a system voltage of 145kV. On the other hand Japan AE Power Systems developed and commercialized single break vacuum circuit breakers for 72/84kV. In late 1970´s, Japanese researchers have also developed a double break 168kV-31.5kA vacuum circuit breaker which is shown in the figure 1.4. But these breakers were too expensive and very large in size.

**Figure1. 4** 168kV, 31.5kA double break VCB in 1979[12]

By 1986, Japanese manufacturers were able to develop a single break vacuum circuit breaker for 145kV-40kA ratings and presented a prototype [11]. In contrast with the developments in US and UK, Japanese manufacturers proved the possibility of commercial feasibility of high voltage vacuum switchgear for practical operations and today they have produced and commercialized a single break 145kV vacuum circuit breaker, double break dead tank type vacuum circuit breaker for 168kV [10] as shown in figure 1.5 and multi break vacuum breakers for 550kV level were published in a conceptual stage [12].

**Figure1. 5** Double break dead tank type VCB for 168kV (left) and single break VCB for 145kV (right) [10]

Later in the 20th century, the amount of research and the investments in developing high voltage vacuum circuit breakers have increased strongly because of the global warming potential of SF6 gas, which is common arc quenching medium used in modern high voltage switchgear. In the context of finding the alternatives to SF6 breakers, China took a strong lead in developing the vacuum interrupter for high voltage ratings. They have already developed a two break 126kV-31.5kA vacuum circuit breaker in 1989, and in early 2000´s a prototype of single break vacuum circuit breaker for 126kV was introduced as shown in the figure 1.6. By 2006, they have reported a prototype of single break vacuum interrupter for 252 kV as shown in figure 1.7 [13].

**Figure1. 6** 126kV two break VCB (left) and 126kV single break VCB prototype (right) [13]

**Figure1. 7** Comparison of 252kV, 126kV and 12kV vacuum interrupters [13]

Currently most R&D efforts of high voltage vacuum circuit breakers are concentrated in East – Asia. Japanese industries have already showed the possibility of advanced breakers two decades ago followed by the strong involvement of Chinese companies. US companies, even though having an early achievement of developing vacuum interrupters for high voltages, didn't commercialize them yet. Coming to European nations, after UK, many countries are now investing to develop vacuum circuit breakers for transmission voltages and their R&D work is reported. [14][15][16]

## 1.3 Motivations for Research into High Voltage Vacuum Insulation

In the view of increasing demand for the vacuum circuit breakers in high voltage levels, there are certain design aspects of the interrupter tube that are starting to gain importance which were not considered as weak points in the medium voltage level. It is not only significant to concentrate on the breaker´s ability to interrupt fault current, but also ensuring the dielectric strength inside the interrupter when the contacts are in open state is important. The internal insulation of an interrupter tube can be divided into two categories. In the first category, the insulation of the vacuum gap between the contacts which are in open state and the insulation of the vacuum gap between the contact rods and the metal shields that are inserted between two insulator blocks are considered. In the second category, the surface insulation of the interrupter´s insulator is important. In the above context, figure 1.8 shows the critical points of a vacuum tube regarding its dielectric strength inside the interrupter tube.

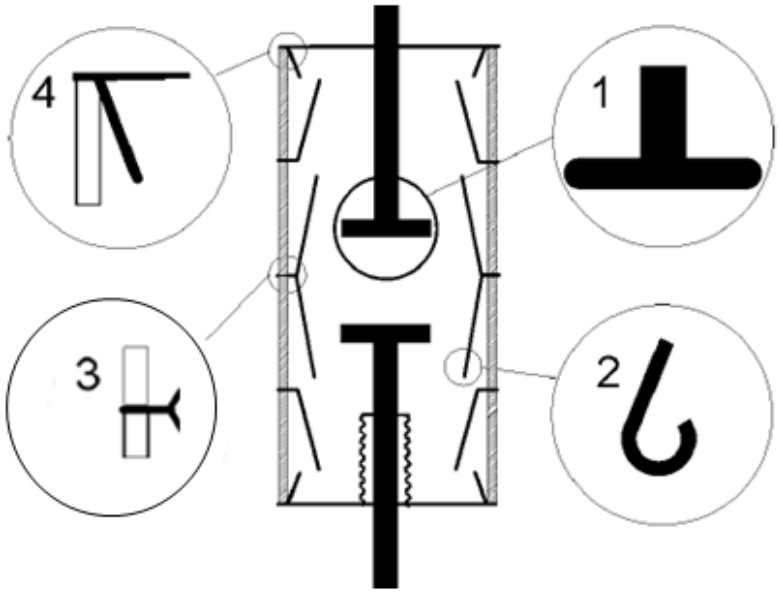


**Figure1. 8** Critical points in the view of dielectric strength inside the interrupter tube 1- Contacts, 2- metal shield ends, 3- unidentified edges of metal shield (outside) and 4- triple points (including surface insulation) [20]

The electric breakdown of the vacuum gap at the critical point 1 i.e. at the contacts has been investigated for a long time. Major theories like cathode heating theory, anode heating theory and clump theory are assumed to play the main role in the breakdown. These theories are briefly explained in chapter 3 of this report. The other critical areas like triple points, unidentified edges of metal shields and the metal shield ends are of main interest in the current research.

The presence of the solid insulator increases the electric field stress at the point where the metal shield, insulator and vacuum comes in contact. This is technically called as triple junction or triple point (4 of figure 1.8). In addition, the flashover along the surface of the insulator is assumed to be triggered by one of the known mechanisms called Secondary Electron Emission Avalanche (SEEA) [17] [18]. It is also assumed that the source of SEEA is the field emitted electron from the highly stressed (field) triple junctions [19]. To avoid the field emission electrons from the triple junctions, various triple junctions in vacuum were created by using different shapes of the insulator at point of contact. These triple junctions were simulated in electrostatic solver of ANSYS Maxwell and their respective electric field distributions were observed. In addition, metal inserts of different depths were place at the both ends of the insulators and the electric field distributions were observed.

The problem of the unidentified edges of the metal shield (3 of figure 1.8) is that these edges will always pose a threat of discharge if they are not properly graded. For the medium voltage applications, the field values may not be high enough to initiate a discharge outside the interrupter tube. But for higher voltages especially when switching small inductive currents, the voltages can elevate up to several times the rated voltage which increases the field stress, and in this case the unidentified edges can be the source of partial discharges. These discharges may be avoided by using high pressurized insulating gas outside but this will affect the mechanical behavior of the bellows. So field grading rings which are conductive in nature are used around the metal shields by extending them outside the insulator along with low pressurized gas insulating medium. The enlarged radius of the grading rings will reduce the field stress considerably and avoid the partial discharge outside the interrupter. The effects of field grading rings and their shapes are clearly observed by simulating each model with ANSYS Maxwell.

When it comes to metal shield ends, generally these metals shields are placed between the two ceramic blocks in order to prevent metal vapor deposition on the insulator surface during arc interruption. In addition, these metal shields will also influence the electric field distribution inside the interrupter tube. The size of the interrupter tube depends up on the distance between the metal shields and the contact rods. As the distance between them is smaller, the size of the tube will also be smaller. But as the distance between metal shield and the contact rod is reduced, the field stress on the surface of the shield end curvatures increases. To optimize the distance, various design variations of metal shield curvatures are built and simulated in ANSYS Maxwell and their respective field distributions are observed. Depending on these field values, an optimum shape of the metal shield can be selected so that a considerable reduction in the distance between the shield and the contact rod can be achieved.

## 1.4 Thesis Structure

The structure of this thesis can be described as followed

- Even though this research is dealing with high voltage vacuum circuit breakers, the basic interruption mechanism is the same as the medium voltage vacuum breakers. Background information about vacuum circuit breakers including interruption mechanism, arch behavior and shielding inside the interrupter tube are explained in chapter 2.

- Chapter 3 gives an insight about the insulation principle inside the interrupter tube. In addition, theoretical explanations about the breakdown mechanisms in various media like gas, vacuum and on the surface of the insulator are also stated clearly.

- All the geometrical designs in this thesis are designed and simulated using a FEM based simulation software named ANSYS Maxwell. Brief introductions to the software including the solvers are given in chapter 4. The simulation of a basic vacuum interrupter design showing the initial results are also presented in chapter 4.

- Parameters that are assumed to influence the withstand voltage of the interrupter tube along with their simulation results are presented in chapter 5.

- Chapter 6 is the final part of this research showing the simulation results by considering the conditions that are close to a real interrupter. The metal shield curvature which considered as another parameter that can influence the withstand voltage of the interrupter is also simulated to finally get an optimized interrupter tube.

- Finally the conclusion is given in chapter 7 along with scope of future work in this field of research.

# Chapter 2

# FUNDAMENTALS OF VACUUM CIRCUIT BREAKERS

Vacuum interruption is currently the leading technology for medium voltages up to 52kV worldwide and is considered as a potential replacement of $SF_6$ circuit breakers for higher voltages. The first vacuum circuit breaker was installed into a grid in the late 1960´s and since then a large number of vacuum circuit breakers have been manufactured. It is projected that more than a million units are being manufactured worldwide annually in the voltage ranges of a distribution network. However, in 1997, the Kyoto Protocol [3] had labeled $SF_6$ as a global warming gas and began to control the usage of it. This leads to an increased effort in the research and development of vacuum interrupters for the lower end of higher voltages like 72.5kV, 145kV and even for 252kV. But as the level of voltage increases, the difficulties in attaining the vacuum insulation also increases and requires a special attention. Before going into the details of the vacuum insulation for higher voltages, basic information about a vacuum interrupter is given in this chapter for a better understanding of its interruption technology.

## 2.1 Basic operation of the vacuum interrupter

Though the vacuum interrupters are mass-produced for different voltage ratings and by different manufacturers with different shapes and sizes, they all have many similarities in their design features and follow a similar interruption mechanism. Figure 2.1 shows the cross section of one such typical vacuum interrupter rated for 12kV 25kA 1250A [21]. The interrupter unit is normally enveloped with cylindrical insulators which are made of ceramic or glass with metal shields attached to them. The main purpose of these shields is to protect the insulator surface from the deposition of metal vapor on it and thus improving and maintaining the dielectric strength of the insulators. In normal conditions, the two contacts are in contact with each other thus ensuring the flow of current to the load. But during the operating conditions, the switchgear mechanism moves the movable contact rod apart from the fixed contact rod to form a gap depending on the voltage rating of the interrupter. This leads to a flow of current through the contacts which instigates a metal vapor arc discharge between them which is termed as vacuum arc. This vacuum arc exists till the next current zero and will get extinguished. The conductive metal vapor condenses on the metal surface in a very short time which quickly increases the dielectric strength of the vacuum.

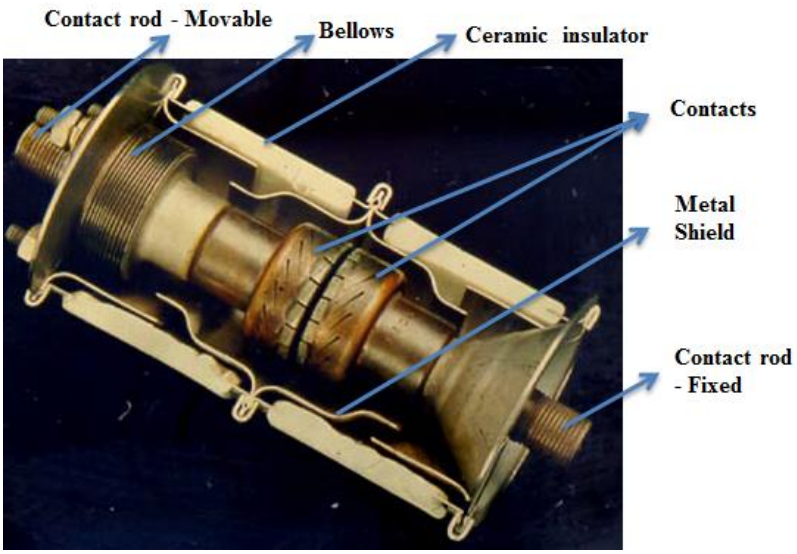


**Figure 2.1** Interrupter rated at 12kV 25kA 1250A [21]

## 2.2 Arc Behavior

The development of the vacuum arc and its behavior is an extremely complicated sequence and requires a better understanding when dealing with the designing of interrupters. Figure 2.2 outlines the important regions between arc initiation and arc extinction [22]. The four major regions of concern are (a) the contacts separation and arc initiation, (b) peak of the arc current where the electrode jets take place and the involvement of metal shields comes into picture, (c) the extinction of the arc at current zero, and (d) recovery of the dielectric strength of contact gap. Interruption of this arc always takes place at current zero and this mechanism should happen in such a way that the dielectric strength between the contacts should recover faster than the transient recovery voltage for a successful interruption [23].

Basically the arc inside the interrupter tube will exist in four different ways. Two of them are in natural forms and the other two are of forced forms. Generally these forms depend on the level of the current and the size of the contact electrodes. For example, for low currents (<5kA), the arc naturally diffuses and spreads over the cathode. During this diffusion, there exist one or more cathode spots which are constantly moving over the cathode surface. These spots repel each other and some of them will get extinguished and some others split into new spots as shown in figure 2.3. Because of this process, the energy of the arc disperses uniformly over the contact surface and reduces its overheating. This lets the interrupter to interrupt the arc easily at the next current zero.

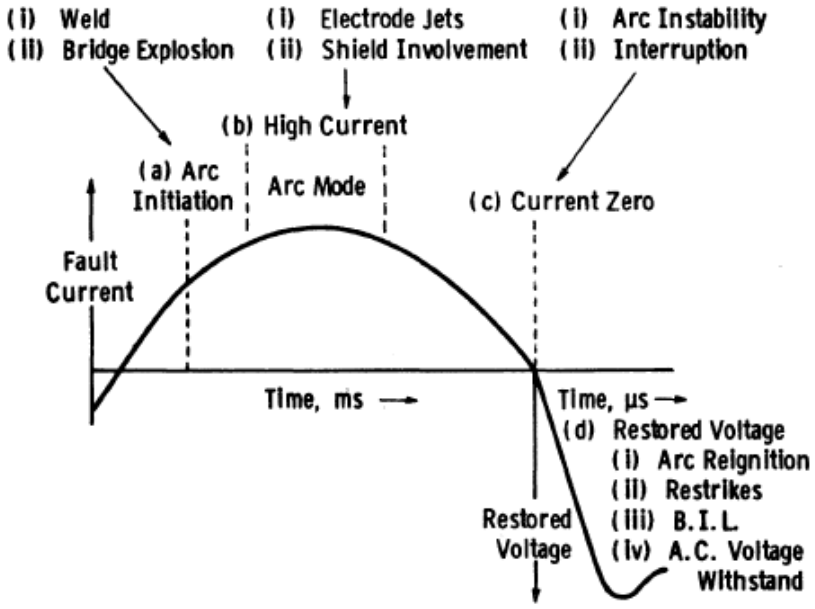


**Figure 2.2** Arcing and interruption phenomena in vacuum

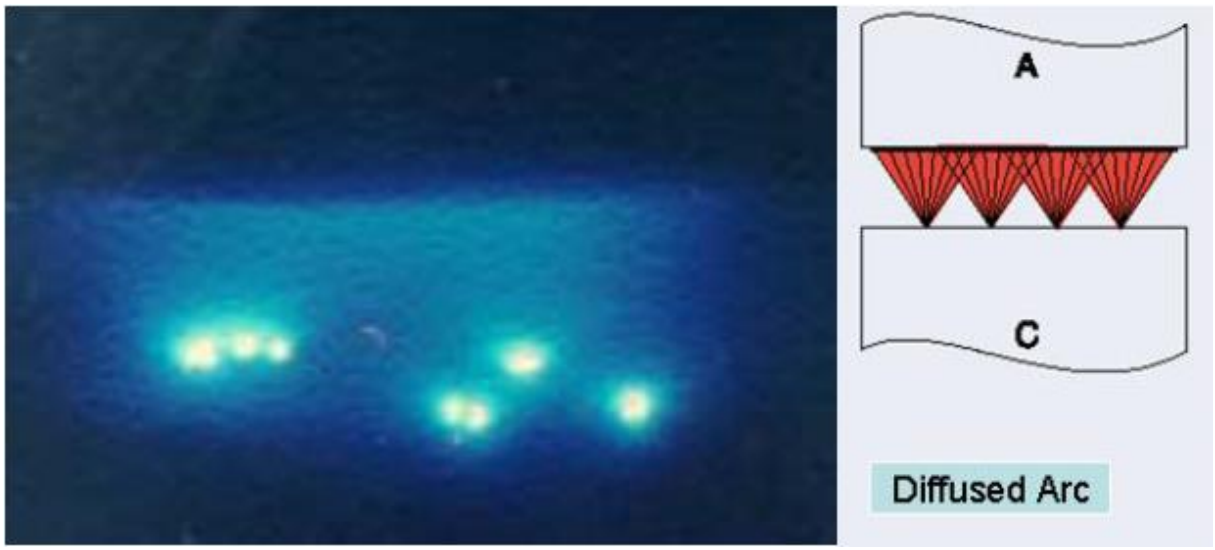


**Figure 2.3** Natural Diffuse Mode on plain butt contact 200A@12kV

At higher currents, things are rather different. For the currents above 5kA, the arc naturally shrinks into a thin column where the whole arc energy is focused over an area of few square millimeters. Subsequently, the surface consists of a boiling contact material due to a very high local temperature at current zero. This boiling material spreads off like a metal vapor and reduces the dielectric strength of vacuum between the contacts which may lead to a restrike due to Transient Recovery Voltage (TRV). Figure 2.4 shows the process mentioned above.

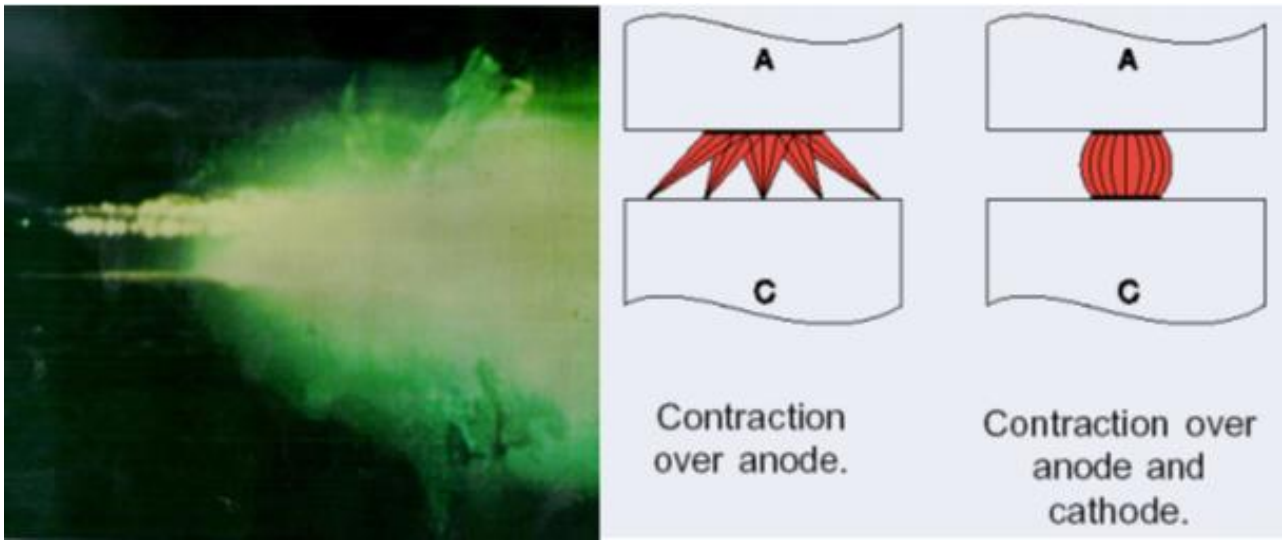


**Figure 2.4** Natural Constricted Mode on plain butt contact at 5KA@12kV

## 2.3 Different types of contacts & contact material

To overcome the above problem, the arc has to be forced to move over the surface of the contacts. In order to achieve this, the shape of the contacts should be in such a way that either a radial magnetic field or an axial magnetic field should exist between them. The selection of contact types depends upon the breaking current and voltage level.

### 2.3.1 Radial Magnetic Field (RMF)

The RMF is generated near the contacts based on their geometry. This magnetic field allows the arc to constrict but forces it to move rapidly around the contact resulting in a uniform distribution of heat over its surface. The contacts of this type are called radial magnetic field electrodes or spiral electrodes (figure 2. 5). In 10ms, the arc may make up to 4 revolutions along the edge of the contact with a speed of 70-150 m/s. This high velocity assures that there is a minimal contact abrasion and at the same time improves the interrupting capability. This technique is very effective in interrupting up to 50kA rms short circuit current. Ingeniously the magnetic field is self-induced by the short circuit current itself. This is possible by forcing the current to move along defined paths which in turn create the Radial Magnetic Field [21] [24].

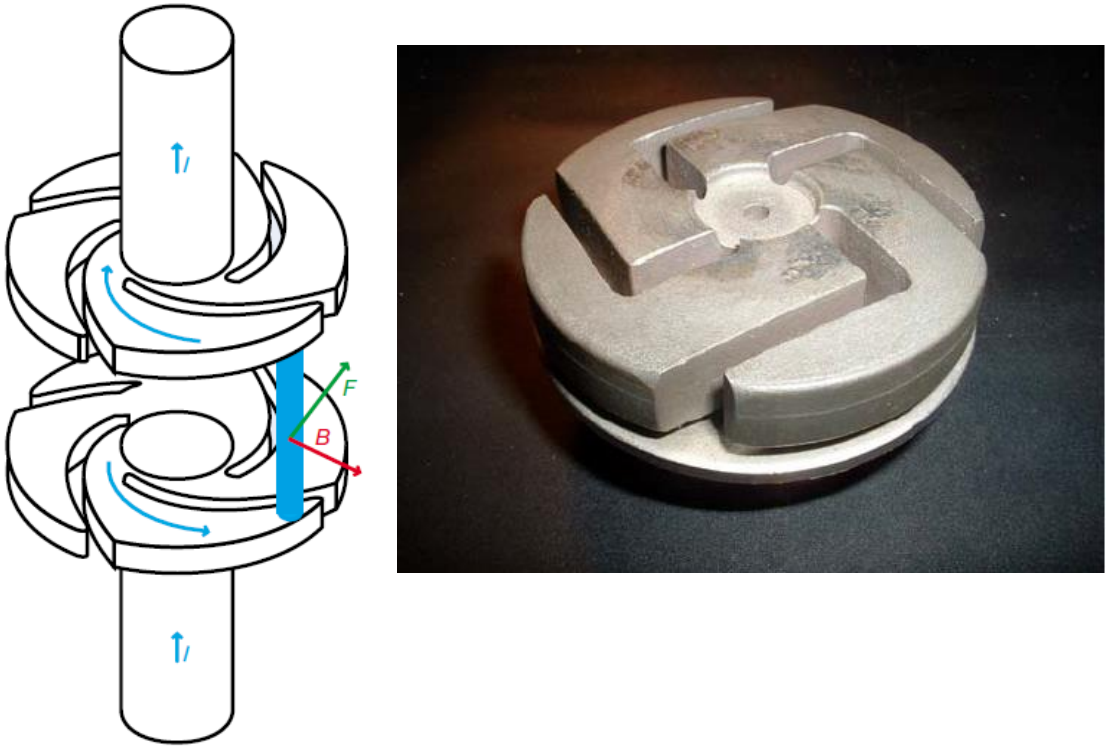


**Figure 2.5** Principle of operation of RMF contacts with B-Magnetic flux density, F- Azimuthal electromagnetic force and I-Current

## 2.3.2 Axial Magnetic Field (AMF)

In contrast to RMF, for high current applications axial magnetic field contacts are preferred where the magnetic field will be applied axially to the arc. This works completely different from the RMF contacts. The AMF contacts, instead of moving the arc, force it to diffuse above its natural constriction point. To elaborate, when a magnetic flux density applied in parallel to the current flow, the mobility of the charge carriers perpendicular to the flow is considerably reduced. This applies especially to the electrons which are having smaller mass than ions. The electrons revolve around the magnetic lines of force as shown in figure 2.6 so that the contraction of the arc is shifted towards higher currents. The arc burns with diffused light and the supply of energy to electrodes is reduced thus making the interruption easy. Many researches has proved that the diffused arc of AMF contact systems result in an outstanding short-circuit interruption capacity. These type of contacts suits especially for currents of 63kA and higher [24] [25]


**Figure 2.6** Principle of operation of AMF contacts and the contact geometry

### 2.3.3 Contact Materials

Contact materials are the important factor in determining the magnitude of interrupting current and voltage withstanding capability. A large number of materials with different combinations have been used over the years. The first material used for the contacts was Oxygen Free High Conductivity (OFHC) copper because of its excellent conductivity and extremely low gas content. But even that low gas content may occasionally result in the degradation of vacuum to a level which might hamper the operation of the device. These contacts when closed against a fault would weld solidly preventing the contacts from opening again. This problem was solved by adding Bismuth to Copper forming Cu-Bi contacts. The presence of Bi brittles the welded portions and makes them weak and easy to break. But the properties of these materials didn‘t match the properties required by the vacuum. Later, a variety of material combinations has been studied and a material with a combination of copper and chromium (Cr) was considered as a suitable material for vacuum switching.

The relation between break down voltage and gap length of Cu-Bi and Cu- Cr by applying an impulse voltage is shown in figure 2.7

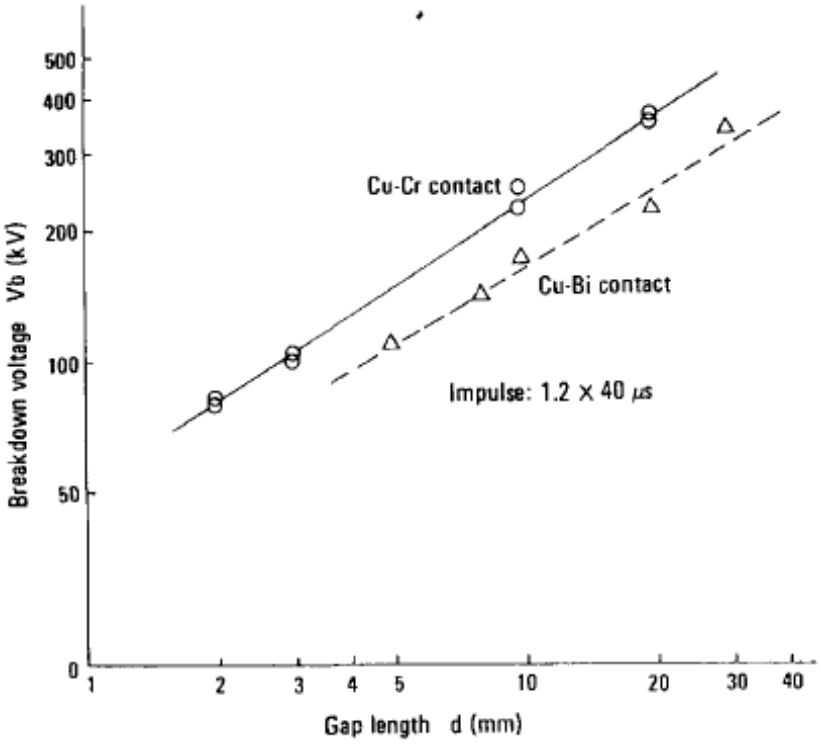


**Figure 2.7** Breakdown voltages of Cu-Cr and Cu-Bi contacts in relation to the gap length [25]

The breakdown voltage of Cu-Cr is approximately 30-40% higher than Cu-Bi material. In addition, the Cu-Cr material combines good dielectric strength, interruption capability and conductivity with a reduced tendency to contact welding. Using Cu can avoid the melting over a large current range and using Cr can achieve a higher withstand voltage (Figure 2.8).

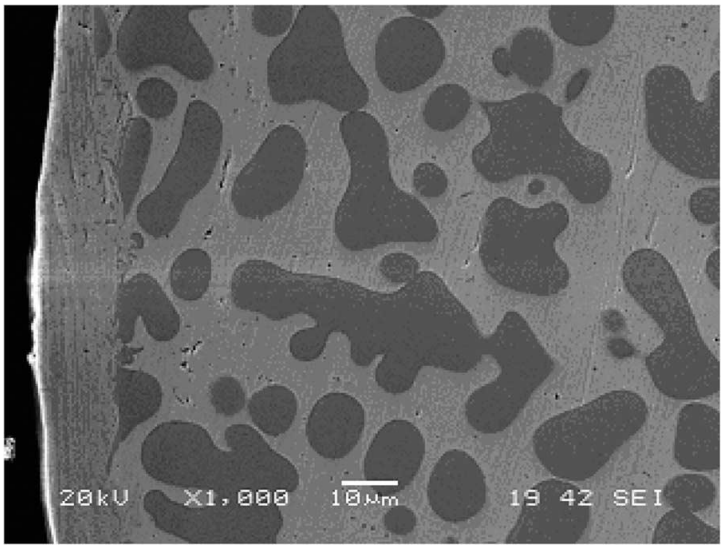


**Figure 2.8** SEM photo of CuCr40 where the black particles are Cr and gray flat part is Cu. [26]

## 2.4 Concept of shielding inside the interrupter tube

As the demand for the research of vacuum interrupters for higher voltages is increasing, certain aspects of the switchgear´s geometry which were not considered as weak points in medium voltage range are starting to become one of the challenges for the design engineers. The dielectric strength of the interrupter tube not only depends upon the contact system but also on the design of shielding. Since, a part of this research also deals with the design variations of these metal shields, this is one of the important sections of the thesis where a basic idea of shielding inside the interrupter tube is explained.

During the arc interruption, metal vapor will be created due to excess heat of the arc. This metal vapor when deposited on the insulator surface reduces the dielectric strength of the insulator. So the metal shields are inserted between the ceramic blocks in order to prevent the metal vapor deposition on the insulator surface. These shields will also help to distribute the electric field evenly throughout the insulation and have the capability to withstand high power frequency voltages and high impulse voltages.

For the medium voltage vacuum interrupters, in most cases it is sufficient to use only a single floating shield as shown in figure 2.1. But when it comes to high voltage vacuum interrupters, there will be a division of several, e.g. four, ceramic blocks to use several floating shields to control the voltage distribution. As shown in figure 2.9 at least 3 floating shields can be arranged in different configurations as shown in figure 2.9. The dimensions of these shields are such that voltage should be equally shared between the shields and the contacts. [27]

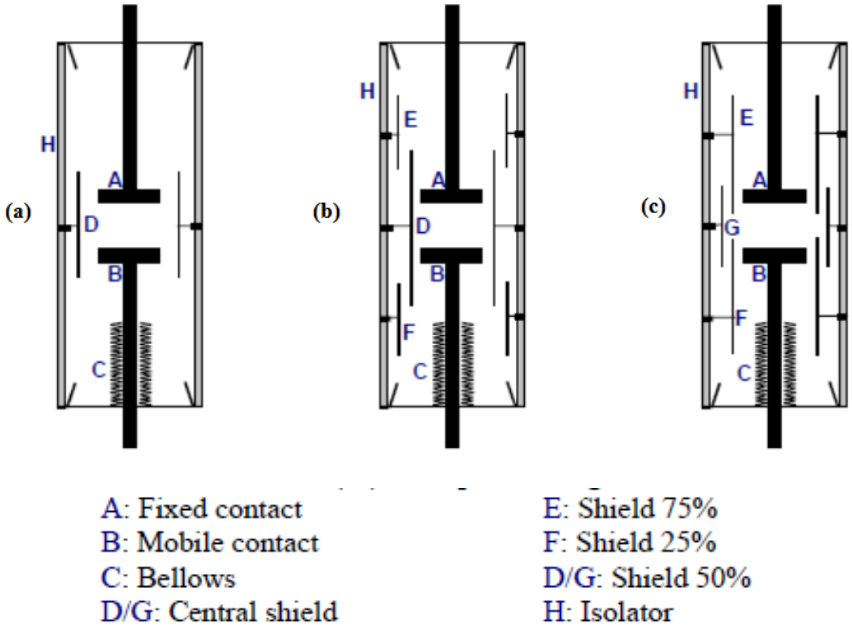


**Figure 2.9** Possible multiple shield configurations for high voltage vacuum interrupters

.

If we look into the above three configurations, when the interrupter is in an open state, the field distribution along the shields will be different in all the three configurations. The possibility of partial breakdown between the contacts and the center shield in type (a) is higher than in type (b) or type (c). In type (b), the center shield D protects E & F from having partial breakdown between the contacts and the shields. But having a breakdown between shield D and the contacts is more likely as the potential difference between shield D and contacts is around 50%. In type (c), the shields E, F protects the center shield G and avoids the partial breakdown between the contacts and the center shield. It is because, the potential difference between the shields E, F and their respective contact rods is only 25%. So the chances of partial breakdown between the contacts and these shields are very less and breakdown between shield G and the contacts can be completely avoided. So from this we can say that the multiple floating shields concept is one of the best solutions for the high voltage vacuum interrupters.

A more detailed explanation of the voltage distribution along the shields is given in chapter 5 and 6.

# Chapter 3

# HIGH VOLTAGE VACUUM INSULATION

One of the important criteria to consider when designing a high voltage vacuum interrupter is to withstand high voltages across the interrupter terminals when the contacts are open. For a design to be successful, the vacuum interrupter must pass a series of voltage tests when placed in an operating mechanism. That means the interrupter´s insulation should not only withstand its rated voltage, but also 2 to 4 times the rated voltage during AC power frequency tests and 4 to 12 times the rated voltage during Basic Impulse Level tests [28]. Special attention should be given to various areas inside the interrupter tube in order to design a successful interrupter for higher voltages. They are explained in the following sections.

## 3.1 Basic Principle of Insulation Design

There are some critical zones in the interrupter tube where the insulation levels are to be maintained within the withstand limits. Figure 3.1 shows these zones along with the components that affect the insulation in these areas [29].

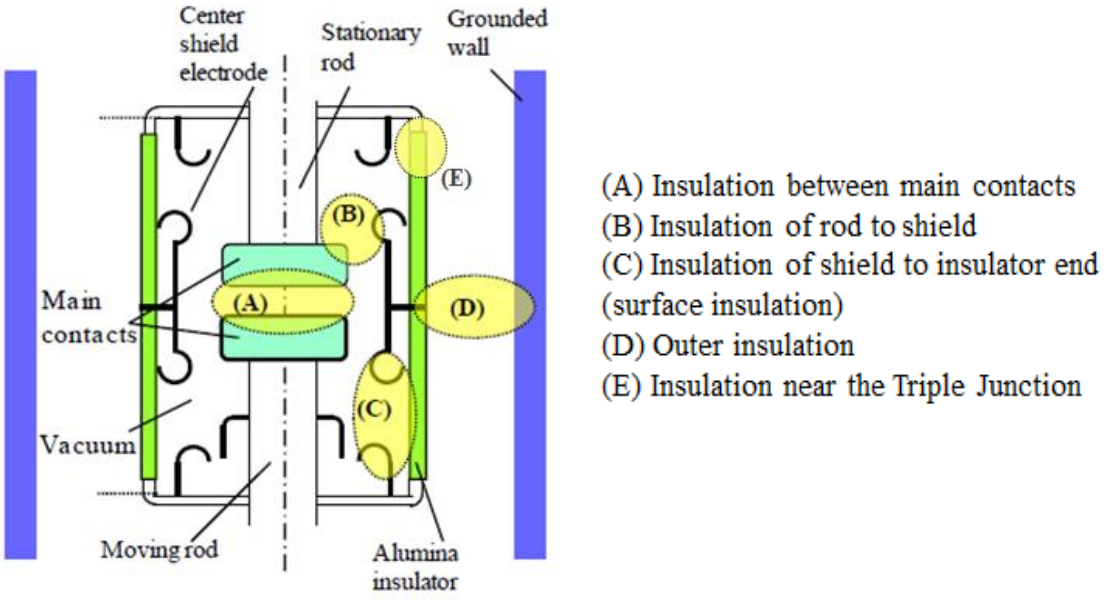


**Figure 3.1** Critical zones inside the interrupter in terms of insulation

From the above figure 3.1, it can be inferred that the withstand voltages at these zones will determine the breakdown voltage of the interrupter. The withstand voltages can be determined by calculating the electric field distribution at the aforementioned electrode arrangements. Local field intensification at any of these electrode arrangements will decrease the withstand voltages considerably. In the present work, the critical zones B, C, D, E i.e. insulation between contact rod and metal shield, insulation between shield and insulator which is often referred to as surface insulation, insulation outside the interrupter tube especially at the metal shield endings, and lastly the insulation at the triple junctions respectively are studied for high voltages, and possible design variations are proposed in order to increase the insulation level inside the interrupter tube. But before going into the design variations, it is important to know how the discharges take place in these areas and their background.

The process of the discharges at these critical zones is different from each other. The discharge mechanisms between the grounded wall and the outer edge of the metal shield and between the contact rod and metal shield are explained in section 3.2 and 3.3 respectively. The process of discharge at the insulator surface and at the triple junctions are interlinked and explained in section 3.4

## 3.2 Breakdown Mechanisms in Gases

Often, the vacuum interrupter tube is placed in the outer housing for two possible reasons. One of the reasons is that it is part of an enclosed arrangement like a metal tank in case of dead tank vacuum circuit breaker as shown in the figure 3.2 (a). The other reason is to improve the BIL and 1-min withstand performance of a given ceramic length significantly and to increase the outer flashover distance to a value sufficient to withstand the test voltages and operating voltages at the ambient air pressure outside the circuit breaker as shown in figure 3.2 (b). In this case the outer housing can be made of porcelain or composite insulator.

In both the cases, the gap between the interrupter tube and the outer housing is filled with dielectric gases at required pressure. The main purpose of these gases is to ensure sufficient dielectric strength in the gap especially in the areas where the sharp edges of the metal shields that are held between the two blocks of the insulator are present as shown in Zone D of figure 3.1.

So it is very essential to know the behavior of the dielectric medium when subjected to high electric stress while designing the insulation system for the high voltage apparatus. It is not sufficient to know only the existing maximum electric field intensity at the electrode, but it is also important to have an idea of the maximum allowable electric field stress for the dielectric that is in use. Generally, the outside gap between the interrupter tube and the grounded wall is filled with gas dielectrics.

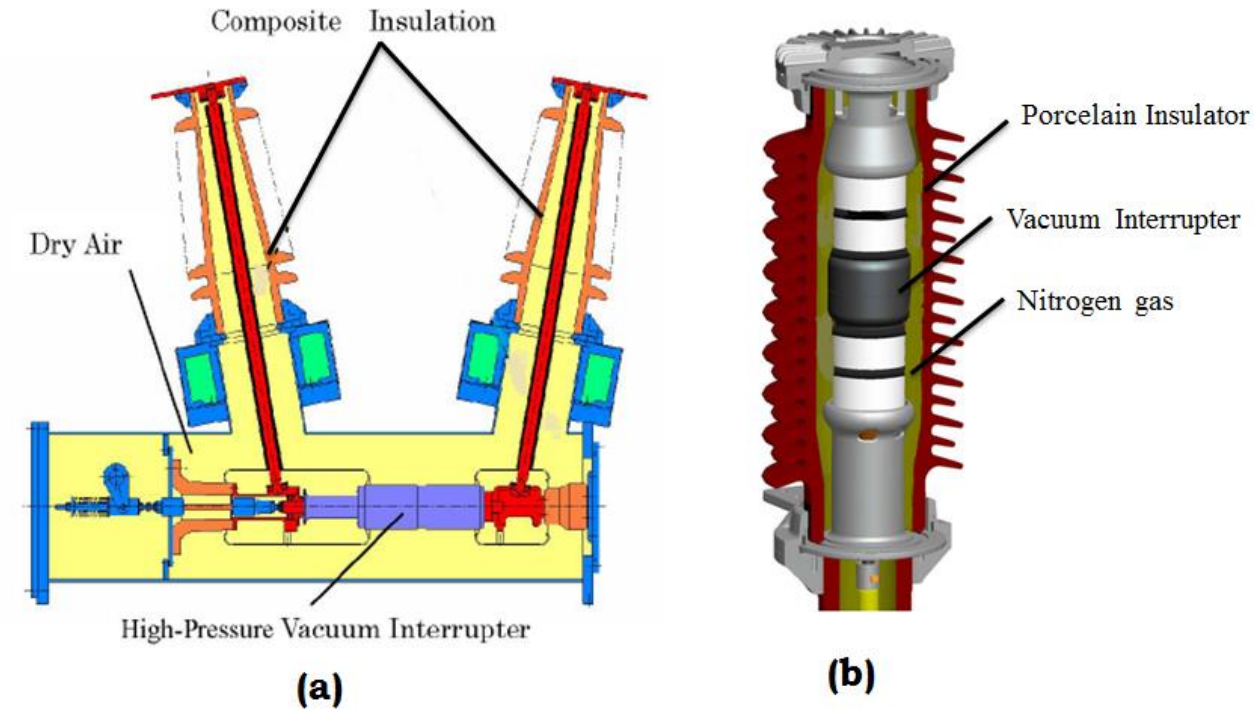


**Figure 3.2** (a) Dead Tank vacuum interrupter [10], (b) Vacuum interrupter with porcelain housing [38]

This gas can be dry air or nitrogen ($N_2$) or carbon dioxide ($CO_2$) or even sulfur hexafluoride ($SF_6$). In our case, the outer insulating medium is either air or nitrogen but not the one of other two as the whole concept of the high voltage vacuum interrupter is being an environmental friendly product. But whatever might be the type of the gas, when the electric field at the outer edge of the metal shield is high, the chances of having a discharge between the highly stressed part and the grounded wall are high.

In the terms of uniform and weakly non-uniform fields (which are mostly considered as ideal conditions) it is eminent that a steady partial discharge will not take place, as the initiation of partial discharge instantly leads to a complete breakdown in the dielectric. That means, if the breakdown of the dielectric occurs at a certain voltage and if $U_i$ and $U_b$ are the partial breakdown inception and the complete breakdown voltages, then

$U_i = U_b$ (for uniform and weakly non-uniform fields)

Similarly, if E would be the field intensity for the uniform field configuration, $E_{max}$ is the maximum field intensity in the weakly non-uniform field configuration, and the average field intensity in the dielectric at the breakdown is $E_b$, then they are expressed as following

$E \approx E_{max} \approx E_b$ (for uniform and weakly non-uniform fields) [30]

However, in our case when we look into the critical zone D of figure 3.1, the electrode configuration is closer to the extremely non-uniform fields (due to a sharp edge of the metal

shield). By applying a sufficient high voltage to this equipment, an electric field $E_{max}$ will appear at the sharp edge and is equal to the field intensity required for breakdown ($E_b$) of the dielectric in uniform or weakly non-uniform fields. Partial breakdown would initiate at this particular location which is experiencing the maximum field intensity in the equipment. In contradiction to uniform and weakly non-uniform fields, the stable partial breakdown will occur in extremely non-uniform field conditions. By further increasing the applied voltage enhances the strength of partial breakdown activity but the complete breakdown of dielectric takes place at a much higher applied voltage. If $U_i$ is the partial breakdown inception voltage and $U_b$ is the voltage required to cause a complete breakdown in the dielectric, then in this case

$$U_i << U_b \text{ (for extremely non uniform fields)}$$

Let's consider a sharp edge – a plane electrode configuration with air as a dielectric medium between them as shown in the figure 3.3 which is similar to our situation and a positive dc voltage is applied to the sharp edge.

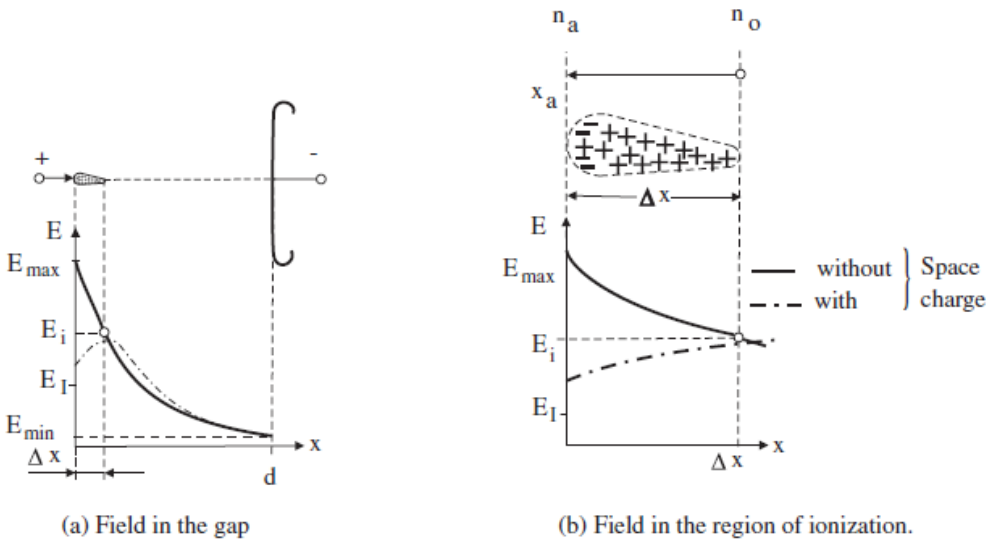


**Figure 3.3** An electron avalanche in front of a positive point electrode (a) field in the gap, (b) field in the region of ionization [30]

Beyond a certain level of the applied voltage $U_I$, it leads to the effect of ionization process that progress in the form of avalanches. On increasing the voltage, the electric field stress at the tip of the electrode increases and at a certain level $E_i$, the air loses its dielectric properties and the partial breakdown or corona initiates in that region. This corona consecutively generates the space charges and thus changes the situation of field intensity completely.

In figure 3.3, E is the applied field intensity which in this case appears close to the sharp edge. Beyond Δx, the field intensity may go below the field intensity that is necessary to initiate the ionization i.e. $E_I$. Thus avalanches are unable to develop themselves after the maximum length of the Δx region.

When a sufficient positive dc voltage is applied to the sharp edge (anode) to initiate an avalanche, a quick absorption of the electrons which are at the head of avalanche will take place. This leaves a positive space charge with heavy and slow ions near the tip. By increasing the applied voltage, the process of ionization develops further and creates stronger space charges. The two polarity charges (in this case alike +ve charges) moving close to each other as shown in figure 3.3 weakens the electric field in the region in front of the tip. Further discharge is only possible when this positive space charge drifts away from anode and diffuses towards cathode. That means when the applied voltage increases further it increases the partial breakdown inception field intensity above Ei. This leads to an intensive corona discharge, which ultimately produces a complete local breakdown. [31]

In order to avoid such discharges, the outer edge of the metal shield is further extended and covered with field grading rings. In that way, the fields in zone D can be considered as weakly non uniform fields. It must be ensured that the electric field intensity at this region should not exceed the $E_{max}$ value, which in turn avoids the discharge between outer shield edge and the grounded wall.

## 3.3 Breakdown Mechanisms in Vacuum

The insulation level between the interrupter contacts (Zone A) and between the contact rod and the metal shield (Zone B) from figure 3.1 requires more attention when designing the geometries of these components. Because, they are the most critical zones that determine the withstand voltage of the interrupter tube. It is necessary to know about the process of discharge that takes place in vacuum when any of the above electrodes are subjected to high field intensity, as this process differs from gaseous medium to vacuum.

According to the theory of Townsend discharge, which is very common in gas dielectrics, the development of current in a gap relies upon the movement of the charged particles. In the absence of such particles, as in the case of perfect vacuum, there should not be any traces of conduction and the vacuum ought to be a perfect medium of insulation. On the other hand, the vicinity of metallic electrodes and the insulating surfaces inside the vacuum, changes the situation. So, even in vacuum, a sufficiently high voltage will result in a breakdown. For the purpose of insulation, the range of vacuum used is in the pressure range of $10^{-4}$ bar to $10^{-9}$ bar.
In the Townsend type of breakdown in a gas, several ionization processes multiply the number of electrons and create an electron avalanche. In high vacuum, even though the electrodes are separated by few centimeters, an electron can pass through the gap without facing any collisions. So, the current growth before the breakdown is not due to the electron avalanches.

Many breakdown mechanisms are proposed in vacuum. They are broadly classified into three categories [32]

1) Particle exchange mechanism
2) Field emission theory
3) Clump theory

## 3.3.1 Particle Exchange Mechanism

It is assumed that in the particle exchange mechanism, when an electrode experiences the high electric field, a charged particle would be emitted from it. When this charged particle impacts on the other electrode, the oppositely charged particles will be liberated. These charged particles, which are influenced by the applied voltage, will be accelerated back to the first electrode and release more charged particles which are similar to the first particle. When this process becomes cumulative, it leads to a chain reaction which in turn leads to the breakdown of the gap. This mechanism involves electrons, photons, positive ions and the absorbed gases at the electrode surfaces. According to Trump and Van de Graff, [33] an electron that exists in the vacuum gap is accelerated towards the anode and on impact releases A number of positive ions and C number of photons. These positive ions and the photons are accelerated towards the cathode and on impact, each photon liberates D number of electrons and each positive ion liberates B number of electrons as showed in figure 3.4. The breakdown will happen if the coefficient of the production of secondary electrons exceeds unity. Mathematically, this condition can be written as

$$(AB+CD) > 1$$

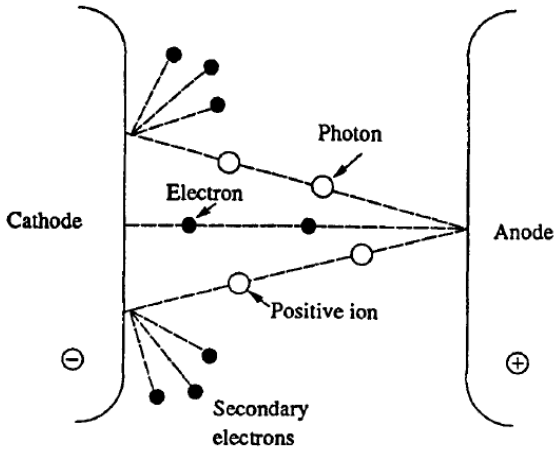


**Figure 3.4** Particle exchange mechanism of vacuum breakdown

Trump and Van de Graff measured these coefficients and proved that they were too small to form a breakdown. They made small changes in this theory by considering the existence of negative ions too and provided a modified equation

$$(AB+EF) > 1$$

where E and F represent the coefficients for negative and positive ions liberated due to the impact of positive and negative ions respectively.

## 3.3.2 Field Emission Theory

The field emission theory is further classified in to two types depending upon the role played by electrodes. [32]

### *3.3.2.1 Anode heating mechanism*

This theory states that due to field emission, the micro-protrusions on the cathode will produce electrons which collide with the anode causing an increase of temperature locally at the anode. This rise in temperature releases gases and vapors from anode into the vacuum gap. The field emitted electrons produce positive ions by ionizing the atoms of the gas. These positive ions reach the cathode and increase the primary electron emission due to space charge formation and produce secondary electrons by colliding with the surface of the anode again. This process continues until a sufficient number of electrons are produced in the vacuum gap which leads to a breakdown as shown in the figure 3.5

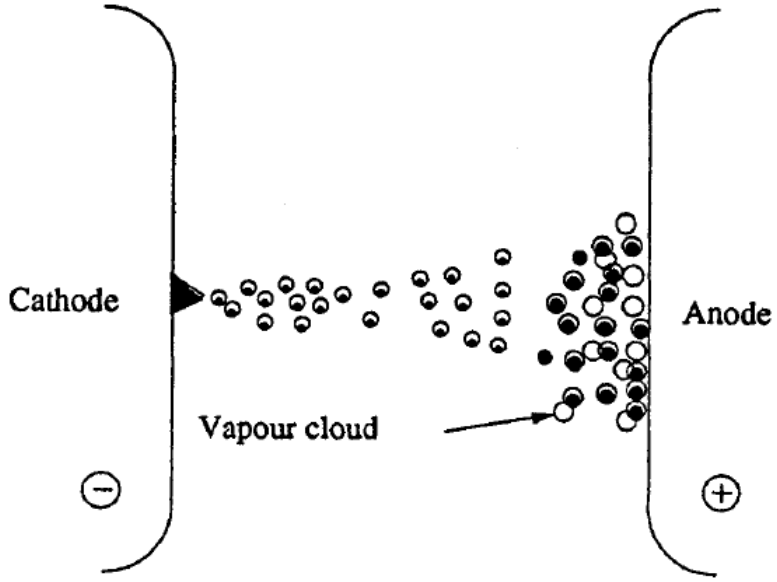


**Figure 3.5** Electron beam anode heating mechanism of vacuum breakdown

### *3.3.2.2 Cathode Heating Mechanism*

This mechanism postulates that when the voltages are close to the breakdown voltages of the gap, the micro projections on the cathode surface are responsible for the existence of the pre-breakdown current. This current is responsible for the resistive heating at the tip of the projection and when the critical current density is reached, the tip melts and explodes thus initiating the vacuum discharge as shown in the figure 3.6. This mechanism is called field emission.

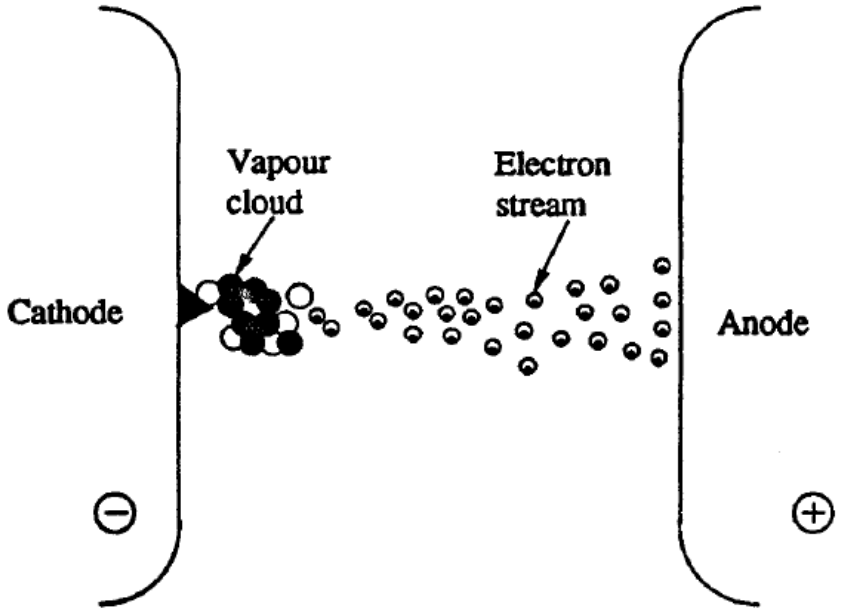


**Figure 3.6** Heating of a micro- projection on the cathode that causes breakdown in vacuum

Thus, the conditions and the properties of the cathode surface influence the breakdown process. Experimental evidence shows that when the cathode experiences an electric field of $10^2$ to $10^3$kV/mm, the cathode heating mechanism will take place.

### 3.3.3 Clump Mechanism

The following are the basic assumptions on which this theory had been developed

(a) One of the electrode surfaces has a loosely bound particle or clump.

(b) When the higher voltages are applied to these electrodes, this clump becomes charged and gets detached from the parent electrode and is accelerated towards the target electrode.

(c) The impact of this clump on the target electrode releases the vapor or gas through which a breakdown will take place as shown in the figure 3.7.

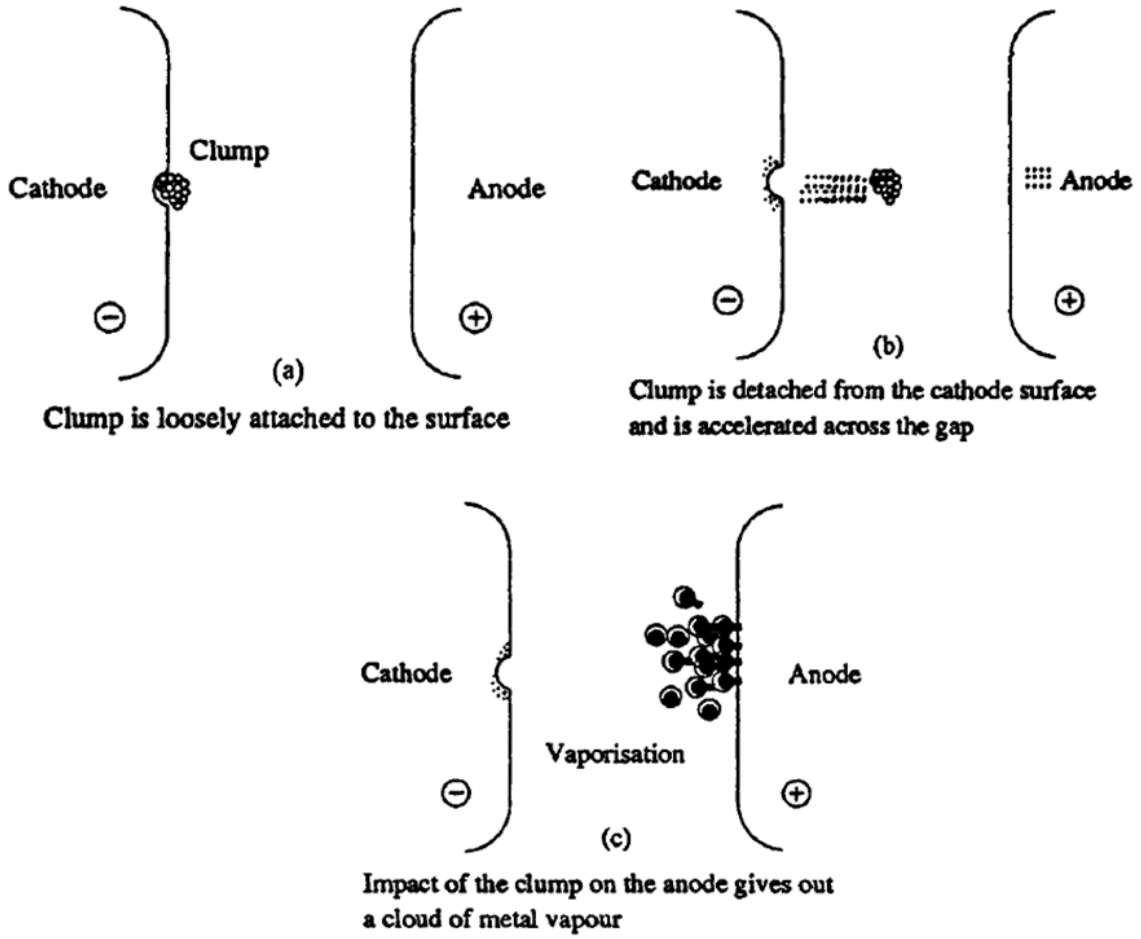


**Figure 3.7** Clump mechanism of vacuum breakdown with stages of (a), (b), (c)

This theory was first proposed by Cranberg [34] who initially assumed that a breakdown will occur when the energy per unit area i.e. W, delivered to the target electrode by the clump exceeds a value C which is constant. The quantity W is the product of voltage across the gap and the charge density of the clump. But this charge density is directly proportional to the electric field on the parent electrode. The criterion for breakdown is given as

$$VE = C$$

Whereas, in the case of parallel plate electrodes, the electric field E is given by V/d with d being the gap distance. So now, the above criterion will become

$$V = (Cd)^{1/2}$$

In this case, the constant C also considers the electrode surface conditions. Cranberg has also conducted some experiments which satisfied this breakdown criterion with a reasonable accuracy.

After looking into the above theories, one can infer that there is no single theory that can define a common process of vacuum breakdown. It appears that each mechanism would greatly depend on the experimental conditions. But on a whole the following conditions play a very crucial role in determining the withstand voltage of an interrupter. They are the length of the gap, geometry of the parts, material of the electrodes, presence of superfluous particles and sometimes the surface treatment.

## 3.4 Surface Flashover Mechanism

The insulation along the surface of the insulator (Zone C) and near the triple junction (Zone E) as shown in the figure 3.1 also requires special attention when designing a vacuum interrupter for higher voltages. Generally, the withstand voltage of a vacuum gap is very high when compared with the withstand voltage of a solid insulator of similar dimensions in vacuum. The reason is that the surface of the insulator is vulnerable to a discharge. This section mainly discuss about the discharges that appear along the surface of an insulator in vacuum.

Basically, the flashover on an insulator surface may be divided into three stages (1) the initiation stage, (2) the development stage, (3) the final stage. Many researchers believe that the surface flashover is generally initiated by the emission of electrons also termed as field emission electrons from the triple junctions. The triple junctions seen in the figure 3.1 Zone E, are the places where the three different materials come in contact. In this research, the triple junctions are formed by ceramic insulator, copper metal shield and vacuum. These triple junctions are basically considered as one of the critical areas in terms of insulation. Sometimes a group of electrons or ions that are generated somewhere away from the insulator can also strike the insulator surface and initiate the emission. So, there is a common agreement on the reasons for initiation of surface flashover. But when it comes to the development stage or intermediate stage, there are many different theories explained by HC Miller. The most commonly accepted theories are mentioned here. [35] [19]

One of the commonly accepted mechanisms for the intermediate stage is a Secondary Electron Emission Avalanche (SEEA). When an electron is emitted from the triple junction due to the high field stress, it will strike the surface of the insulator and produce additional electrons by secondary emission. These secondary electrons will again collide with the surface and generate the tertiary electrons. This process will continue until an avalanche take place which is called as SEEA and this avalanche leads to a flashover as shown in figure 3.8.

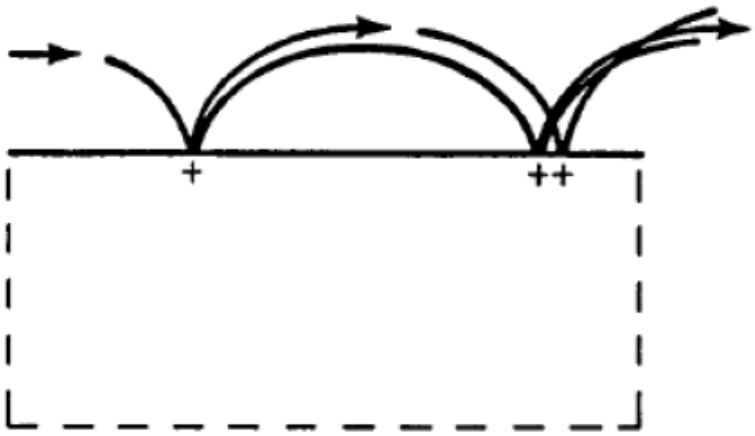

**Figure 3.8** Secondary Electron Emission Avalanche (SEEA)

Another common mechanism that is considered as a reason for the development stage of the surface flashover is the formation of an electron cascade in the conduction band of the insulator. This process takes place almost inside the insulator. The electric field accelerates the electrons within the insulator and thus by gaining energy, these electrons start to make inelastic collisions. When their energy exceeds the band gap of the insulator, they create an electrode cascade just inside the insulator along the surface. A fraction of these electrons will be emitted into the vacuum and the field on the surface of the insulator will accelerate them towards the anode. This will increase the flow of electrons along the insulator.

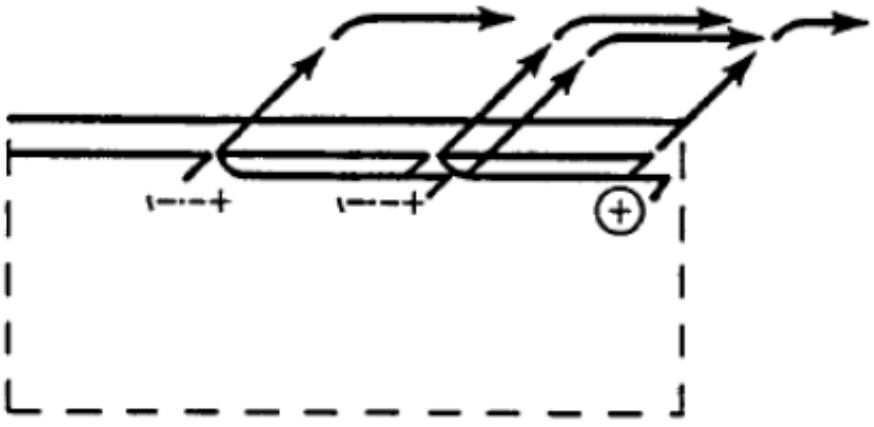

**Figure 3.9** Electron cascade inside the insulator

The process looks very similar to SEEA but the background procedure is different as shown in figure 3.9. The electron cascade will create an amount of holes in the valence band and some of these holes will form a positive surface charge.

When it comes to the final stage of the surface flashover, it is largely believed that desorbed surface gases from the surface of the insulator play the major role. The cascaded electrons just

inside the insulator´s surface will make inelastic collisions creating enough energy to liberate the adsorbed gas molecules. The final flashover will occur in the desorbed surface gas. Similarly, the gas desorption theory also assists the SEEA and leads to flashover. When the electrons from SEEA strike the surface, some releases the new electrons and some may excite the adsorbed gas molecules on the insulator surface and release them in to the vacuum. If the density of these released gas molecules is adequate to shorten the mean free path of the electrons in SEEA, the secondary emitted electrons collide with gas molecules as shown in figure 3.10 and assists SEEA further, leading to complete breakdown.

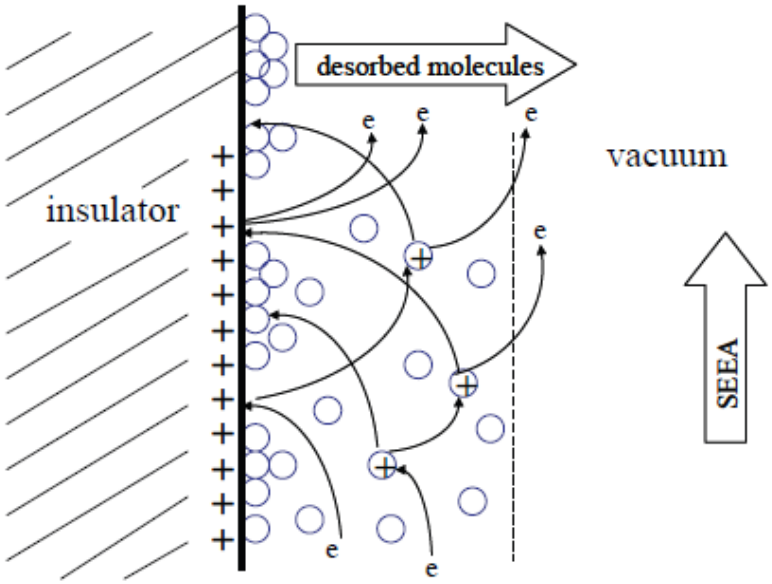


**Figure 3.10** Process of gas desorption assisting SEEA [36]

Gray made numerical calculations of the estimated density of the neutral gas next to the surface of the insulator. He established that the densities are in the range of $2x10^{17}$ $cm^{-3}$ to $2x10^{21}$ $cm^{-3}$. He has also assumed that the final stage of the surface discharge was filamentary in nature and was steady with gas breakdown phenomena [37].

In this research, the area of interest is to overcome the initial stage itself. That means the triple junction emissions and also the electrons which are generated away from the insulator that strike the surface of the insulator are to be avoided. The electrons generated away from the insulator, in this case, are assumed to be from the high stressed metal shields.

# Chapter 4

# MODELING & SIMULATION OF A BASIC INTERRUPTER MODEL

For building an interrupter model and to simulate the electrostatic behavior of its insulator and metal shield, it is required to have an insight into Maxwell equations. As most practical problems in electromagnetics cannot be solved only by using analytical methods, it is necessary to use numerical methods in an efficient way to get the appropriate results. Again, using numerical methods manually is time consuming and sometimes it is very difficult to solve. In order to overcome these complications, a general purpose simulation software named ANSYS Maxwell of version 16.0 is used to perform the electrostatic field analysis of the interrupter tube. This Maxwell software uses Finite Element Method (FEM) as its backend process. In this chapter, an introduction to the basics of electromagnetism in terms of Maxwell's equations, very basic information about FEM and field analysis of the basic interrupter model is explained.

## 4.1 Maxwell´s Equations and the Types of Fields

Maxwell´s equations are a collection of four complex equations that define the science of electromagnetics. These equations describe how the electric and the magnetic fields interact with each other and are influenced by other objects. From the table 4.1, the Gauss law of electricity explains how the electric fields are produced by electric charges, the Gauss law of magnetism explains how the magnetic fields are produced by the currents and by the change in electric fields, the Faraday´s law of induction describes that a changing in electric field gives rise to change in magnetic field and finally the Amperes law states that, change in electric fields and currents will produce magnetic fields. In table 4.1, D represents electric flux density or also called as electric displacement with unit $C/m^2$, E represents electric field measured in V/m, B implies magnetic flux with unit T, H is the magnetic field with unit A/m and J is the current density with unit $A/m^2$, and $\rho$ represents charge density with unit $C/m^3$ [39] [40].

| Name | Differential form | Integral form |
|---|---|---|
| **Gauss's law for electricity** | $div\,.\vec{D} = \rho$ | $\oiint_{\partial v} \vec{D}\,d\,\vec{A} = \iiint_{v} \rho dV$ |
| **Gauss's law for magnetism** | $div\,.\vec{B} = 0$ | $\oiint_{\partial v} \vec{B}\,d\,\vec{A} = 0$ |
| **Faraday's law of induction** | $curl\ \vec{E} = -\frac{\partial}{\partial t}\vec{B}$ | $\oint_{\partial A} \vec{E}\,d\,\vec{s} = -\frac{\partial}{\partial t}\iint_{A} \vec{B}\,d\,\vec{A}$ |
| **Ampère's law (with Maxwell's extension)** | $curl\ \vec{H} = \vec{J} + \frac{\partial}{\partial t}\vec{D}$ | $\oint_{\partial A} \vec{H}\,d\,\vec{s} = \iint_{A} (\vec{J} + \frac{\partial}{\partial t}\vec{D})d\,\vec{A}$ |

**Table 4.1** Differential and Integral forms of Maxwell´s equations [41]

Basically the electromagnetic fields are classified into two types.

(a) Static fields: The static fields are further categorized into electrostatics and magnetostatics. In electrostatics, as the name suggests, the fields are static i.e. they are independent with respect to time. So the term *curl E* = 0. Applying this assumption to Faradays law of table 4.1 gives that the time varying magnetic fields = 0. $\frac{\partial \mathbf{B}}{\partial t}$ Strictly speaking, even if the electric currents or magnetic fields exist, they must not vary with time and even if they vary with time, it must be a very slow variation. Similarly, in magnetostatics, the magnetic fields are time independent. So here the currents are stationary which is in contrary with electrostatics where the charges are stationary.

(b) Time varying fields: The most common problem to study is the dependency of fields with time. As the charge moves, they not only generate electric fields, but also magnetic fields (from Amperes law) and when this magnetic field changes, it produces an electric field. That means a time dependent magnetic field will produce a time dependent electric field (Faradays law) [42].

## 4.2 Introduction to ANSYS Maxwell

ANSYS Maxwell is a high end interactive tool that uses Finite Element Analysis (FEA) in order to elucidate electric and magnetic simulations. Maxwell solves the electromagnetic field issues by solving Maxwell´s equations from table 4.1 in a finite region of space with suitable boundary settings and user specified settings in order to get definitive results. The following flow chart gives the brief idea about the type of methods that can be used to analyze the electromagnetic problems.

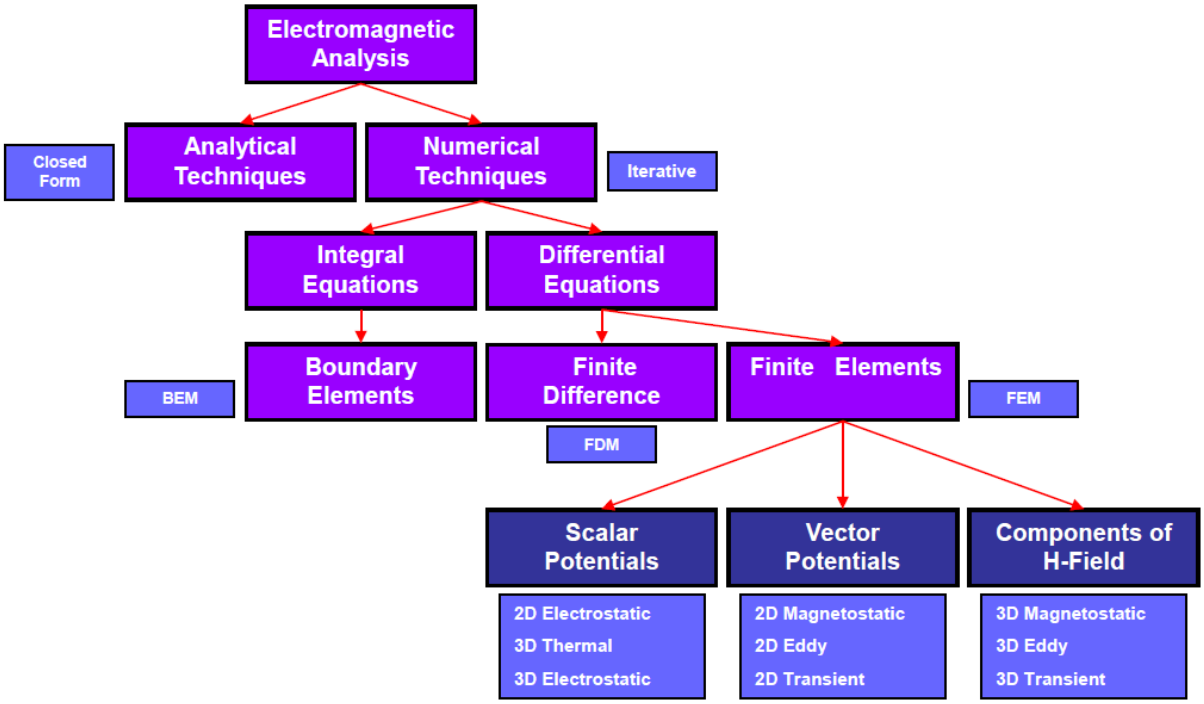


**Figure 4.1** Different methods of electromagnetic analysis [43]

From the figure 4.1, it can be seen that the electromagnetic problems are solved either by analytical procedures or by numerical procedures. When it comes to numerical procedures, the solving process is an iterative process and uses differential equations and integral equations. In order to solve integral equations, the Boundary Element Method (BEM) is used whereas for differential equations the Finite Element Method (FEM) or Finite Difference Methods (FDM) is used. ANSYS Maxwell uses FEM in order to calculate scalar potentials, vector potentials and components of magnetic fields as well depending upon the type of solvers defined by users.

### 4.2.1 Solution Types

An appropriate Maxwell solver should be selected based on the application of the problem. These solvers are almost similar for both 2D and 3D except for an AC conduction solver which is only available in 2D and the electric transient solver which is only available in 3D. Since this whole research was done in Maxwell 2D, a brief explanation of 2D solvers is given below. In Maxwell 2D, the solvers are categorized into Magnetic solution types and Electric solution types with each having three different solvers. [44]

***Magnetic Solution Types:*** The following are the three different solves that fall under the category of magnetic solution types.

*(a) Magnetostatic Field Solver:* It calculates the static magnetic field that exists in a structure when excited with DC currents and permanent magnets. For both linear and nonlinear materials,

the magnetic field may be computed. Based on the energy stored in the magnetic field, force, torque, inductance matrix and flux linkages can be calculated.

*(b) Eddy Current Field Solver:* In contrary with the above solver, the eddy current solver calculates the oscillating magnetic field when the structure is excited with AC currents. All eddy current effects including skin effects are considered in order to calculate current densities.

*(c) Transient Magnetic Solver:* This solver computes the transient magnetic fields that are caused by permanent magnets, conductors and windings when excited by time varying voltage or time varying current. Rotational and translational motion effects can be included in the simulation.

***Electric Solution Types:***

*(a) Electrostatic field solver:* This solver calculates the static electric fields resulting from stationary charge distribution or applied potentials. Electric field E and Electric flux density D are automatically calculated from the potential.

*(b) AC Conduction Field Solver:* This solver computes the AC voltages and current density distribution in a material having both conductive and dielectric properties when excited with AC voltages. Current flow and the admittance matrix can be computed from the calculated fields.

*(c) DC Conduction Solver:* When the model is excited with DC voltages, this solver computes the DC currents that flow in a lossy dielectric material. In contrary with AC conduction solver, here it is possible to calculate the conductance matrix from the obtained electric field solution.

All the simulations in this research were done with the solvers categorized under electric solution types.

## 4.2.2 Finite Element Method

The Finite Element Method in Maxwell refers to a process from which the solution is achieved numerically from an arbitrary geometry by breaking it down into simple fragments called finite elements. In Maxwell 3D, the fundamental unit of the finite element is tetrahedron, whereas for Maxwell 2D it is a triangle. The assembly of all the triangles in 2D and tetrahedrons in 3D is referred as the finite element mesh or simply mesh. For 3D, as shown in figure 4.2, the components of the field that are tangential to the edges of an element are openly stored at the vertices and the component of the field that is tangential to the face of an element and perpendicular to an edge is saved at the center point of particular edges. The values of a vector field at an inner point are incorporated from the nodal values. Then the desired field of each element is estimated with a $2^{nd}$ order quadratic equation. For example, $\mathbf{A_x(x,y,z) = a_0 + a_1x + a_2y + a_3z + a_4xy + a_5yz + a_6xz + a_7x^2 + a_8y^2 + a_9z^2}$ **.** So in a 3D simulation the field quantities are calculated for those 10 points.

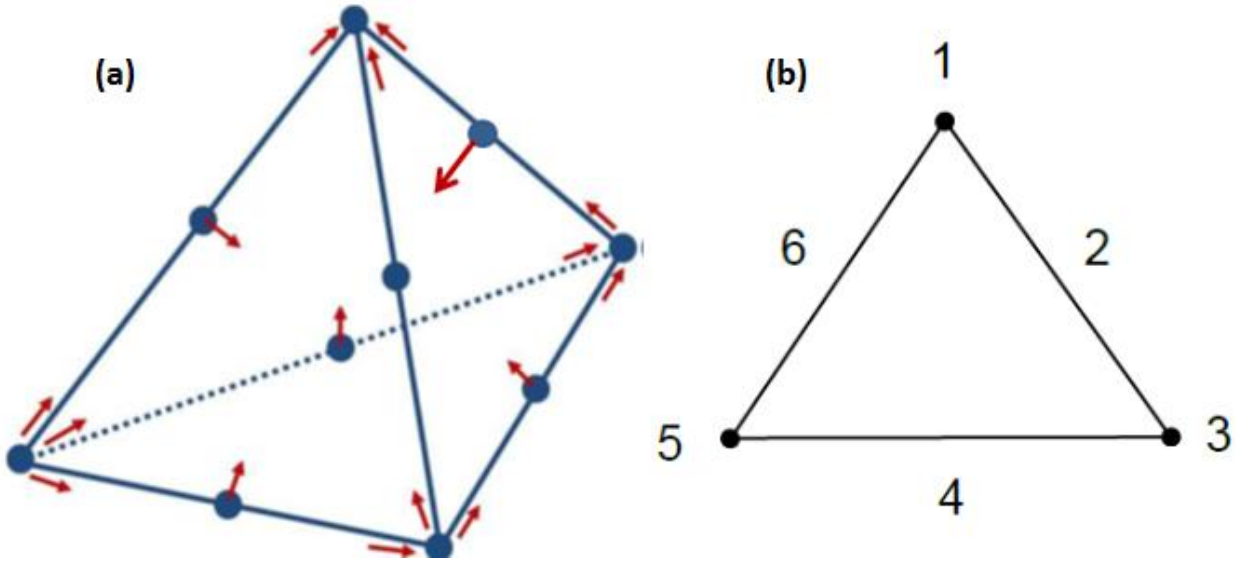


**Figure 4.2** Finite elements (a) Tetrahedron for 3D and (b) Triangle for 2D

Similarly in 2D simulations, the required field in each element is approximated with a 2nd order quadratic equation like $\mathbf{A_x(x,y) = a_o + a_1x + a_2y + a_3x^2 + a_4xy + a_5\ y^2}$ **.** The field quantities are calculated for six points as shown in figure 4.2.

Once the tetrahedral or the triangles are defined, the finite elements are placed in a large sparse matrix equation [S][H] = [J] which is solved using standard matrix solutions like Sparse Gaussian Elimination.

*Error Evaluation:* For each solver, there is some fundamental defining equation that provides an error evaluation for the solved fields. From the entire solution volume, the energy produced by these error terms is calculated. This energy is compared with the total calculated energy and will generate the percentage error energy.

$$percent\ error\ energy = \frac{error\ energy}{total\ energy} \times 100\%$$

The value of percentage error is displayed after each solution pass and is used to give information about convergence of the solution with respect to the adaptively refined mesh. The figure 4.3 shows a flow chart of the process of meshing and its dependency on the energy error.

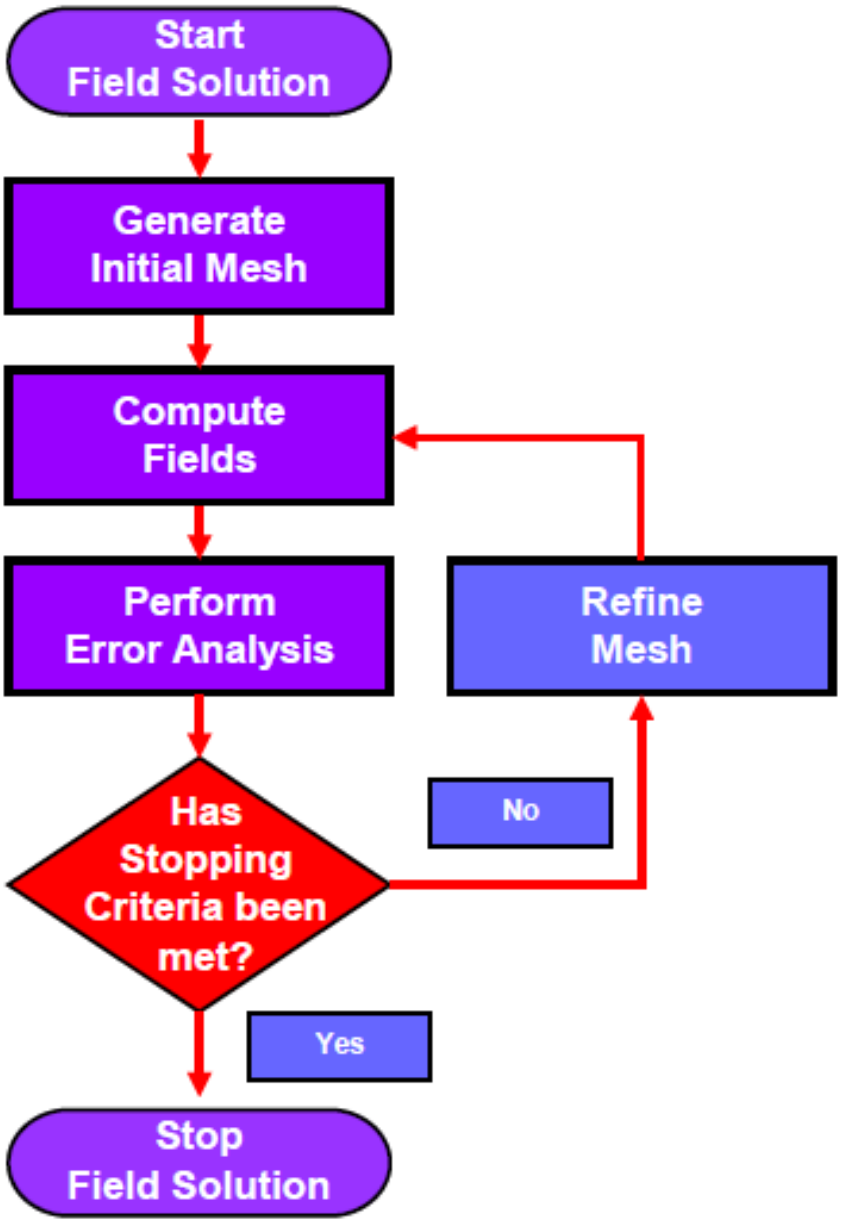


**Figure 4.3** Adaptive meshing with respect to energy error [43]

During the analysis, the system refines the initial mesh iteratively in order to reduce the size of individual elements in the areas where the error is high. This helps to get the accurate solution. After the first pass of the analysis, the software calculates the change in total energy from the previous pass. This difference is called delta energy (%). The mesh refinement continues until both percentage energy error and percentage delta error are below the target percent error specified by the user.

The flowchart in figure 4.4 gives the complete process that takes place in Maxwell from defining the geometries to analyzing the results once the solution type is selected.

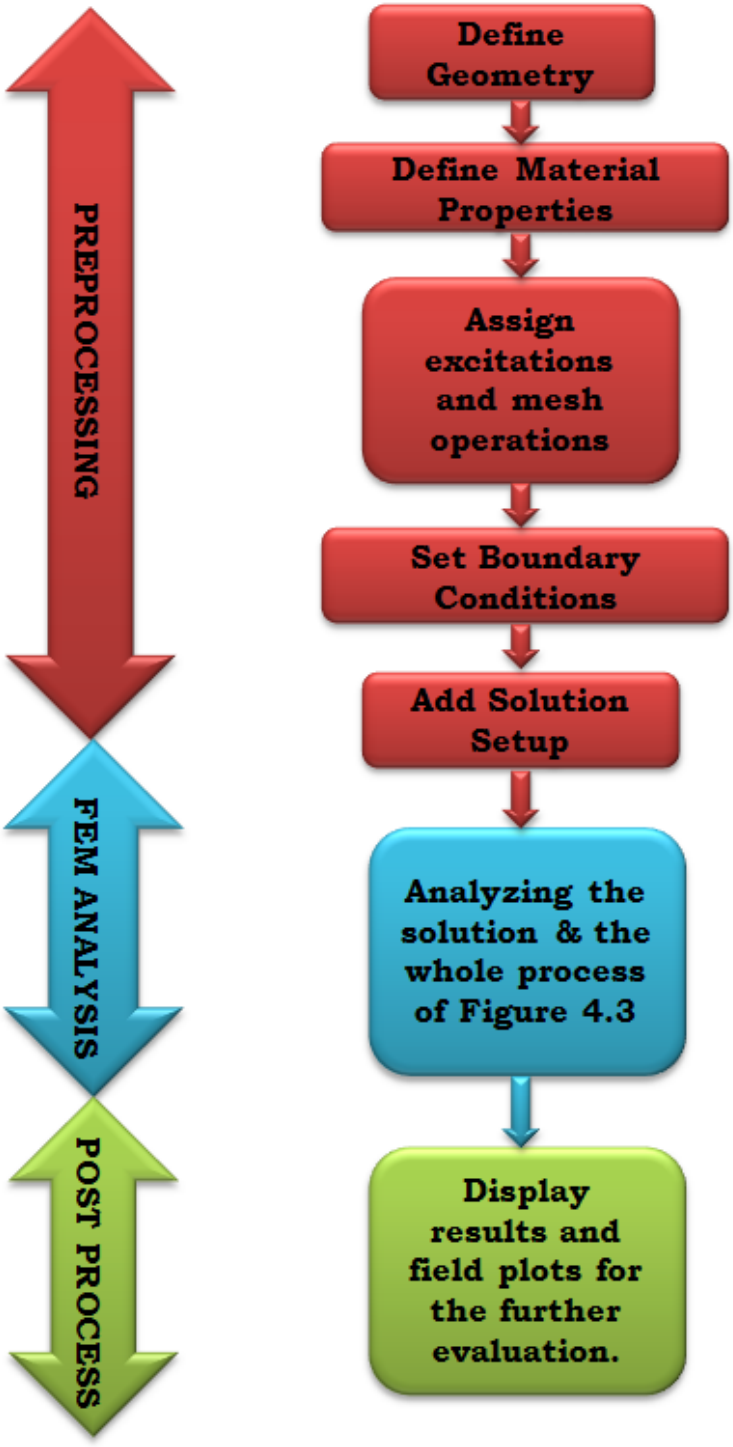


**Figure 4.4** Flow chart of complete process in ANSYS Maxwell

## 4.3 Modeling and Simulation

In this section, the initial simulation of a vacuum interrupter in ANSYS Maxwell 2D is shown. Based on figure 4.4, the task sequence of building a vacuum interrupter and analyzing its results are as follows.

1. Building the geometry of the interrupter
2. Setting up the material properties
3. Meshing and excitations
4. Setting up the boundary conditions
5. Defining the solution set up and analyzing
6. Visualization of solution i.e. Post processing

In the following sections, the above steps are executed and the results of the interrupter simulation for a given geometry are demonstrated.

### 4.3.1 Geometry modeling and assigning the materials

For the initial simulation, a patented 72.5 kV vaccum interrupter is taken as a reference for the dimensions of the interrupter model simulated in this research [45] Figure 4.5 shows the sketch of the vacuum interrupter unit. This model is built in axis symmetric i.e cylindrical about Z axis. The 2D geometry, when sweeped with 360° around the z-axis of a cylindircal coordinate system, it looks similar to the real time interupter unit as shown in figure 4.6.

Coming to the dimensions of the interrupter tube that are derived from the patent [45], the thickeness of the insulator wall has been taken as 6mm and height of the each block of the insulator is considered as 80mm. The thickness of metal shields is taken as 1mm. The diameter of the fixed contact is 40mm and for the movable contact with bellows is 70mm. The length of the center shield envelop is 110mm. The dimensions of other parts are self assumed values and are subjected to change in the following chapters. They are considered as the parameters to improve the performance of the interrupter tube.The diameter of the tube is 200mm. The radius of the curvature of the metal shield is 2.5mm. The distance between the two metal shield is 45mm. The distance between the metal shield and the insulator is 5mm. The shape of the insulator end is 45° to the metal shield. All the above dimensions are indicated in the following figure 4.5.

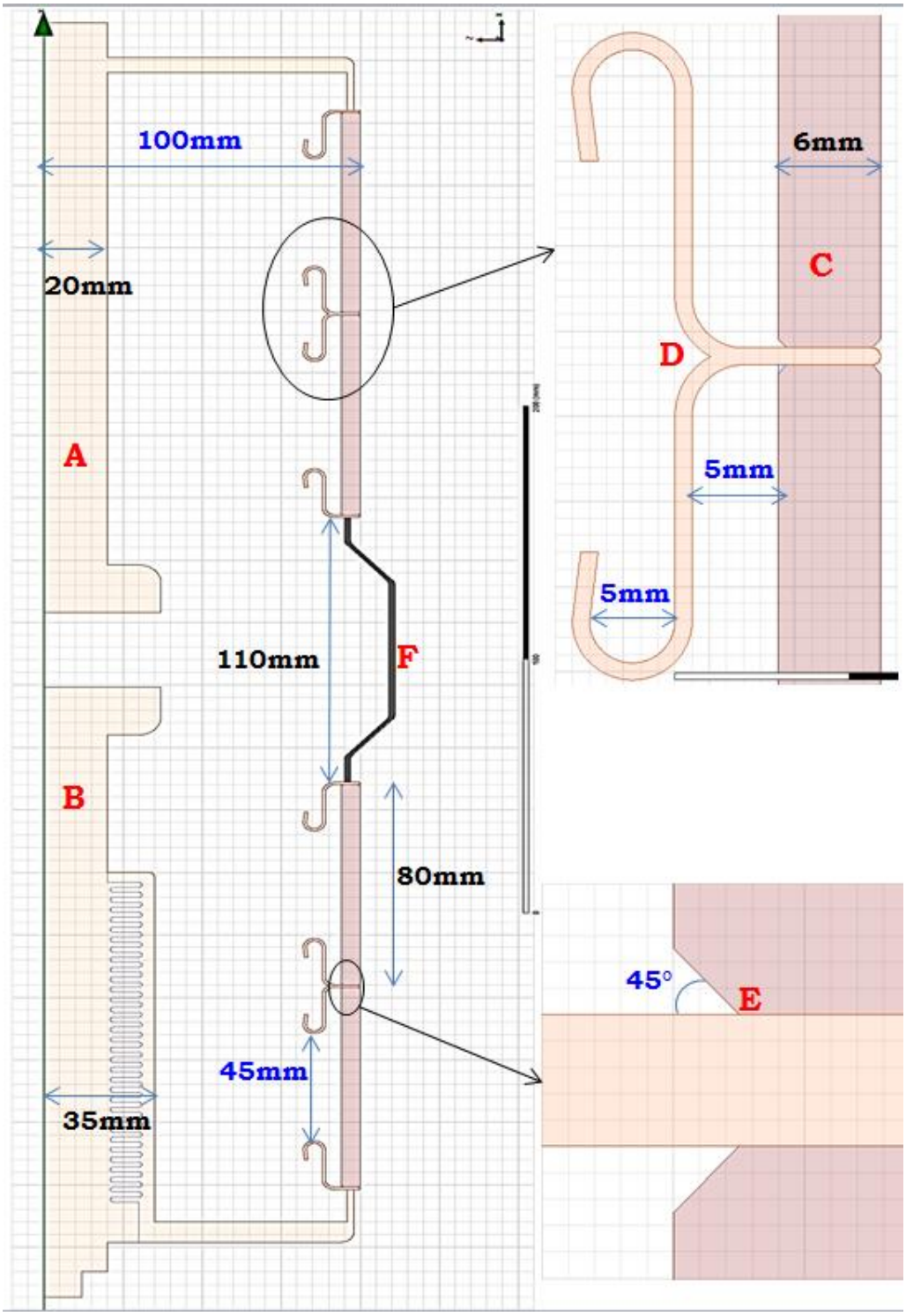


**Figure 4.5** Geometrical representation of a 72.5 kV Vacuum Interrupter in 2D with the following parts. **A:** Fixed contact, **B:** Movable contact with bellows, **C:** Insulator, **D:** Metal Shield, **E:** Triple Junction, **F:** Center Shield

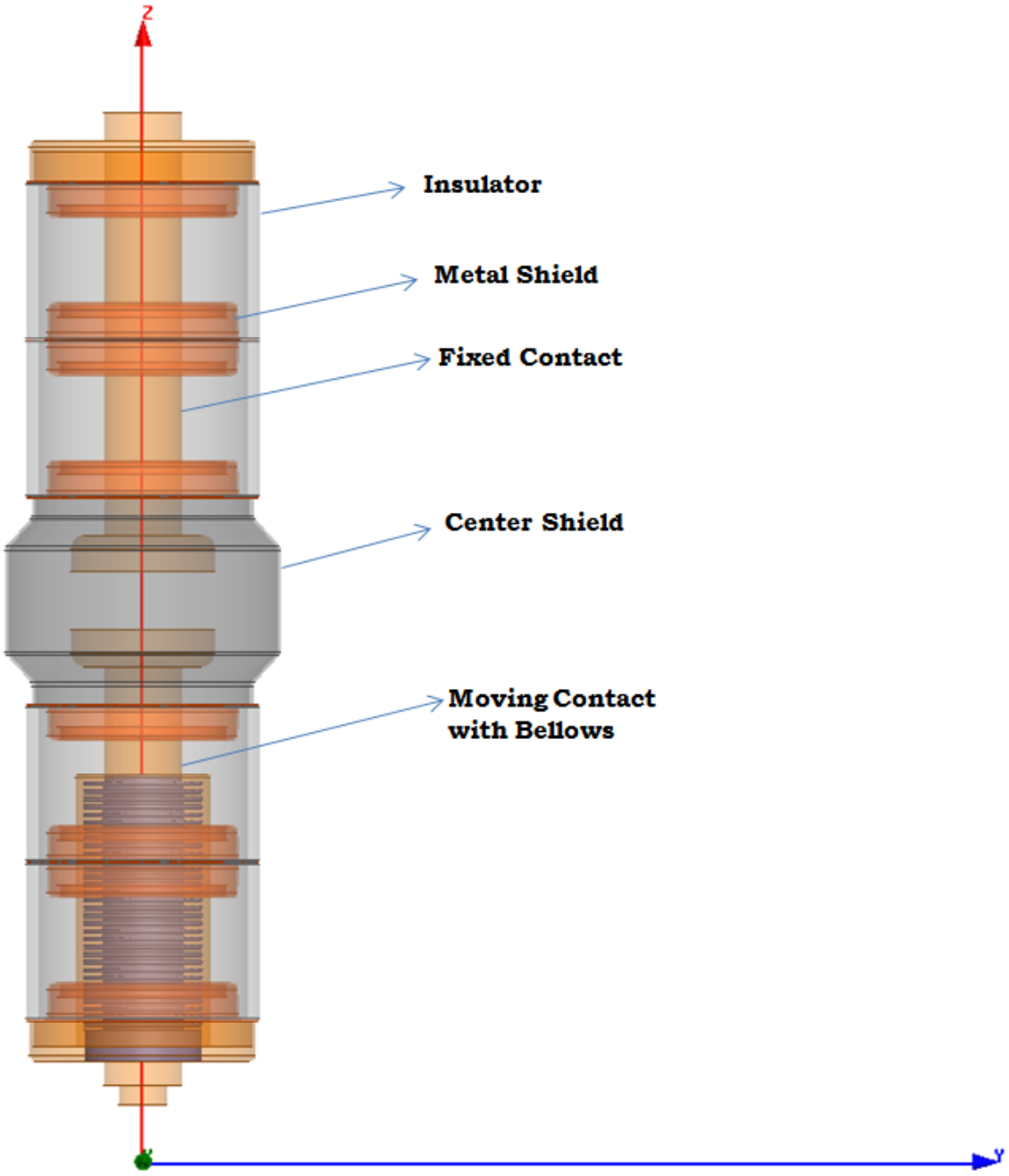


**Figure 4.6** 2D geometry when swept with 360° around Z-axis turns into 3D model

With respect to the type of the materials assigned to the individual parts, the insulator blocks of the inerrupter are made of alumina ceramic with relative permittivity ($\varepsilon_r$) of 9. The fixed contact, movable contact and the metal shields are made of copper with $\varepsilon_r$ of 1 and the conductivity of 58e6 S/m. Finally the center shield is made metal. If a material is not assigned to a part, then by default it is considered as a vacuum.

### 4.3.2 Meshing and Excitations

Once the geometry is built, the next step will be assigning a mesh to the model. In Maxwell´s static solvers, the mesh is automatically refined to achieve the required level of accuracy in the field computation. There are two types of initial mesh settings in Maxwell 2D. They are Ansoft Classic mesh and Ansoft TAU mesh. All the models in this research are simulated using Ansoft TAU mesh as it is advanced and gives more accurate results when compared with Classic mesh. To achieve a required level of accuracy in the results, the mesh needs to be refined in areas where the fields are of interest. Adaptive meshing provides an automated mesh refinement capability. There are mainly three different mesh operations which can be assigned to the model. They are (a) On Selection, (b) Inside Selection, and (c) Surface approximation. The On Selection based refinement will limit the edge length of all the triangles formed on the surface of the selected object. The Inside Selection refinement will limit the edge length of all triangles formed inside a selected object. For models mentioned in this research, the Inside Selection mesh refinement is used. The difference between the mesh formed without mesh operation and with mesh operation is showed below in figure 4.7.

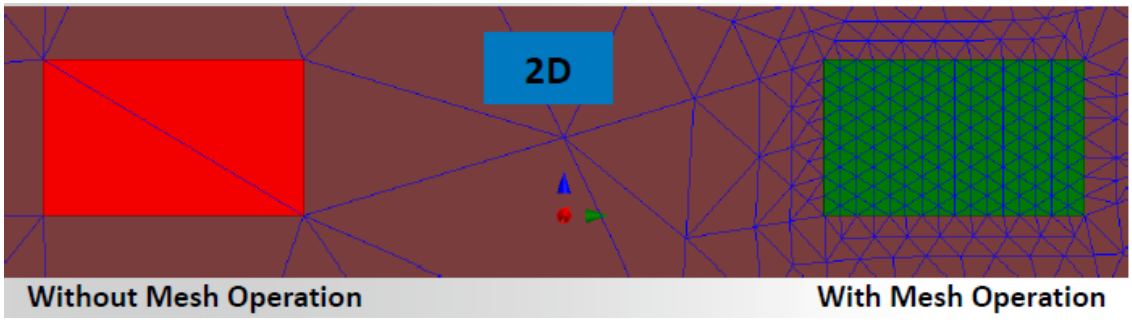


**Figure 4.7** Inside Selection mesh refinement

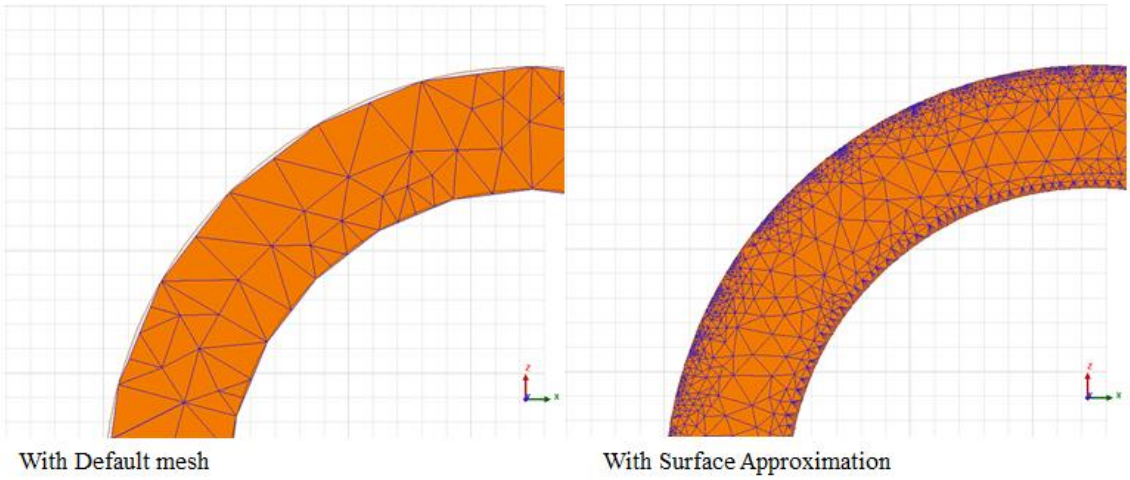


**Figure 4.8** Mesh near the metal shield curvatures with surface approximation operation

But, when it comes to curved surfaces, the Surface approximation mesh operation is used to get a good quality mesh and can be used to increase the mesh density especially at curvatures. In the present model, this operation is used mainly for the grading rings and metal shields which have curvatures. An example of an application of surface approximation on metal shield curvature is shown in figure 4.8.

Regarding the excitations, since the solver used in this simulation is an electrostatic solver, it is allowed to give DC voltages. When the vacuum interrupter is in open position, one of its contacts is at ground potential and other one is at high potential. So in this case, from the figure 4.5 the fixed contact is considered to be at ground potential (0%) and is excited with 0 volts and the movable contact is considered to be at high potential (100%) and is excited with 100 volts. By this way, the 0V is considered as a 0% and 100V is considered as 100% and the resultant field values can be showed in % values which would be easier for evaluation for initial purposes. In chapter 6, the higher potential is considered as 325 kV, which is the rated lightning impulse withstand voltage for rated 72.5 kV interrupters.

### 4.3.3 Setting up Boundary Conditions

Once the mesh operations and excitations are defined to the model, the boundary conditions have to be assigned. In order to assign boundaries, a region has to be drawn around the geometry which is known as simulation region. This simulation region is needed in order to specify a finite region in which FEA calculations will be carried out. The region should completely enclose the geometry and its dimension is normally 2-3 times the maximum length of the geometry and is considered as vacuum by default.

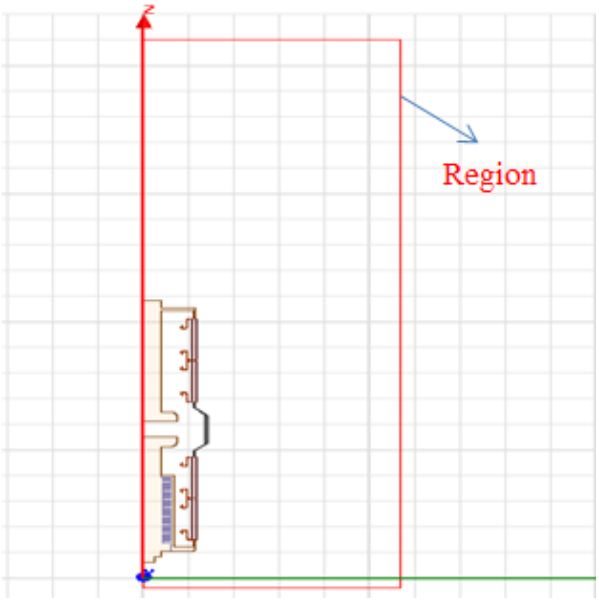


**Figure 4.9** Simulation region that is covering the interrupter geometry completely

After creating the region, boundary conditions should be given to it. These boundary conditions define the behavior of the electric field at the edges of the simulation region. There are different types of boundaries depending upon the applications.

| **Boundary Type** | **E-Field Behavior** | **Used to model...** |
|---|---|---|
| Default Boundary Conditions (Natural and Neumann) | Field behaves as follows:<br><br>• Natural boundaries — The normal component of **D** changes by the amount of surface charge density, tangent component of **E** is continuous. No special conditions are imposed.<br><br>• Neumann boundaries — **E** is tangential to the boundary. Flux cannot cross a Neumann boundary. | Ordinary E-field behavior on boundaries. Object interfaces are initially set to natural boundaries; outer boundaries are initially set to Neumann boundaries. |
| Symmetry | Field behaves as follows:<br><br>• Even Symmetry (Flux Tangential) — **E** is tangential to the boundary; its normal components are zero.<br><br>• Odd Symmetry (Flux Normal) — **E** is normal to the boundary; its tangential components are zero. | Planes of geometric and electrical symmetry. |
| Balloon | Two options are available:<br><br>Charge — The charge at "infinity" balances the charge in the drawing region. The net charge is zero.(Use for capacitance calculations)<br><br>Voltage — The voltage at "infinity" is zero. | Electrically insulated structures (Charge option) or electrically grounded structures (Voltage option). For the voltage case, the balloon boundary will not be equipotential in general. |
| Master and Slave (Matching) | The E-field vector on the slave boundary is forced to match the magnitude and direction (or the negative of the direction) of the E-field vector on the master boundary. | Planes of symmetry in periodic structures where **E** is oblique to the boundary. |

**Table 4.2** Boundary condition for electrostatics problem [44]

From table 4.2, it is clear that the Boundary types, Symmetry and Master & Slave are more effective to symmetric geometries. The Balloon boundary type is used for the applications where the device is in open air and the boundary limit is infinite. But in this case, the vacuum interrupter

model is not symmetric and is not an application of open air as the interrupter model in real applications is enclosed with a porcelain insulator. So in these simulations, the default boundaries i.e. Natural and Neumann boundaries are applied.

### 4.3.4 Solution Setup and Analyzing

After having defined the geometry, material properties, FEM mesh, excitations and boundaries, an adaptive solution setup should be defined, based on which the Maxwell runs its simulation. In this step the user should assign the maximum number of passes to be simulated and percentage error. The simulation will stop when any of these criteria are met. When the maximum number of passes is reached before the percentage error has been achieved, the simulation will stop but is considered as a non-converged solution. The higher the number of passes and lower the percentage error, the number of mesh triangles increases, which further improves the accuracy of the solution. Here, the number of passes is given as 15 and percentage error as 0.1. Once the solution setup is done, the model should be analyzed for the solution. After analyzing the model and when the stopping criterion has been met, the simulation will stop and display the solution data as shown in figure below.

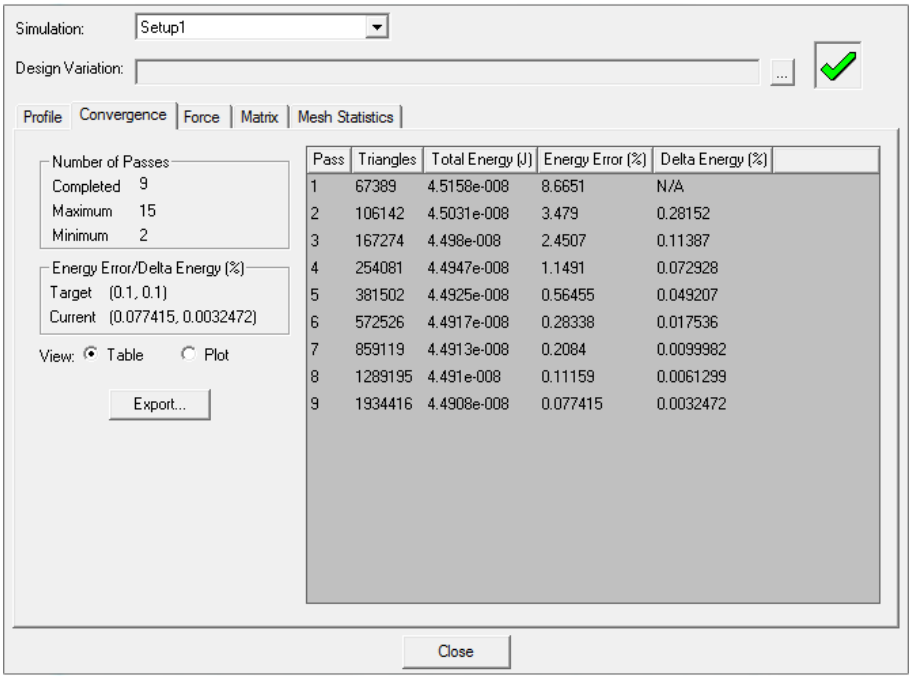


**Figure 4.10** Solution data showing the number of passes and percentage error

From figure 4.10, it can be seen that the solution has converged at pass number 9 when the energy error is less than the assigned value i.e. 0.1. The numbers of mesh triangles that are created in the model are shown in the triangles section and the number is increased with passes.

### 4.3.5 Post Processing

After designing the model and attaining the solution, we need to answer the question: How does the electric field distribution inside the interrupter tube look like? To answer this, it is necessary to execute post processing which means reviewing the results of the analysis. This is one of the important steps in the analysis as it is helpful to understand how the applied potential affects the electric field distribution based on the geometry, mesh and so on. The following images will explain the potential distribution, field distribution and influence of the mesh.

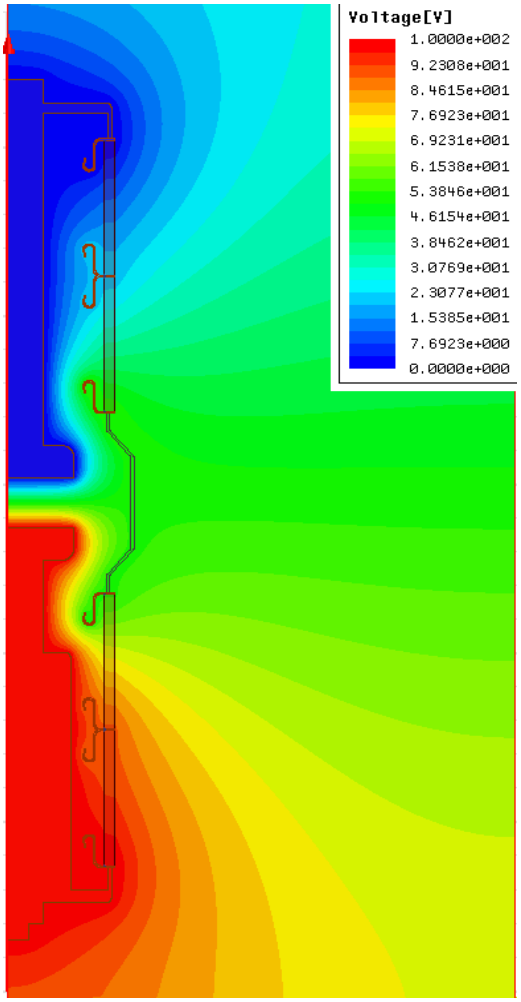


**Figure 4.11** Potential field plot of the interrupter model

Figure 4.11 shows the potential distribution inside the interrupter tube. As explained in the section 4.3.2, the fixed contact is assigned with 0V and the movable contact is assigned with 100V. The metal shields inside the interrupter will experience different potentials because of which the field distribution is affected. The schematic representation of the potential distribution on each metal shield is shown below.

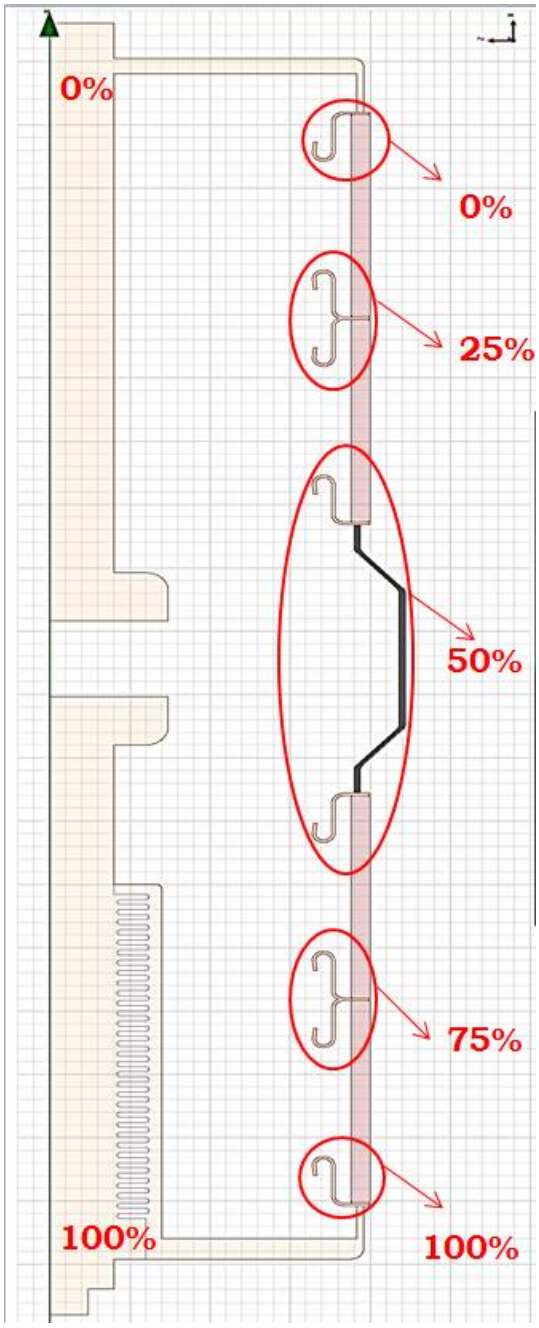


**Figure 4.12** Potential distributions on each metal shield when one contact is at 0% and other at 100% potential

The potential distribution in figure 4.12 shows that each metal shield experiences a different potential based on their position. This potential distribution and the geometry configurations are the primary reasons why the electric field distribution is different at different metal shields as shown in figure 4.13.

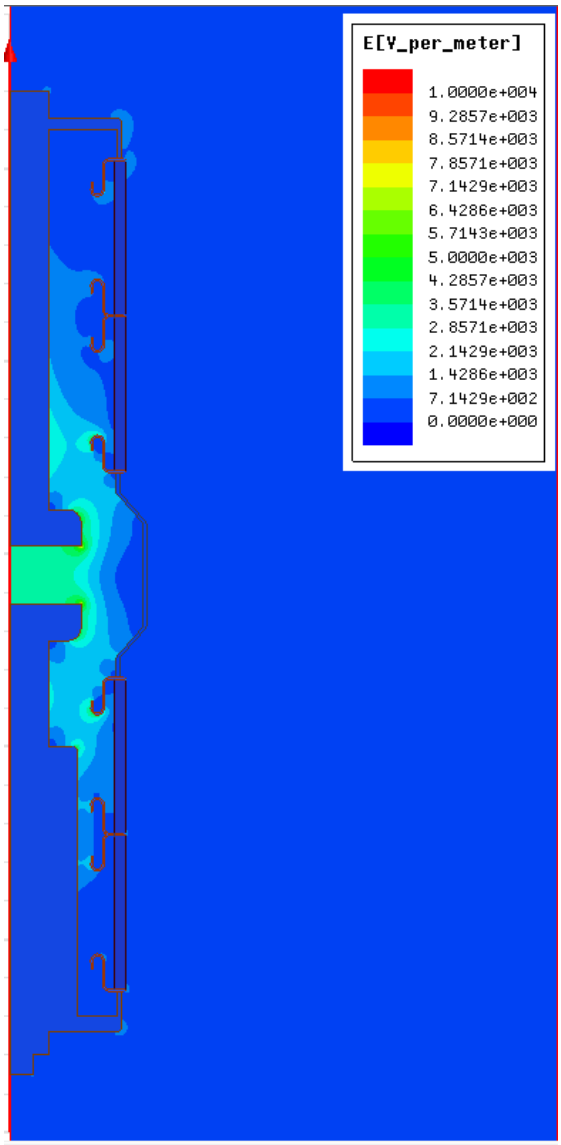


**Figure 4.13** Electric field plot of the interrupter model

In the whole research the electric field will be discussed in V/mm or kV/mm. This electric field plot helps to understand the critical regions in the geometry. It shows where the field stress is high and where changes in geometry are needed. Since this work deals with the critical regions like triple junctions, metal shield edges and near the metal shield curvatures, the field stress at these regions are showed in following images (Figure 4.14). But when it comes to the triple junctions, plotting the electric field at this region is tricky. It depends very much on the mesh configuration as shown in figure 4.15. So near the triple junctions care should be taken that mesh must be very fine to get accurate results.

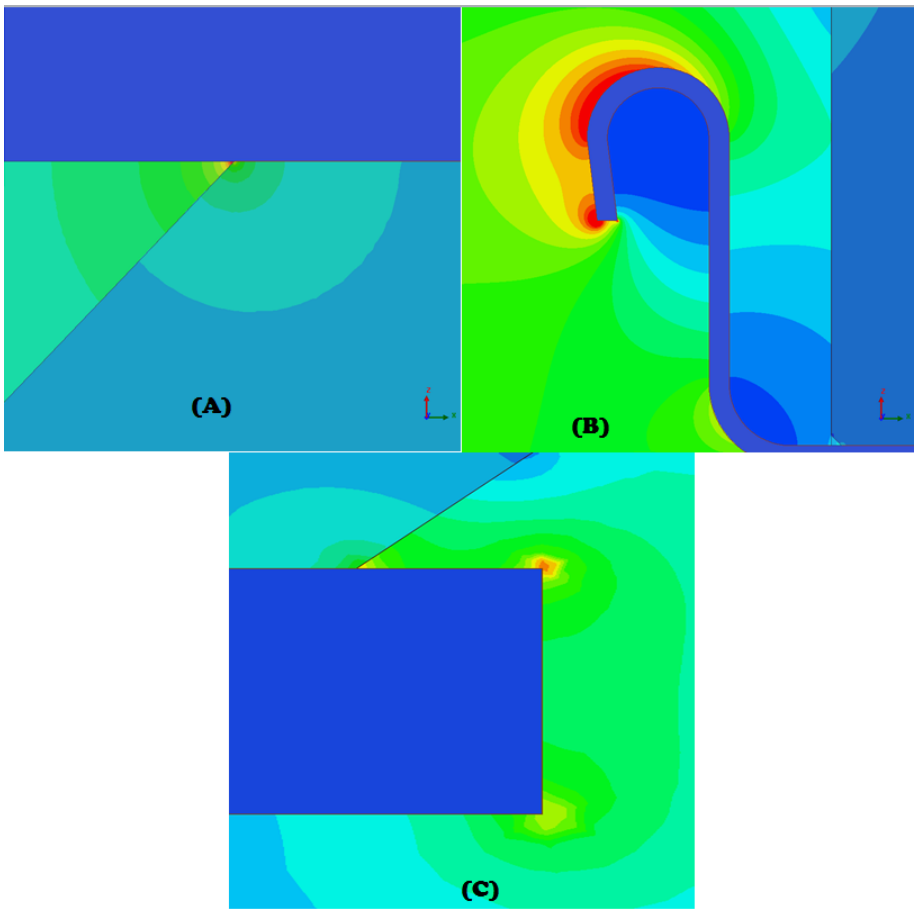


**Figure 4.14** Electric field stresses of a metal shield at 50% potential: (A) Triple Junctions, (B) Metal shield curvatures, (C) metal shield edge

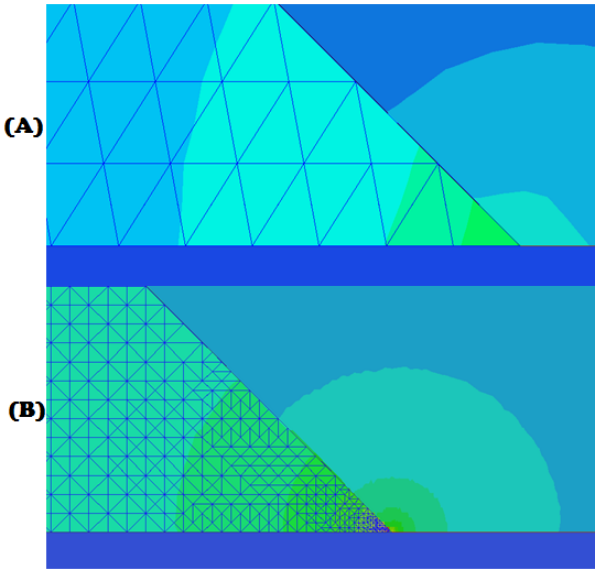


**Figure 4.15** Triple Junction (A) without fine mesh and (B) with very fine mesh

The field stress in the critical areas, as shown in figure 4.14, is one of the primary reasons for having surface flashovers inside the interrupter unit and reducing its withstand voltage.

## 4.4 Concept of Field Grading

Electric field grading or stress control refers to the techniques of controlling local enhancements of the electric field in various devices. As voltage levels are increasing and the sizes of components are shrinking, the demand for integration of different functions in a single device is steadily growing. In order to make products competitive with these properties, field grading is crucial. For example, smaller insulation thickness leads to reduction in material costs and temperatures but results in higher electric fields which may leads to breakdown mainly at the critical regions such as the interfaces or the triple points. [46]

Field grading methods are mainly classified into two main classes. A) Capacitive field grading which is generally achieved with electrode geometry of appropriate shape of the conductive parts and high permittivity materials. B) Resistive field grading by using special materials with appropriate current-field characteristics. The main task during a product development of many electrical devices is to identify a suitable field grading technology for a given application.

In the next chapter, different geometrical parameters which are assumed to have an influence over the field stress at the critical regions inside the high voltage vacuum interrupter are discussed.

# Chapter 5

# PARAMETERS INFLUENCING THE WITHSTAND VOLTAGE OF THE INTERRUPTER & THEIR SIMULATIONS

In this chapter different parameters that affect the electric field distribution inside the vacuum interrupter are analyzed. Figure 5.1 illustrates the places where the changes in geometry may be needed in order to improve the dielectric strength inside and outside the interrupter. Based on the regions of figure 5.1 and the literature survey, various geometrical parameters are considered and simulated in this chapter.

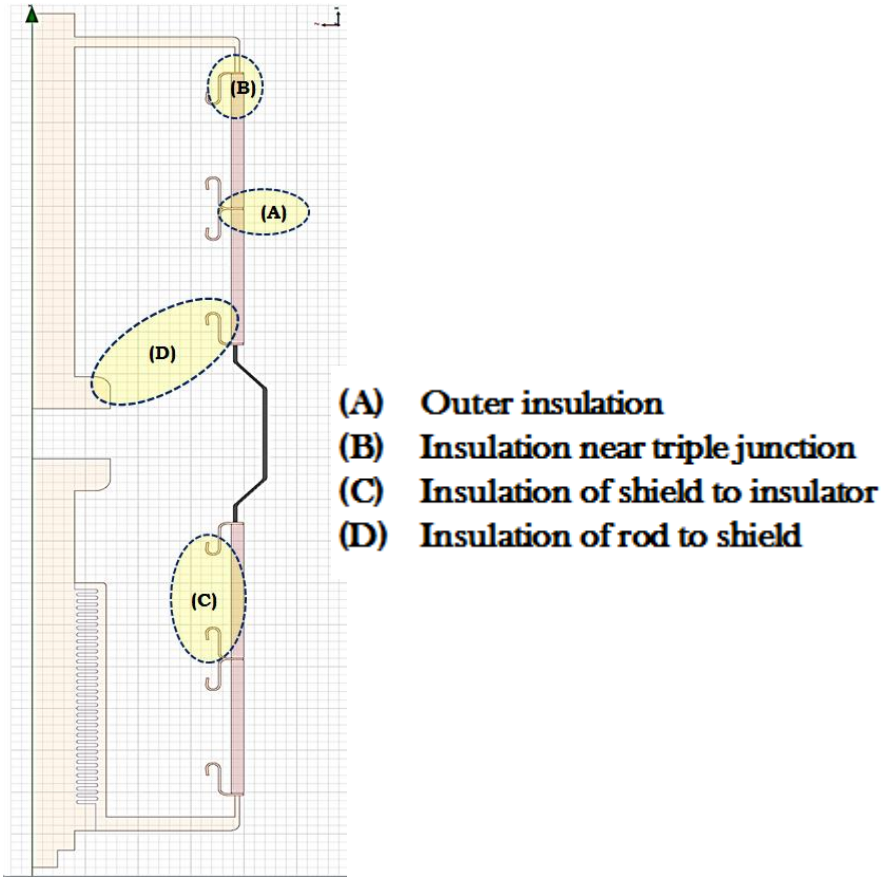


**Figure 5.1** Critical zones inside the interrupter in terms of insulation

For the outer insulation, field grading rings of different shapes are studied. In addition, the effects of different conductivities of these grading rings are also considered. For the insulation near the triple junction, shape of the insulator and metal inserts at both ends of the insulator are studied and simulated. For the insulation of shield to insulator, distance between the metal shields and the distance between the metal shields and the insulator are assumed as influencing factors and are simulated with different variations. In chapter 6, the insulation of rod to shield and the shape of the metal shield curvatures are considered as parameters and simulated.

## 5.1 Field Grading Rings

When we consider a vacuum interrupter in an open state, one of its two contacts will be at high voltage potential i.e. 100% and the other one will be at the ground potential i.e. at 0%. In ideal conditions, the center shield will be at 50% potential. But in practical applications, the potential at the center shield will be floating because of the presence of stray capacitances. This floating potential leads to an unequal field distribution which further leads to a higher field stress on some of the metallic elements inside and outside the interrupter tube.

In general, metal shields at ceramic joints will have a higher field stress at its edges as the thickness of the metal shield is 1mm. That leads to indefinite sharp edges after manufacturing. The high field stress at these undefined edges can result in breakdowns through the gas. In addition the triple junction emissions can result a breakdown on the surface of the ceramic insulators. There are two ways to avoid the breakdown from the edges of these metal shields. One way is to fill the gap between the insulator and outer housing with a high pressurized gas which has high dielectric strength. But during the switching of small inductive currents, there is a chance of voltage elevation up to several times the rated voltage, and in this case the undefined edges can be the source of partial discharges because of very high field stress. In addition to this, the high pressure can be the reason for high mechanical stress on the elastic bellows and can lead to damage of these bellows. The other alternative is using a low pressurized gas, and the metal shield edges are extended outside the insulator and to cover the shield edges with grading rings which are conductive. Because of their conductive nature, they reduce the field strength at the edges by a strongly enlarged radius and thus the discharges can be prevented. Care must be taken to ensure that the rings are not in contact with the ceramic insulators to avoid breakdown along the surface of the ceramics.

A simple model with ceramic insulators and metal shields without grading rings as shown in figure 5.2 is built in Maxwell. The upper metal shield is excited with 0V and lower metal shield is excited with 100V. This model will help us to observe the field distribution near the metal shield edge. The zoomed image shows the geometry of the edge of the metal shield. Figure 5.3 shows the plots of the potential distribution and the electric field distribution. The electric field stress on the metal shield edges can also be seen in the figure. This unwanted high stress at the corners of the edge may be responsible for discharges in the gas or on the insulator surface.

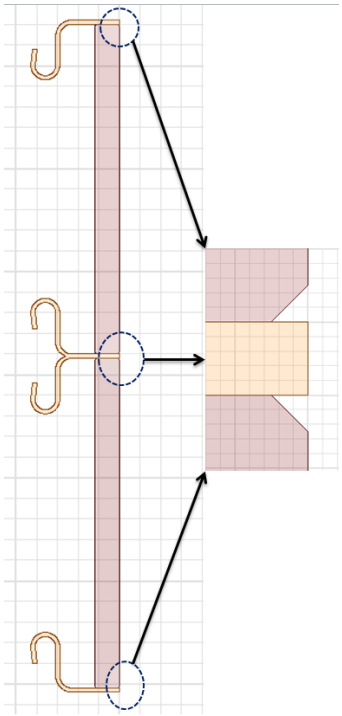

**Figure 5.2** Geometry of ceramic blocks, metal shield and shield edge

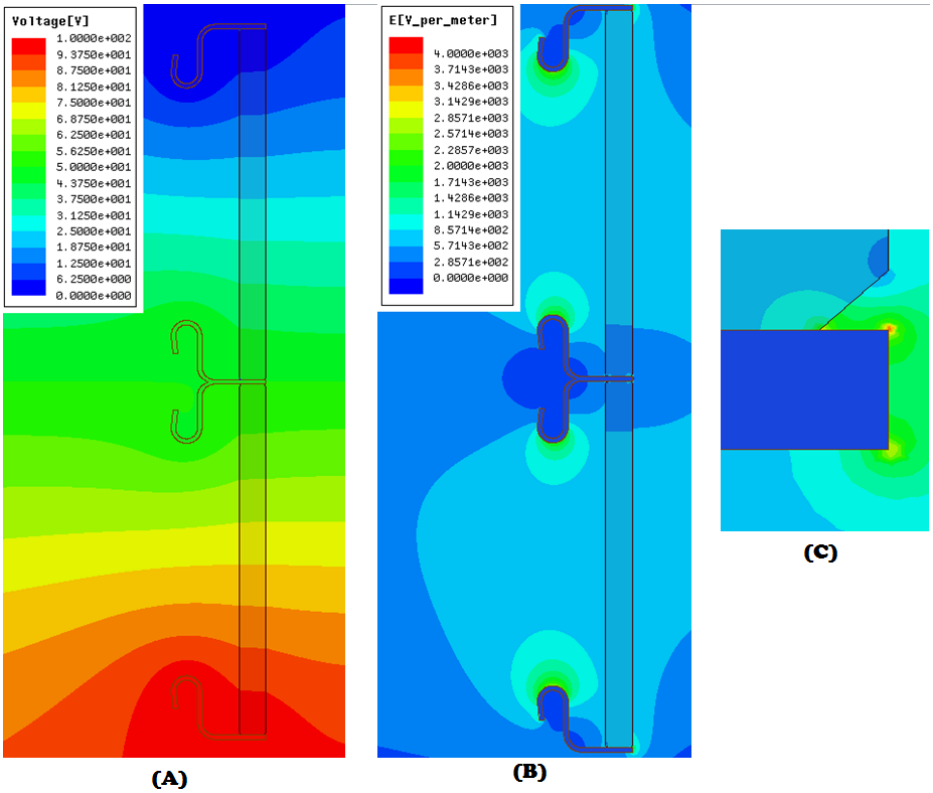


**Figure 5.3** (A) Potential distribution, (B) Field distribution, and (C) Electric field stress at one of the shield edges

In order to avoid this high stress, these metal shields are extended to the outside and covered with grading rings. This geometrical arrangement along with the grading rings is shown in figure 5.4. Here, the thickness of each grading rings is of 10mm radius and is made of aluminum which is a very good conductor. The influence of different conductivities of grading rings will be discussed in the next section. In this section, all the simulations are made with grading rings made of aluminum. From the figure, it is clear that the maximum field stress near the edge of the metal shield has been reduced to almost half when compared with field stress without grading rings.

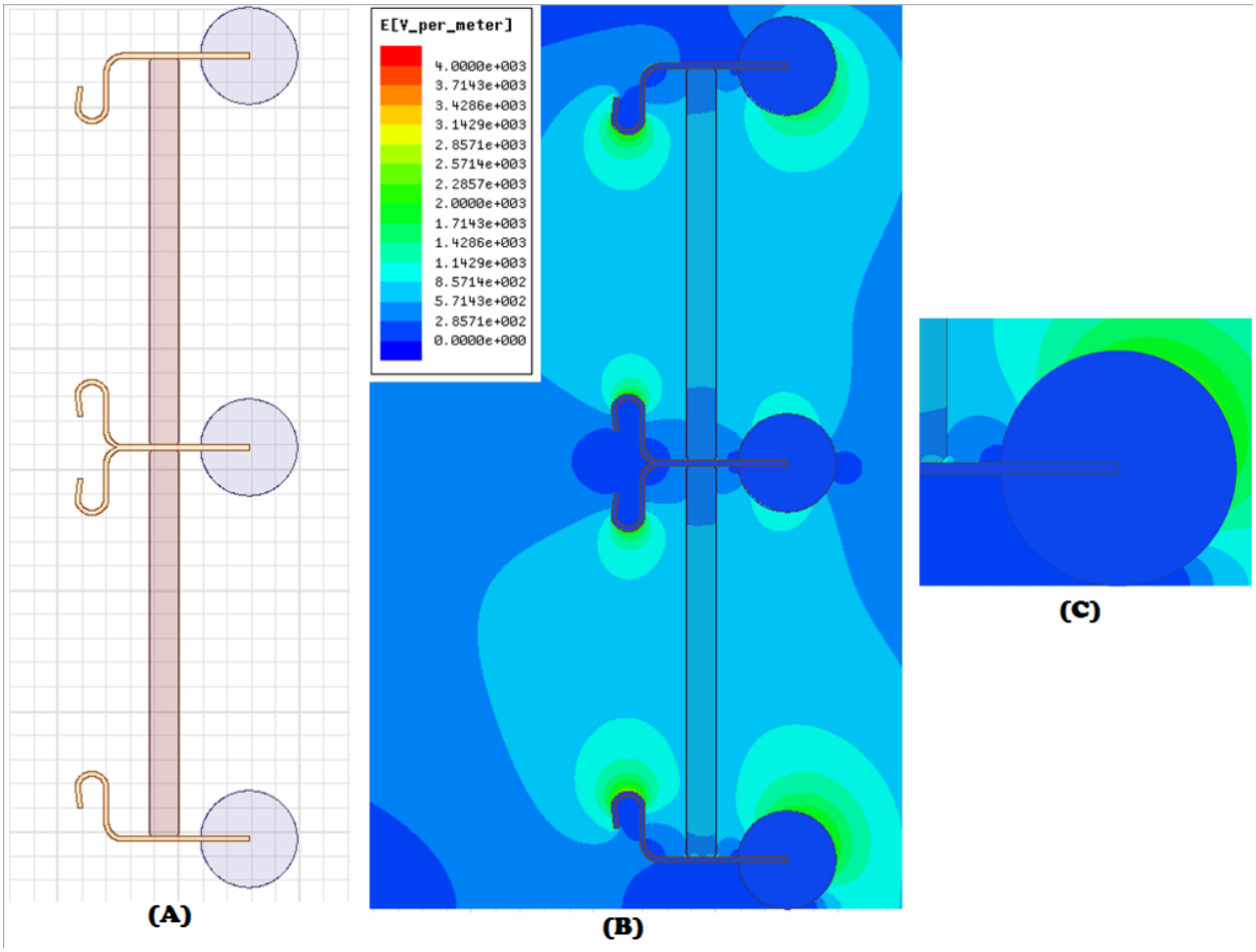


**Figure 5.4** (A) Interrupter unit with field grading rings, (B) Electric field distribution, (C) Field stress near the edge of the metal shield

Further, it is assumed that the shape of the grading rings may have an influence on reducing the stress at the triple junctions outside the interrupter. In order to observe this influence, two principal variables are considered: the radius of the ring and the distance between the ring and the insulator. The shape of the grading rings can alter the equipotential distribution at the triple junction thus influencing the stress at the triple junction.

The effect of the radius of grading ring and its distance to the insulator are studied in the following simulations. Figure 5.5 shows the various models of which the first three models are

varied to observe the effect of changes in distance (1-3) and the other three are modeled to observe the effect of change in radius.

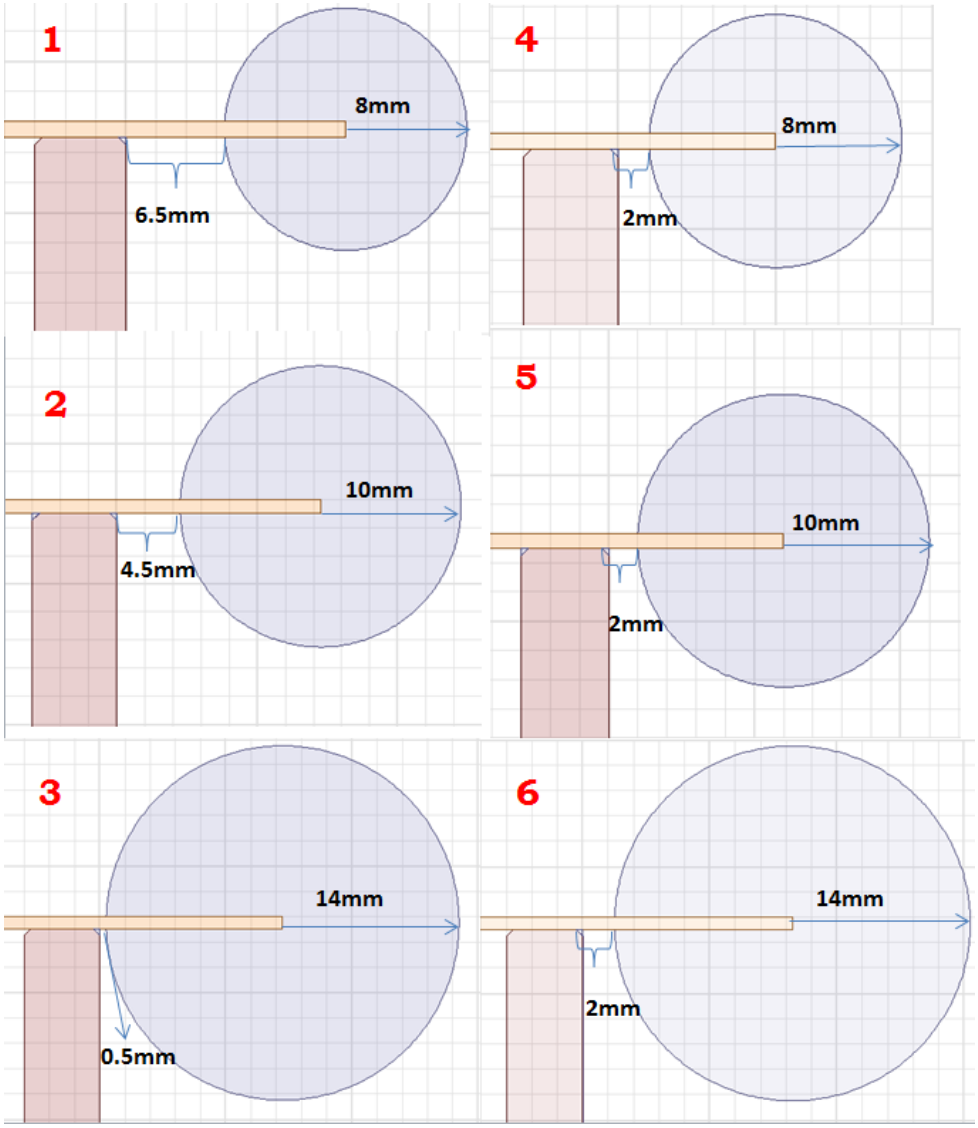


**Figure 5.5 (1)** Grading ring with the radius of 8mm and a distance of 6.5mm. **(2)** Grading ring with the radius of 10mm and a distance of 4.5mm. **(3)** Grading ring with the radius of 14mm and a distance of 0.5mm. **(4)** Grading ring with the radius of 8mm and a distance of 2mm**(5)** Grading ring with the radius of 10mm and a distance of 2mm. **(6)** Grading ring with the radius of 14mm and a distance of 2mm

The first three models in Figure 5.5 show that as the radius of the grading ring increases, the distance between the insulator and the ring decreases. So by simulating these three models, the effect of distance can be observed. On the other hand to see the effect of an increase in radius, the other three models were developed. In these models, the radius of the ring is increased while keeping the distance between the insulator and the ring constant. All these models are simulated and their field plots were plotted to observe the effect of the changes.

Figure 5.6 shows the equipotential lines around the grading ring at the cathode metal shield (0V). It is clearly visible that the shape and the distance of the grading rings effect the potential distribution especially on the outer surface of the insulator and near the cathode triple junction (outside). These potential distributions in turn affect the electric field stress.

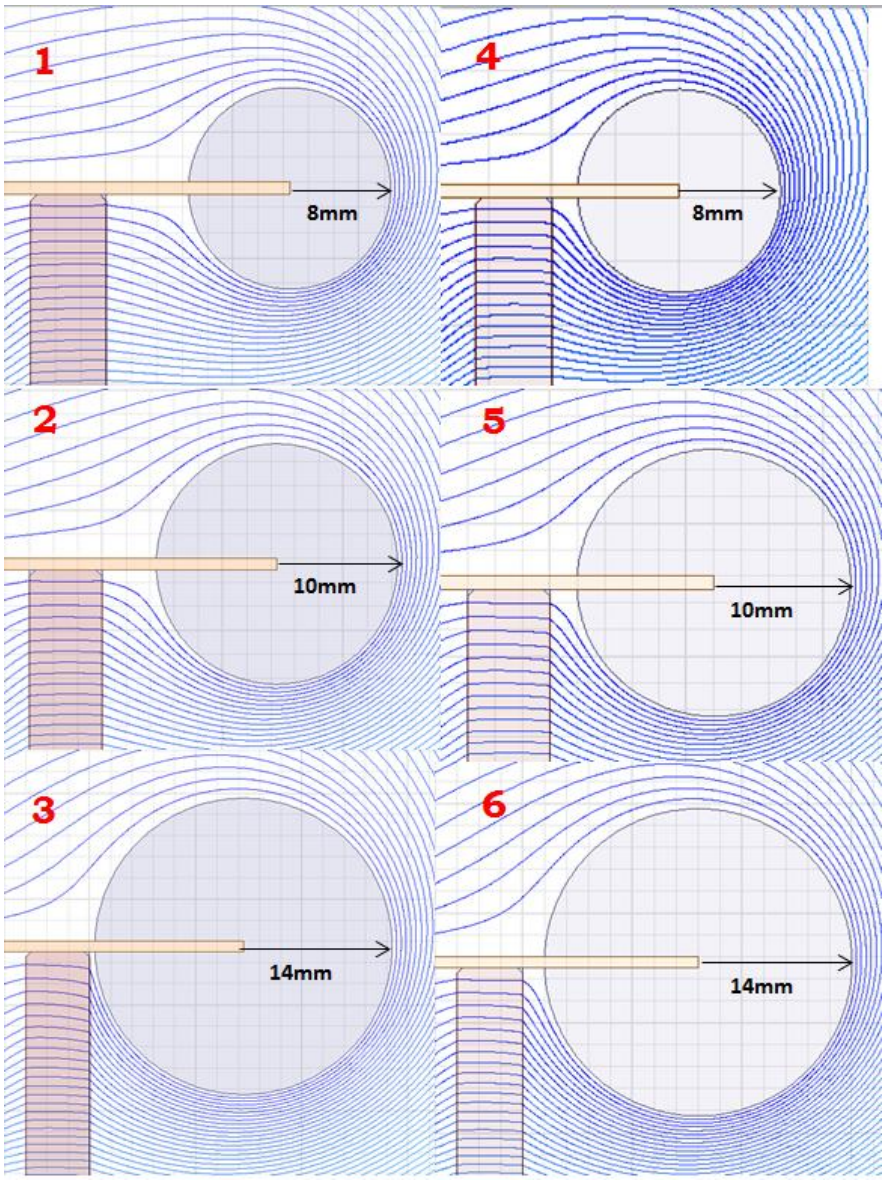


**Figure 5.6** Change in equipotential lines or potential distribution based on the distance from the insulator and radius of the rings

In order to observe the electric field distribution, electric field values are plotted along the outer surface of the upper insulator block. With these graphs, the effect of the shape of the rings on the field stress at the outer triple junctions as well as on the outer insulator surface is clarified. Figures 5.7 shows the graphs to observe the effect of varying the distance to the insulator and figure 5.8 show the graphs to observe the effect of changing the radius.

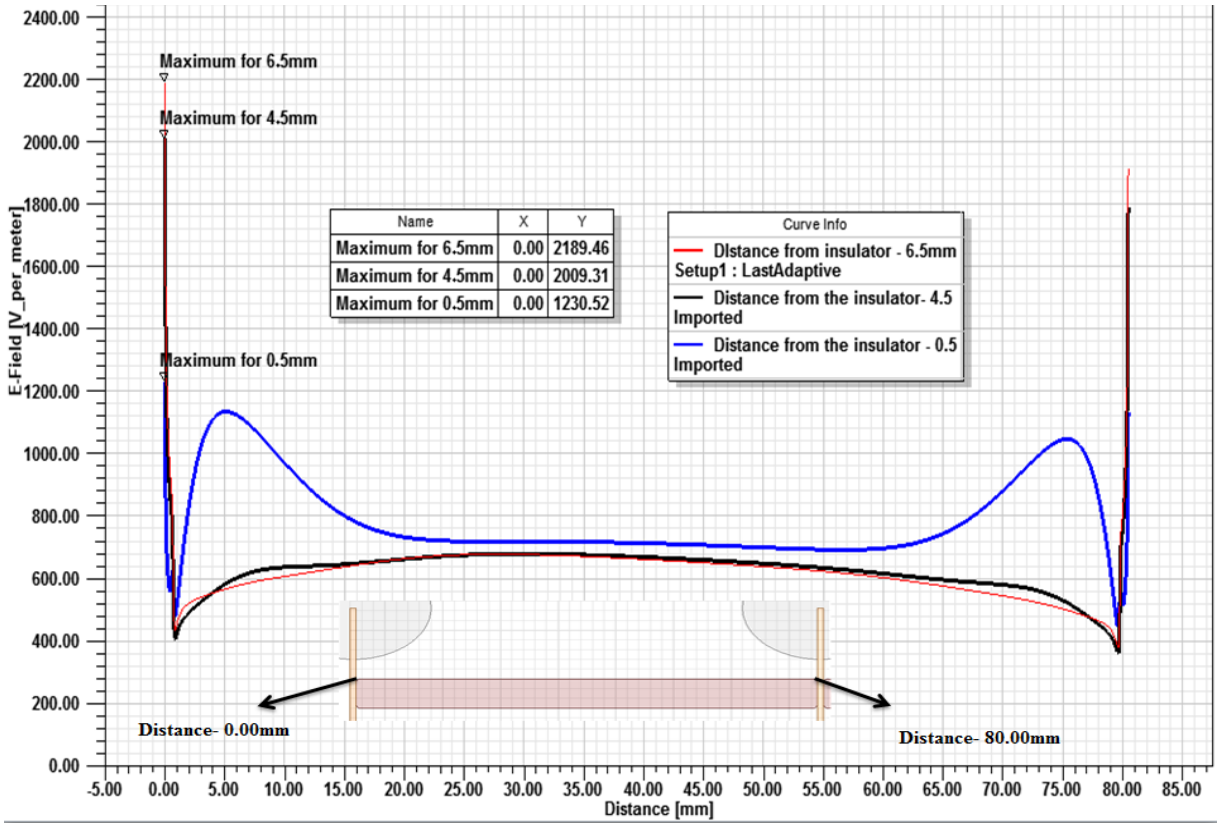


**Figure 5.7** Electric field values along the outer surface of the ceramic showing the effect of change in distance to the insulator

From the figures 5.5 and 5.7, it is clearly visible that for the grading ring of radius 8mm which is 6.5mm away from the insulator, the field stress at the outer triple junction is around 2.2kV/m. Similarly the grading ring of radius 10mm which is having a distance of 4.5mm from the insulator has around 2kV/m field stress at the outer triple junction. And finally, for the grading ring of radius 14mm and the distance of 0.5mm from the insulator, the field stress is around 1.2kV/m. From all these values it is evident that as the distance between the grading ring and the insulator decreases, the field stress at the outer triple junction decreases. But at the same time, the stress on the ceramic surface increases.

From the images of 4, 5 and 6 of figure5.5 and from figure 5.8, by keeping the distance between the insulator and ring as constant i.e. 2mm, the effect of change in ring radius can be seen. For a ring with the radius of 8mm the field stress at the outer triple junction is around 1.94kV/m. For the ring with the radius of 10mm, the field stress at the triple junction has reduced to around 1.83kV/m and lastly for the ring with radius of 14mm, the stress at the triple junction has further reduced to around 1.64kV/m. So, the increase in radius decreases the stress at the outer triple junction and has a lesser effect on the field stress on the ceramic surface. But it is clear that the effect of change in distance is more pronounced compared with the effect of radius.

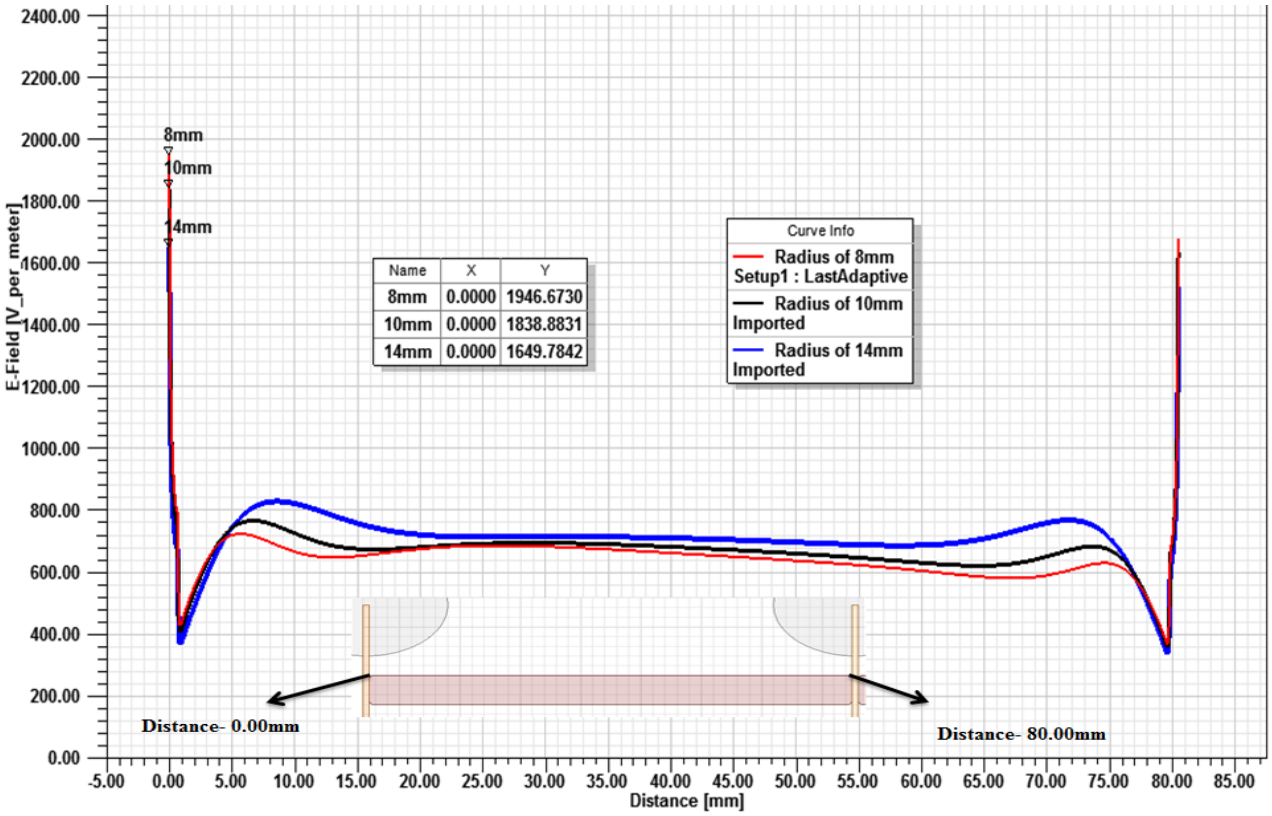


**Figure 5.8** Electric field values along the outer surface of the ceramic showing the effect of change in radius

Furthermore, by keeping the distance constant, the effect of the height of the grading ring is observed by modeling the grading rings in the shape of ellipses as shown in the figure 5.9. The first ellipse from the figure has a vertical radius of 10.5mm and horizontal radius of 13.5mm. The second ellipse has 13.5mm vertical radius and10.5mm horizontal radius. And the final ellipse has 17.5mm vertical radius and 14mm horizontal radius. Figure 5.10 shows the electric field values plotted along the surface of the same ceramic block that is used for the previous calculations.

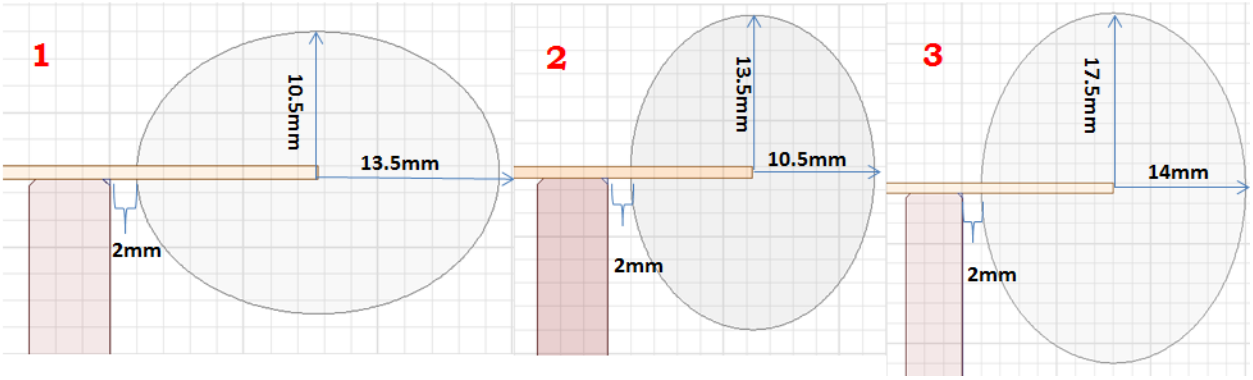


**Figure 5.9** Grading rings of elliptical shapes with constant distance of 2mm from the insulator

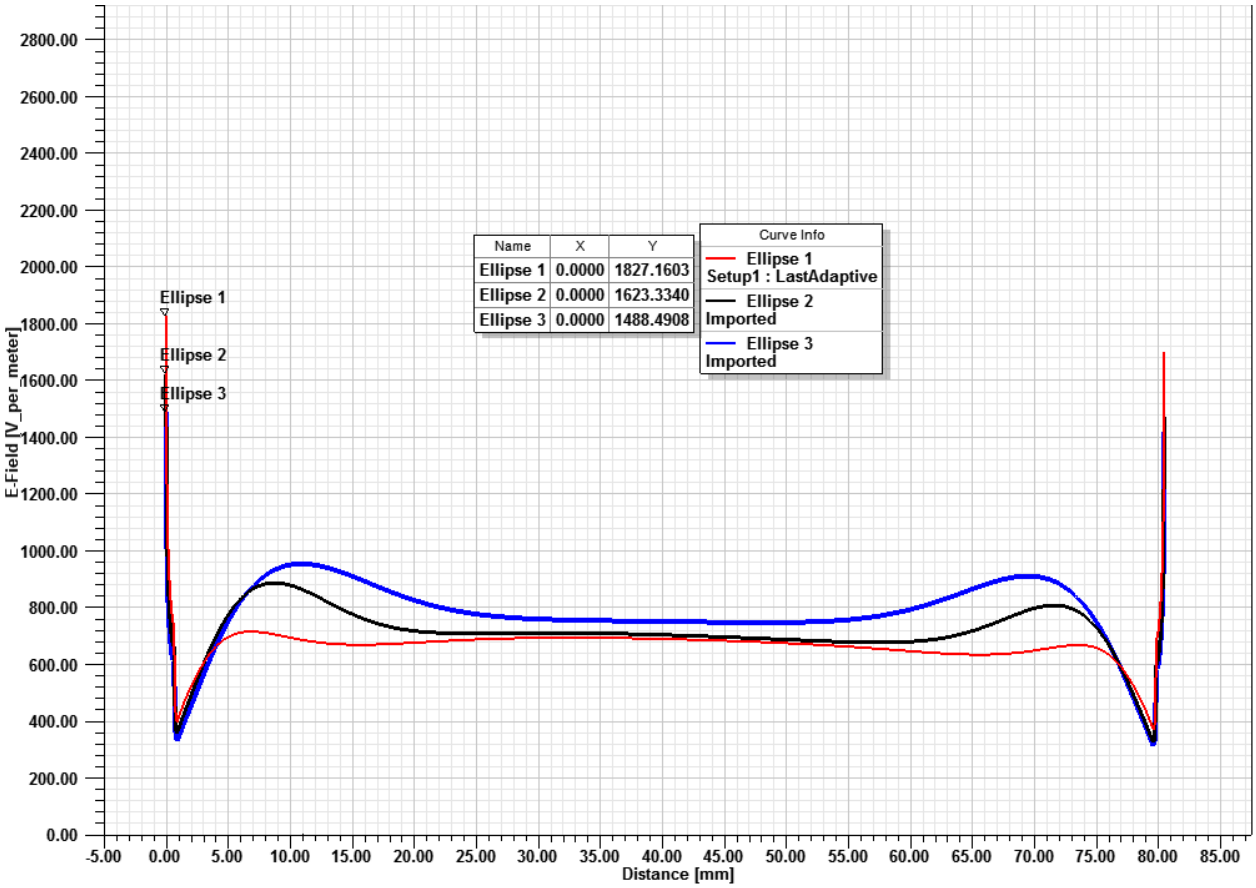


**Figure 5.10** Electric field values along the outer surface of the ceramic showing the effect of elliptical shaped rings

From the field values in figure 5.10, it is understood that for the elliptical shape with vertical radius of 10.5mm, the stress at the triple junction is 1.8kV/m. For the elliptical shape 2 with vertical radius of 13.5mm, the field stress at the triple junction is 1.62kV/m and finally for the elliptical shape with vertical radius of 17.5mm, the field stress at the triple junction is 1.48kV/m. So, from the above values it can be inferred that, as the height of the ring increases (vertical radius), the field stress at the triple junction decreases.

By observing all the shape variations of the grading ring and the variation in the distance between the ring and the insulator, it is clear that the grading with lesser distance from the insulator and having a larger height (vertical radius) will considerably reduce the field stress at the outer triple junction. But, care should be taken to make sure that the ring is not too close to the insulator as this increase the field stress on the outer surface of the insulator.

## 5.2 Conductivity of the Grading Rings

In addition to the shape of the grading rings and their distance to the insulator surface, the conductivity of the grading rings is also assumed to have an influence. So the grading rings of different conductivities are simulated to study the influence on the electric field around the grading ring. To observe the effect of conductivity of the material, an AC conduction solver is used instead of an electrostatic solver to obtain better results. The following are the grading rings of different conductivity ranges that are used in the simulations.

1. Grading ring with the conductivity of $10^{6}$S/m.
2. With conductivity of $10^{3}$S/m.
3. With conductivity of 10 S/m.
4. With conductivity of $10^{-1}$ S/m and relative permittivity of 10
5. With conductivity of $10^{-3}$ S/m and relative permittivity of 10

The first three rings are treated as conductive rings and the last two rings are treated as insulating rings.

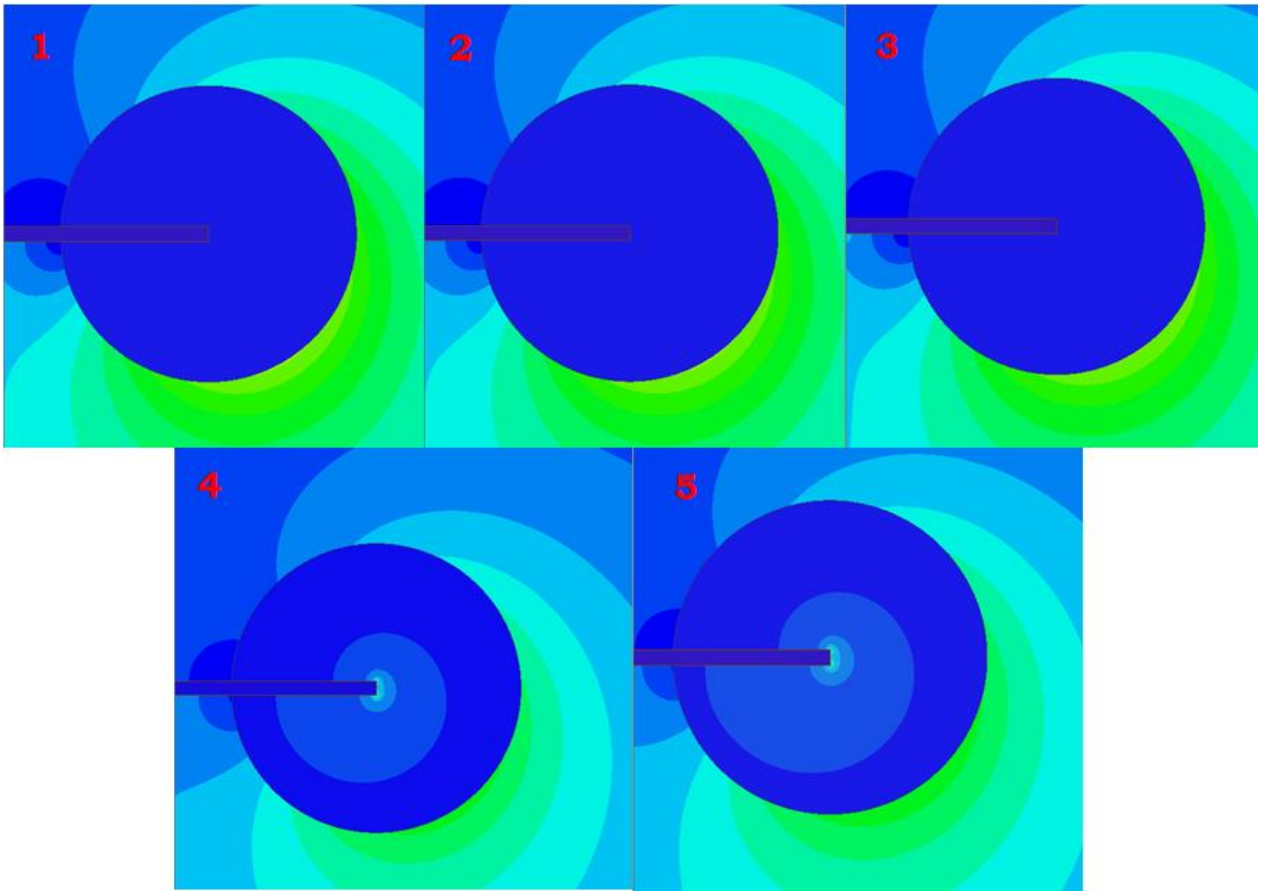


**Figure 5.11** Electric field plots inside and around the grading ring with respect to their conductivities

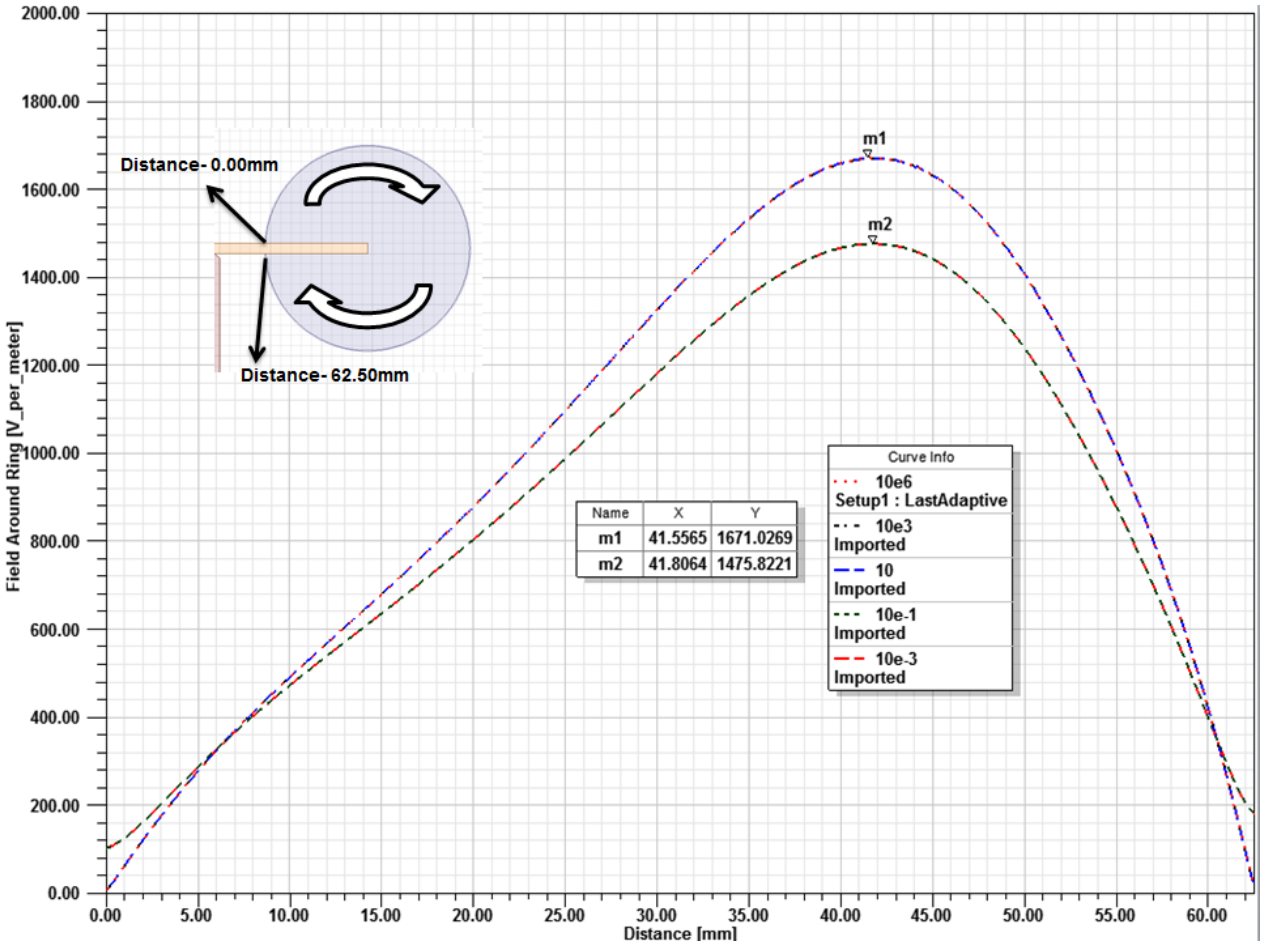


**Figure 5.12** Electric field values on the surface of the grading rings of different conductivity

All the models are simulated with 0V 50 Hz at upper metal shield and with 100V 50Hz at lower metal shield. The figures 5.11 and 5.12 show the electric field plots inside and around the field grading rings with different conductivities. The field patters of 1, 2, 3 which are considered as conductive rings in figure 5.11 and their graphs in figure 5.12 suggest that there is no change in field distribution inside the ring as well as around the ring irrespective of changing the conductivity from $10^6$ to 10 S/m. On the other hand the rings with insulator properties i.e. with negative conductivity show high field intensity at the end of the metal shield i.e. at the center of the grading ring and low field intensity around the ring (1.47 kV/m) when compared with conductive rings (1.67 kV/m) which can be clearly seen from figures 5.11 and 5.12 respectively. However, the increase in field intensity inside the grading ring is considered to be more dangerous than the high field intensity around the grading ring. So the grading rings must be conductive and the conductivity range can be varied from a pure conductor ($10^6$ S/m) to a partial conductor (10 S/m) depending on the availability of the material and the cost of the material. In the present research, all the grading rings are considered to be a pure conductor and assigned with the aluminum material.

## 5.3 Shape of the Insulator

When an insulator is subjected to high voltages, it has a tendency to acquire a large positive charge on its surface. There is a possibility that this positive surface charge may be an essential link in the sequence of events that leads to flashover through Secondary Electron Emission Avalanche (SEEA) as proposed by Boersch [17]. In this process, electrons with enough energy impact on the insulator surface to eject secondary electrons resulting in a positive charge on the surface. One of the sources of this primary electron is the triple junction. The breakdown field depends upon the structure of this triple junction where metal, insulator and vacuum meet. The SEE characteristics of the insulator determine the electric field strength required to cause a surface flashover on the surface of the insulator in vacuum.

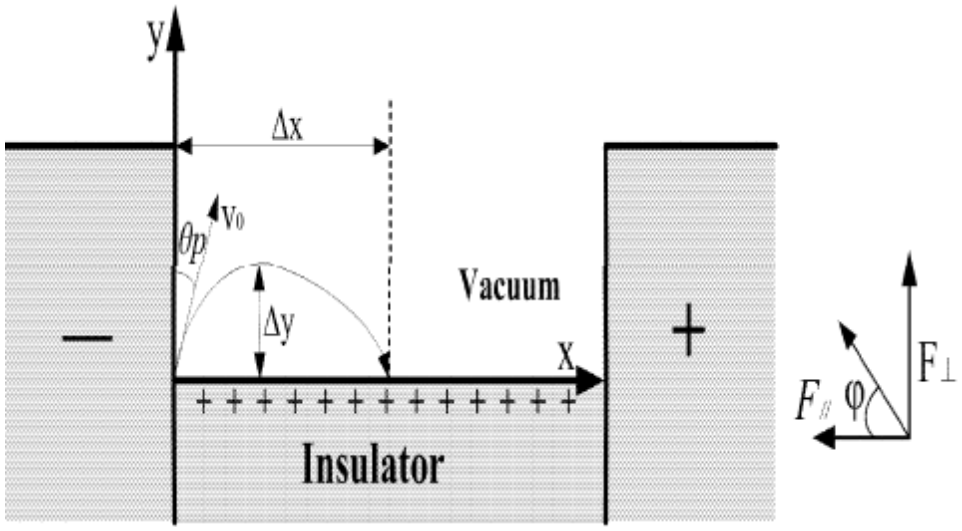


**Figure 5.13** Mechanism of primary electron emission and its propagation along the insulator surface

From figure 5.13 it can be seen that a primary electron is emitted with electric field from the cathode triple junction to vacuum with an initial velocity V0 and angle θp. The first electron collision has energy and is represented in the form of an equation shown below [47]

$$E_i = \tfrac{1}{2} m_e v_i^2 = E_p \left( 1 + \frac{4F_{//}^2}{F_\perp^2} \cos^2 \theta_p + \frac{4F_{//}}{F_\perp^2} \sin\theta_p \cos\theta_p \right) \qquad (1)$$

where $V_i$ is the velocity of the electron at the time of its impact on the insulator surface, $m_e$ is the effective mass of the electron, $F_{//}$ is the parallel component of electric field and $F_\perp$ is the normal component. The terms in the bracket indicate the energy gain ΔE that the electron obtains during the travelling along the surface. ΔE is mainly dependent on the angle of emission θp and also the ratio of parallel and normal component of the electric field. As explained in section 3.4, the final flashover will probably take place due to the layer of desorbed gases. The expression of the flashover voltage by taking the desorbed gases into account is shown below

$$V_t = \left| \frac{M \cdot L \cdot v_{gas} \sqrt{2A_0 \cdot m_e} \cdot \left| \tan\varphi \sin\theta_p + \sin^2\theta_p \right|}{\varepsilon_0 \cdot \gamma \cdot \tan^3\varphi \cdot \left| \cos\theta_p + 2ctg\varphi \sin\theta_p \right|} \right|^{1/2} \quad (2)$$

where M is the amount of desorbed gas molecules per $cm^2$ which is sufficient to cause a breakdown, L is the length of the insulator, $V_{gas}$ is the average velocity of the desorbed gas molecules from the insulator surface, $A_o$ is the electron emission energy, $m_e$ is the mass of the electron, and φ is the angle between the electric field and the insulator. From the figure () the value of tan φ is give in the equation below.

$$\tan\varphi = \frac{F_\perp}{F_\parallel} \quad (3)$$

As the angle φ increases, the ratio of the parallel component of the electric field ($F_{//}$) to the perpendicular component of electric field ($F_\perp$) decreases. Now from equation 1, as the term $F_{//}/ F_\perp$ decreases, the energy of electron collision is reduced. This helps in avoiding secondary electron emission. So a reasonable geometry of the insulator can improve the angle φ.

Another factor that affects the breakdown voltage across the insulator surface is the shape of the insulator. Figure 5.14 shows the results of Anderson [48] and Milton [49] which states that the surface flashover field depends greatly on the insulator angle with the metal shield.

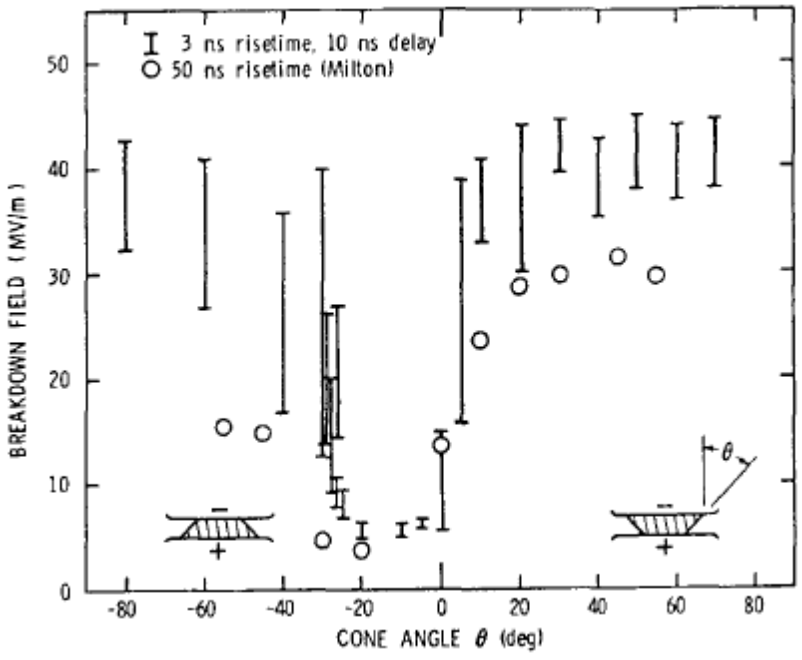


**Figure 5.14** Surface flashover fields with respect to insulator angle, PMMA insulator, d=6mm [48] [49]

For the 50 ns pulses, it can be taken from the figure that the flashover field increases for the positive angles like +15° to+70° and a little increase for -30° to -80°. The minimum flashover field is observed for the angles of -5° to -20°. This behavior strongly suggests that changing the angle of contact between the insulator and the metal shield affects the flashover field by modifying the local field at the inner triple junction as well as effecting the electron propagation along the inner surface of the insulator.

Based on the above discussions, four different shapes of insulators as shown in the figure 5.15 which make different contact angles with the metal shields are simulated.

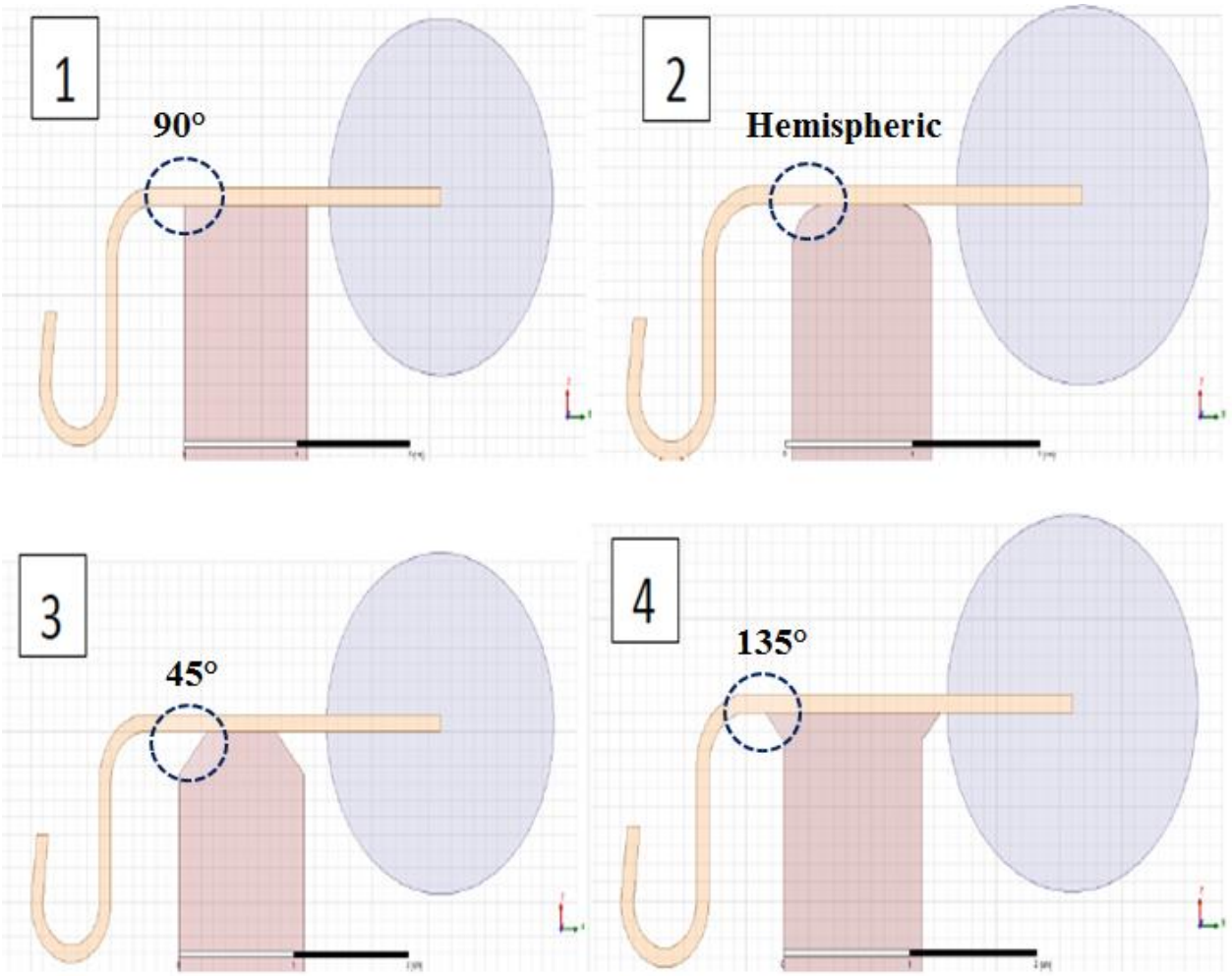


**Figure 5.15** Different shapes of insulators (1) Flat end with 90° angle of contact, (2) hemispheric shape with 2.5mm radius, (3) 45° angle of contact, (4) 135° angle of contact

The upper metal shield is excited with 0V and the lower metal shield is excited with 100V. The resultant field plots give the details of electric field at the triple junctions. These details help us to understand the effect of the shape of the insulator on the electric field at the triple junction vicinity. The electric field plots of four different insulators are shown below.

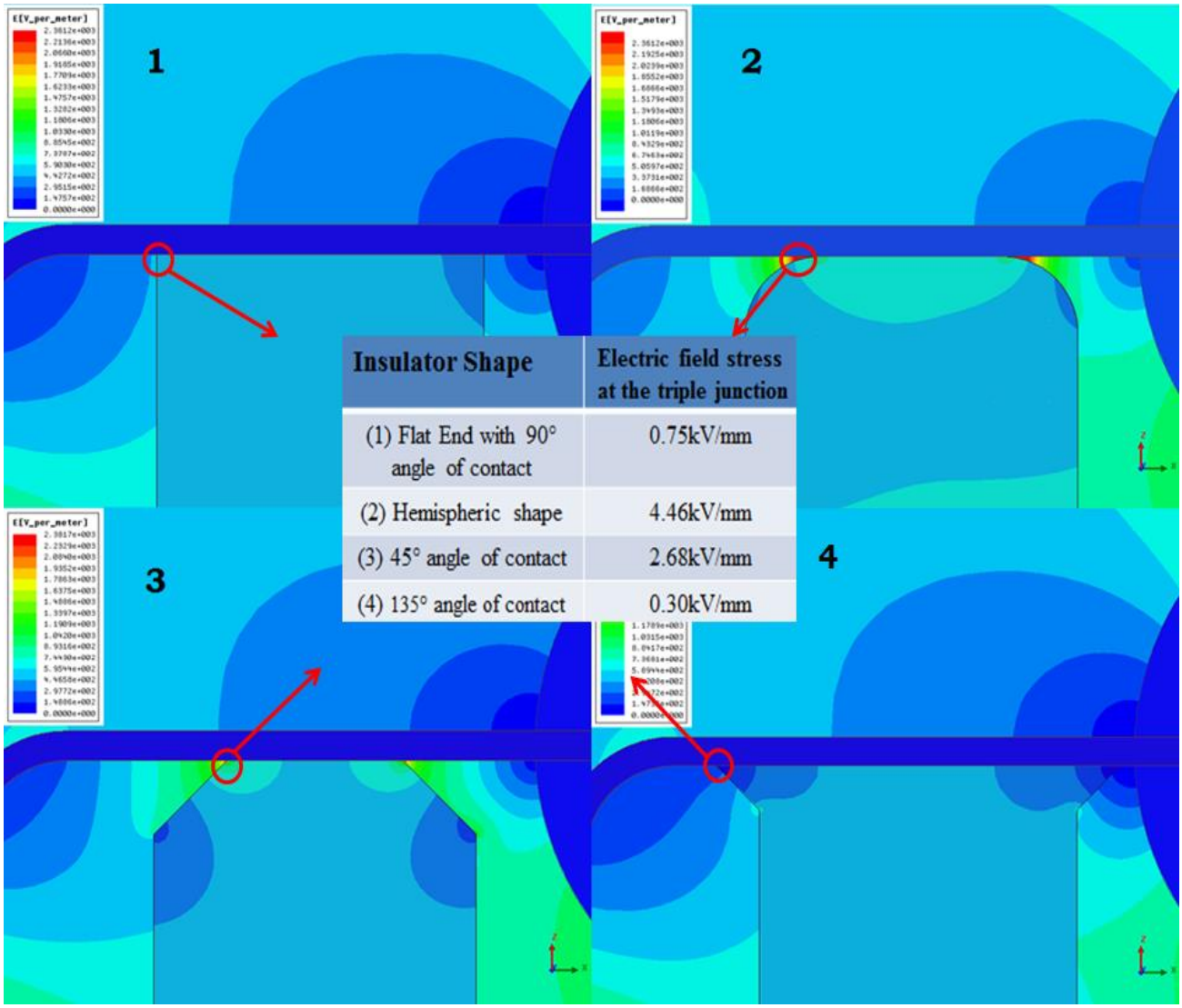


**Figure 5.16** Electric field plots of (1) Flat end insulator, (2) Hemispheric end, (3) 45° end insulator, (4) 135° end insulator

From the above field plots, it is evident that the shape of the insulator has a significant effect on the field stress near the triple junction. For the flat end insulator (1), the field stress near the triple junction is around 0.75kV/m. For the insulator with hemispheric end with 2.5mm radius (2), the field stress near the triple junction is around 4.46kV/m. For the insulator with the 45°angle of contact (3) with metal shield have a field stress near the triple junction around 2.68kV/m. And finally for the insulator with 135° angle of contact (4) with metal shield, the field stress near the triple junction is around 0.30kV/m.

In addition, based on the experiments done by Yamano et.al [50], it is proved that the direction of electric lines of force with respect to the insulator surface influences the Secondary Electron Emission Avalanche (SEEA). They stated that if the electric field lines are parallel to the insulator surface near the triple junction, the electrons emitted from the cathode triple junction are inclined to develop a SEEA along the insulator surface. On the other hand, when the electric field

lines are perpendicular to the insulator surface near the triple junction, the electrons generated from the triple junction are unable to develop a SEEA. So, the electric lines of force are plotted for the above four models to see their direction with respect to the surface of the insulator.

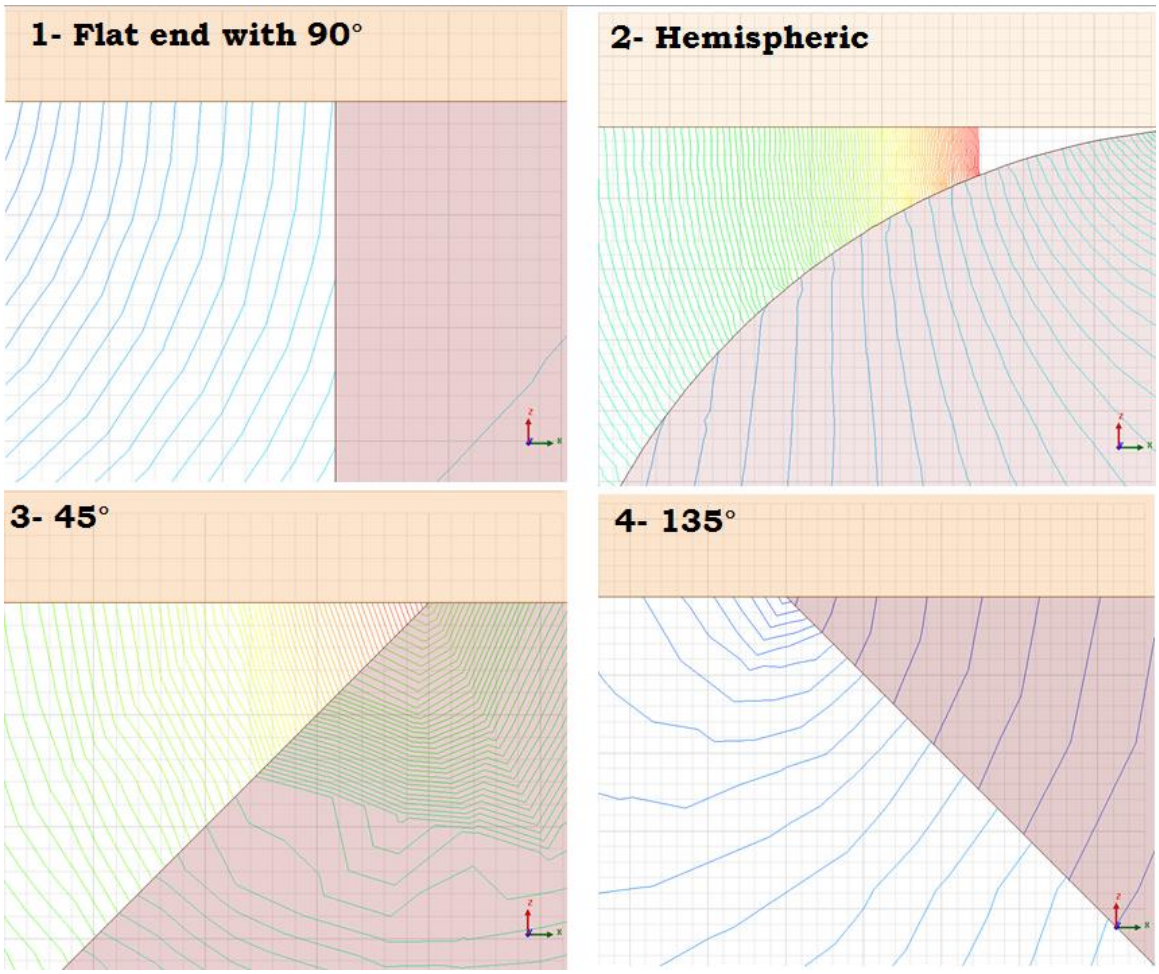


**Figure 5.17** Direction of the electric field lines with respect to insulator surface

From the figure 5.17, it can be observed that for the insulator shape (1) the field lines are almost parallel to the insulator surface which let the electrons develop a SEEA. For the insulators (2) and (3), the field lines are of slant nature. But, since the field stress at the triple junction for these two models is comparatively very high, the number of ejected electrons will be more. These electrons, due to the direction of field lines, may not develop a SEEA but create a large negatively charged area. Whereas for the insulator shape (4), the field lines are almost perpendicular to the surface and since the field stress is very low at the triple junction, the number of ejected electrons can be either zero or very small.

Figure 5.18 (a) shows the image of an assumed electron hopping mechanism on the surface of the insulator which is responsible for initiating SEEAs. The same concept is applied to a typical insulator with angle of contact of 45° with metal shield and the insulator with angle of contact of 135° with metal shield as shown in the figure 5.18 (b) and (c) respectively. θp is the angle with

which the electron is emitted. Based on the figure 5.13 and the equation 1, it is clear that as θp increases, the primary electron collision energy $E_i$ decreases. From the triple junction arrangements of 45° and 135°, it can be assumed that the angle θp of 135° triple junction arrangement can be larger than that of 45° arrangement.

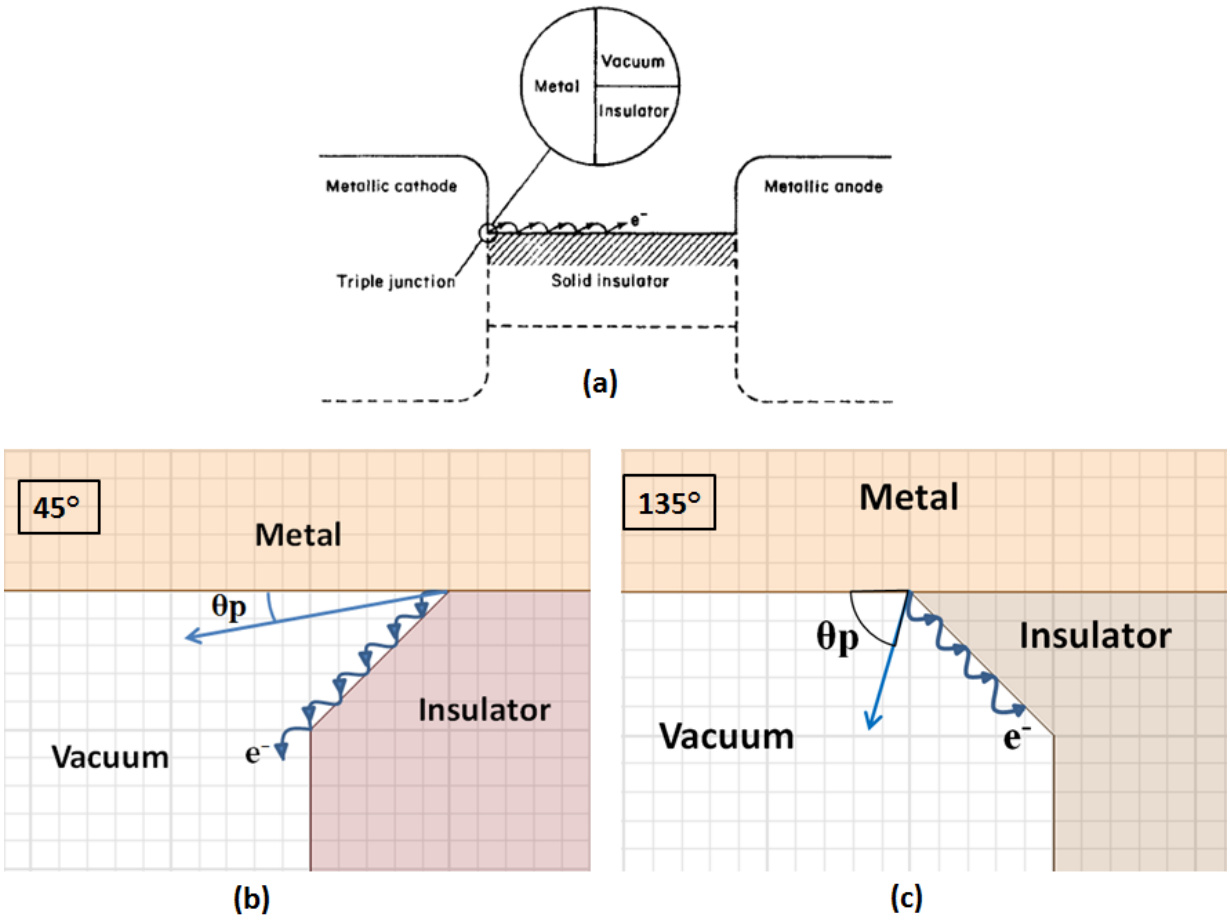


**Figure 5.18** (a) Electron hopping mechanism that may leads to SEEA, (b) assumed hopping mechanism for 45° arrangement, (c) assumed hopping mechanism for 135°arrangment

Based on the above discussions the following points are clear. (1) For 45° arrangement, since the electric field intensity at the triple junction is high the electron emits with comparatively large amount of energy and with θp being small, the collision energy will be high. In addition the electric field lines are not exactly perpendicular to the insulator surface which all together leads to a secondary electron emission that has a potential to create a discharge. (2) On the other hand, for 135° arrangement, the electric field intensity at the triple junction is very low and the electron emitted from the junction (if emits) will have very less amount of energy and with θp being comparatively large, the collision energy will be low. Further, the electric field lines are perpendicular to the insulator surface which ceases the electron emission process and may avoid the surface discharge making the 135 ° arrangement as an optimized solution to avoid triple junction emissions.

## 5.4 Metal Inserts

Another effective way to reduce the field stress at the triple junction is by using metal inserts at both ends of the insulator. Trump and Cook [51] used metal inserts for post insulators in $SF_6$ gas and found that the electric field stress has been considerably reduced at the areas of metal inserts. Nitta et.al [52] had also performed flashover measurements on cylindrical insulators with metal inserts in $SF_6$ gas. In our research, the influences of metal inserts with different depths in insulators in vacuum are studied. Ceramic insulator of 45° and 135° angles of contact are used to study the influence. Figures 5.18 and 5.19 shows the arrangement of metal inserts of different depths in a 45° insulator and a 135° insulator. In both cases the width of the ceramic is 6mm and the width of the metal insert is 4mm. The height of metal inserts is varied form 0.5mm to 2mm.

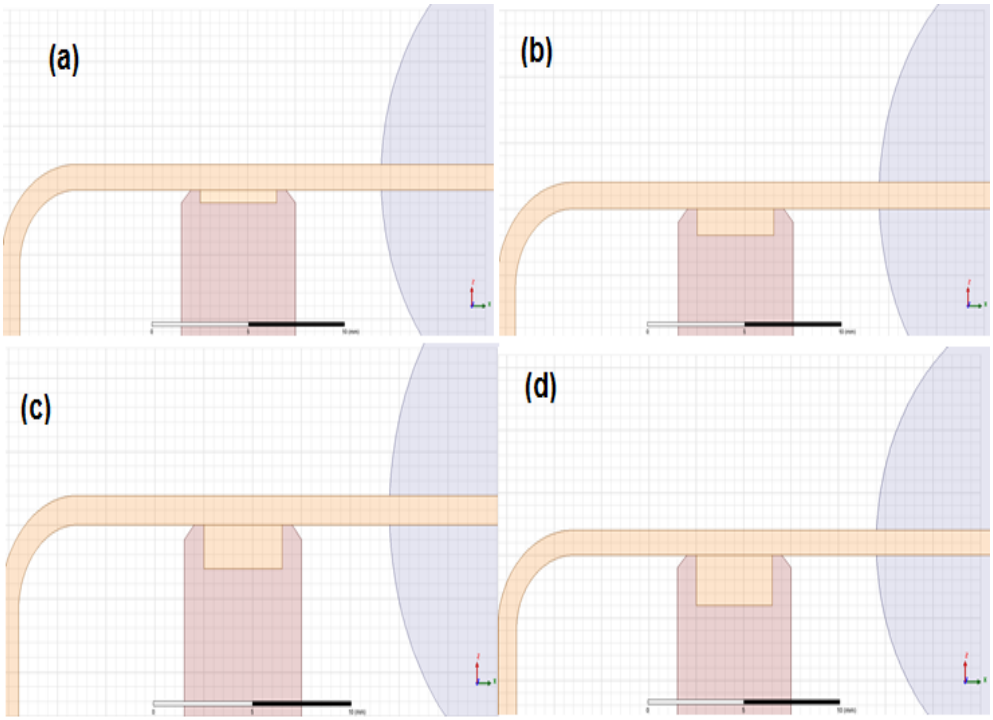


**Figure 5.19** 45° ceramic insulator with metal inserts of (a) 0.5mm deep, (b) 1mm deep, (c) 1.5mm deep and (d) 2mm deep

For all models, the upper shield is excited with 0V and the bottom metal shield is excited with 100V. Electric field values along the inner surface of the insulator starting from the cathode triple junction to the anode triple junction are plotted in a graph for each model. All these graphs are then compared with each other to observe the influence of metal inserts as well as their depths on the field stress at the triple junctions. Figure 5.20 shows the graphs for a 45° ceramic insulator and figure 5.21 shows the graphs for a 135° ceramic insulator. It is clear from the graphs that the metal inserts at the both ends of the insulator have reduced the field stress at the triple junctions at the inner side of the insulators. As the height of the metal insert increases, the stress at the triple junction decreases.

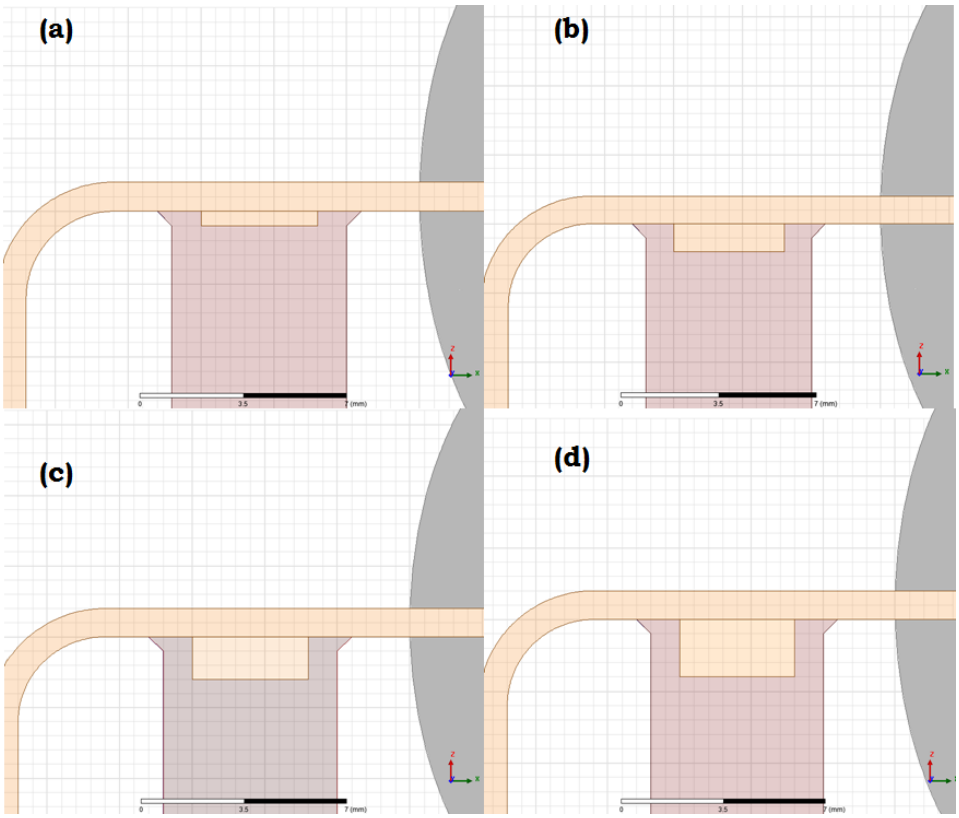


**Figure 5.20** 135° ceramic insulator with metal inserts of (a) 0.5mm deep, (b) 1mm deep, (c) 1.5mm deep and (d) 2mm deep

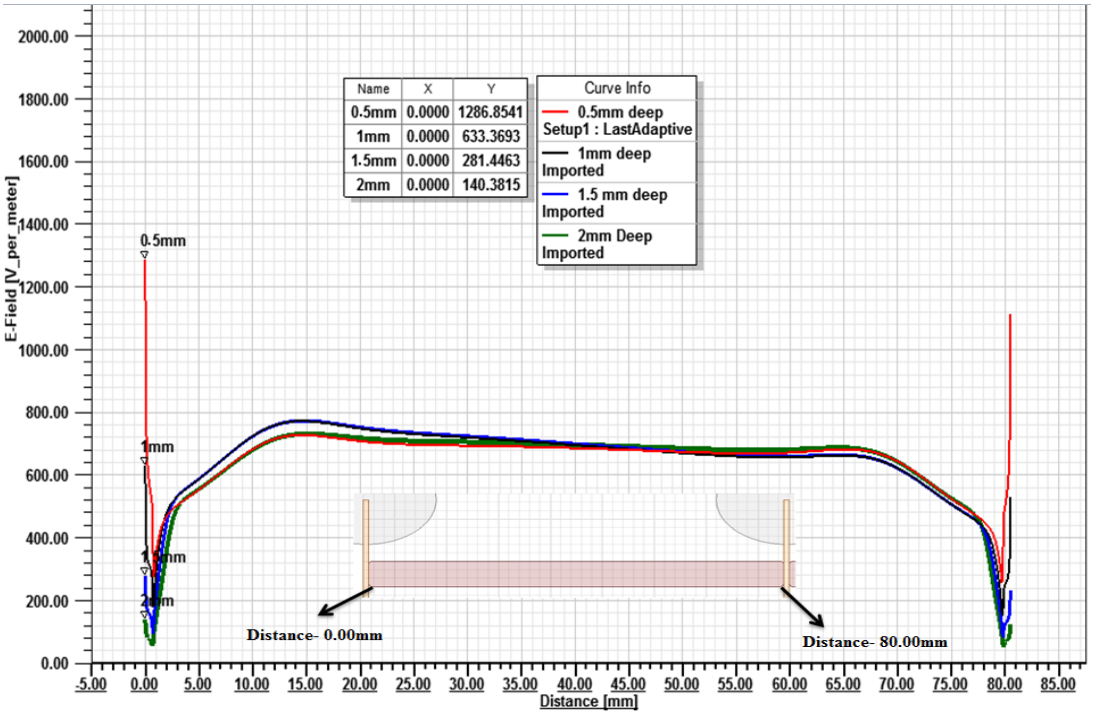


**Figure 5.21** Electric field values across the surface of the insulator of 45° with different metal inserts

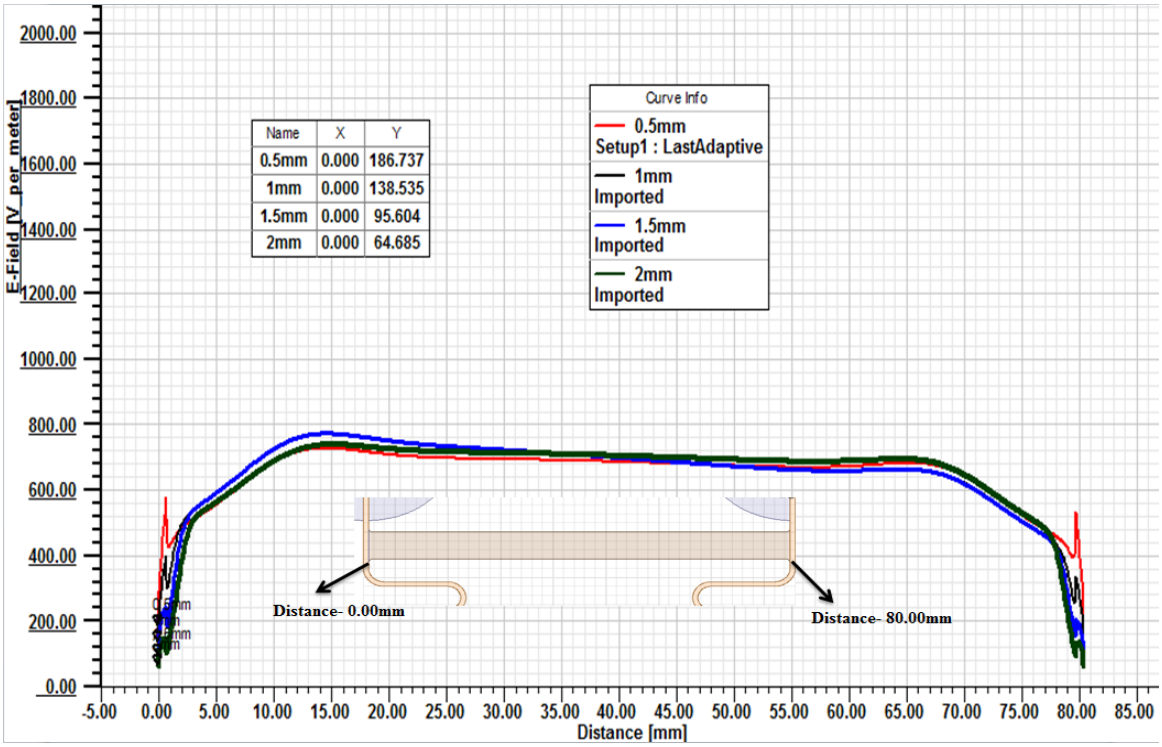


**Figure 5.22** Electric field values across the surface of the insulator of 45° with different metal inserts

Table 5.1 shows the comparison of the influence of the metal inserts for 45° insulator and 135° insulator.

| **Depth of Metal Insert** | **E-Field at CTJ for Insulator** | |
|---|---|---|
| | **45°** | **135°** |
| Without Metal Insert | 1.78kV/m | 0.19kV/m |
| With metal insert of 0.5mm deep | 1.29kV/m | 0.19kV/m |
| With metal insert of 1mm deep | 0.63kV/m | 0.14kV/m |
| With metal insert of 1.5mm deep | 0.28kV/m | 0.10kV/m |
| With metal insert of 2mm deep | 0.14kV/m | 0.06kV/m |

**Table 5.1** Comparison of electric field at the Cathode Triple Junction (CTJ) with respect to the depth of metal inserts

From the above discussions, it is clear that using a grading ring will reduce the stress at the outer edges of the metal shields. The shape and the distance of the rings to the insulator have a considerable effect on the field stress at the outer triple junction. When it comes to the inside of the insulator, the shape of the insulator at the triple junction and placing the metal inserts have a considerable effect on the field stress at the CTJs. By implementing these parameters, the high field stress at the critical zones A and B of Figure 5.1 can be reduced.

## 5.5 Height of the Metal Shields

In order to observe the dielectric strength at zone C of figure 5.1 i.e. insulation of shield to the insulator, the length of metal shield is assumed as one of the influencing parameters. As the length of the metal shield increases, the distance between two metal shields decreases. Four different models have been built with the distance between metal shields decreasing from 53mm to 23mm by increasing the length of the metal shield. The geometrical arrangements of these four models are shown in figure 5.22. The model (a) has the shortest metal shields with a distance of 53mm between the shields. The model (d) has the longest metal shields with a distance of 23mm between the shields. For all the models, the upper metal shield is excited with 0V and the bottom metal shield is excited with 100V. All the models are built with 45° insulator. The electric field plots of the four models can be seen in the figure 5.23. From the plots, it can be observed that the overall field strength increases gradually with decrease in distance between the shields. In addition to the overall field strength, the field strength on the surface of the insulator is also plotted as shown in the figure 5.24. From the plots it is clear that as the distance between the metal shields decreases, the field stress on the insulator surface especially near the metal shield curvature increases.

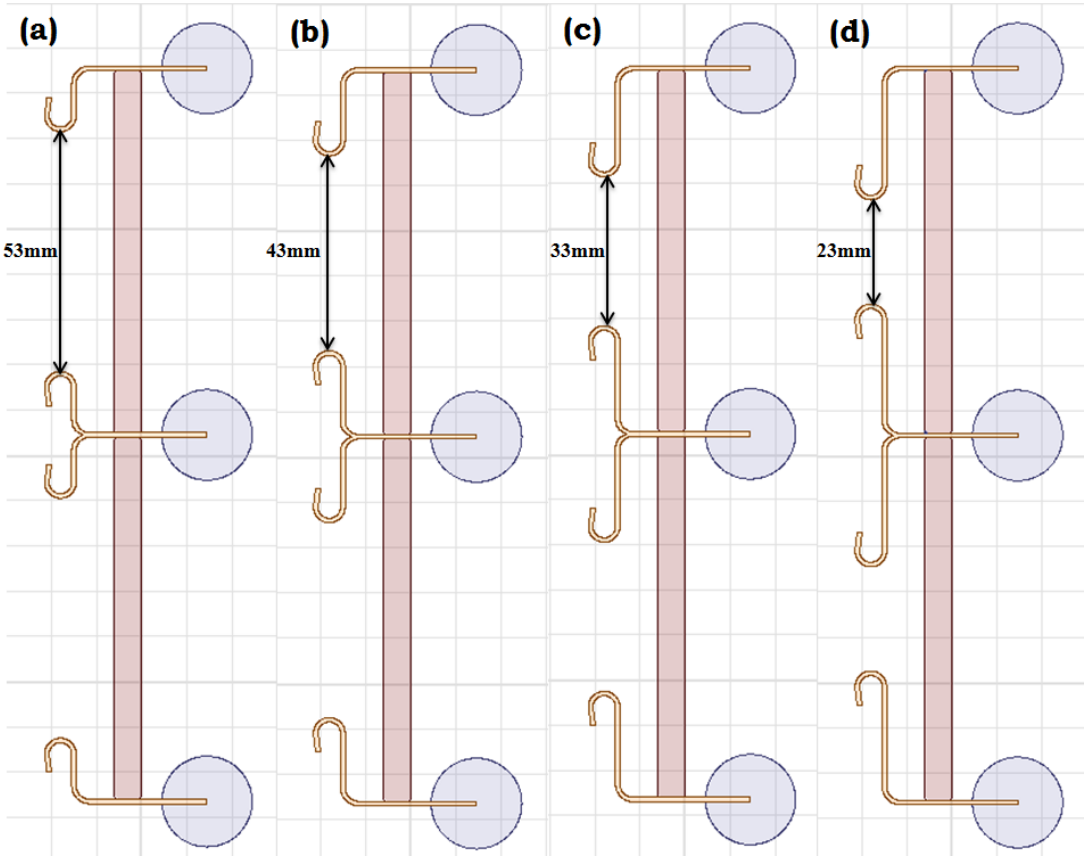


**Figure 5.23** Different distances between metal shields (a) 53mm, (b) 43mm, (c) 33mm and (d) 23mm

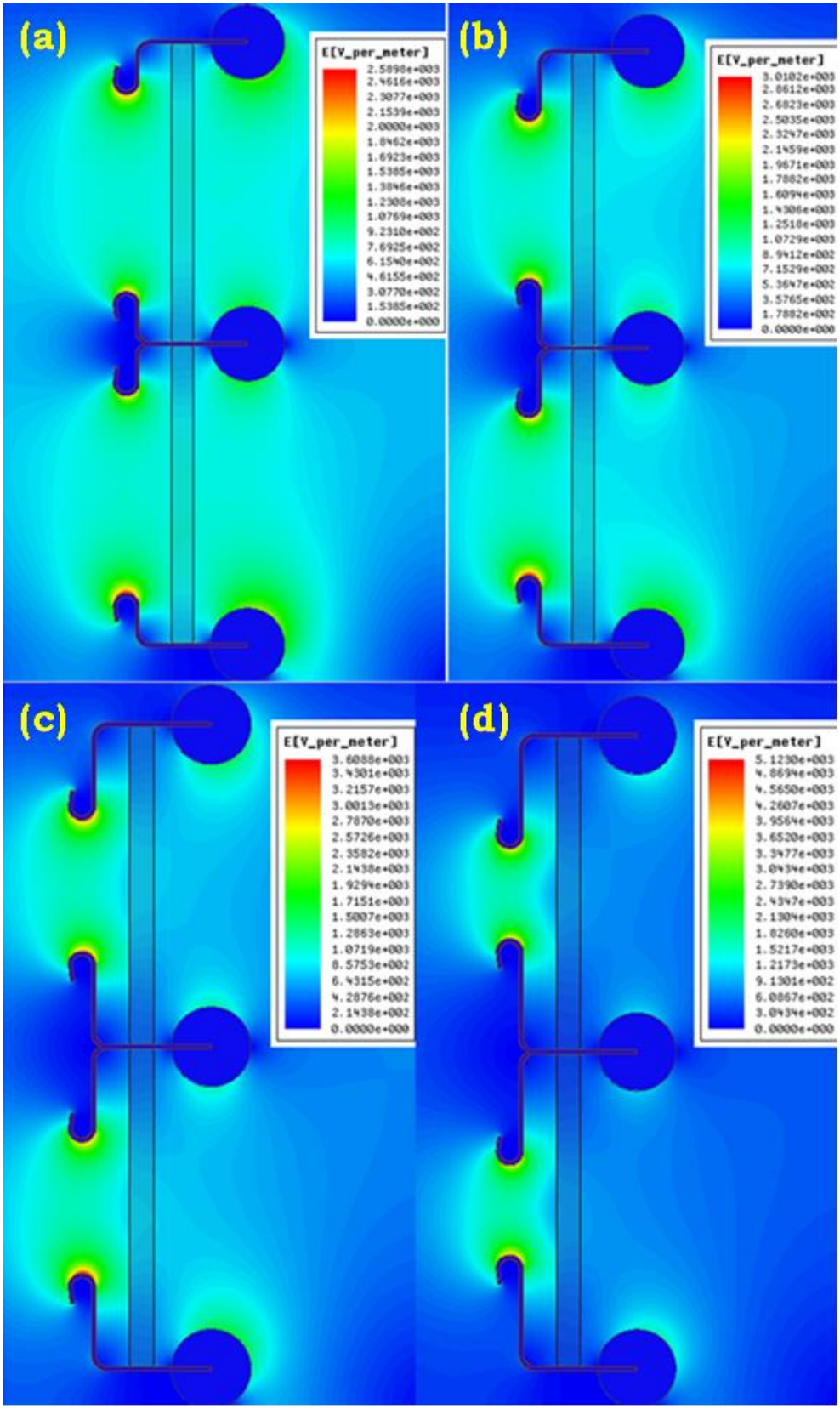


**Figure 5.24** Electric field plots of models with different distances between the metal shields

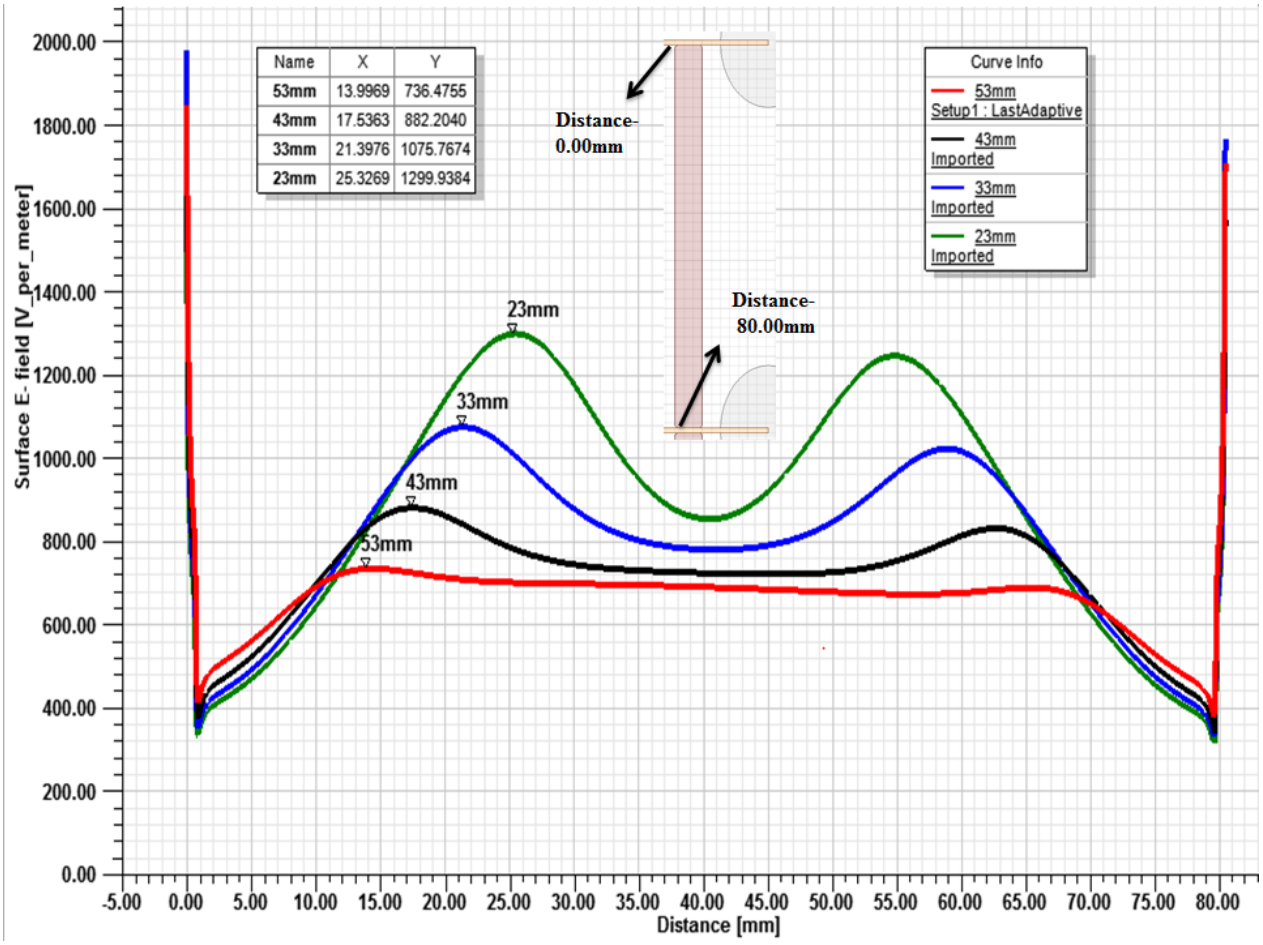


**Figure 5.25** Electric field values across the surface of the insulator with different distances between metal shields

Table 5.2 gives the information about the overall electric field strength and also the maximum stress on the insulator surface for each model.

| Distance between the metal shields | Maximum field stress (on the shield curvature) | Maximum field stress on the insulator surface |
|---|---|---|
| Distance of 53mm | 2.59kV/m | 0.74kV/m |
| Distance of 43mm | 3.01kV/m | 0.88kV/m |
| Distance of 33mm | 3.60kV/m | 1.10kV/m |
| Distance of 23mm | 5.12kV/m | 1.30kV/m |

**Table 5.2** Dependence of surface field stress and maximum field strength in the model on the distance between the metal shields

Based on the above values, it is implicit that as the height of the metal shield increases, the overall field strength and the field stress on the insulator surface increases. In the following section, the influence of the distance between metal shield and the insulator is studied.

## 5.6 Distance Between the Metal Shield and the Insulator

In addition to the height of metal shield, the distance between the metal shield and the insulator is also assumed to be of the parameters that influence the insulation between shield and insulator. So in order to observe the influence, four different models are built with the distance between metal shield and the insulator changed from 5mm to 2mm. The geometrical arrangements of the four models are shown in the figure 5.25. All the models are excited similar to the other parameters i.e. 0V at the top metal shield and 100V at the bottom metal shield. The electric field plots are also plotted and shown in the figure 5.26. The electric field plots show that the overall electric field is not significantly affected by the change in distance. But if we see the graphs of electric field values along the surface of the insulator from figure 5.27, it is clearly visible that the field stress on the surface increases with decrease in distance between the shield and the insulator.

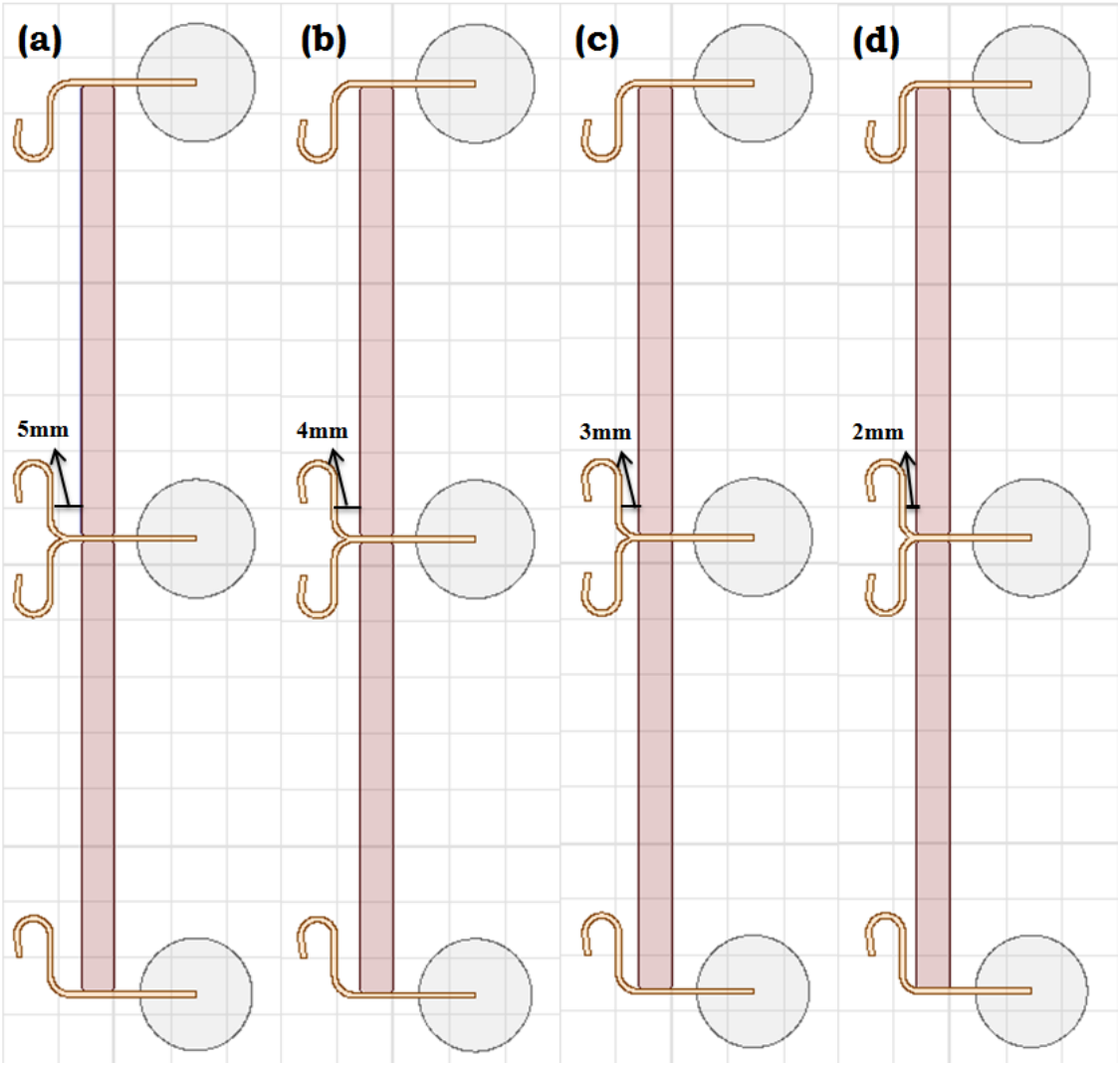


**Figure 5.26** Different distances between the metal shield and the insulator (a) 5mm, (b) 4mm, (c) 3mm and (d) 2mm

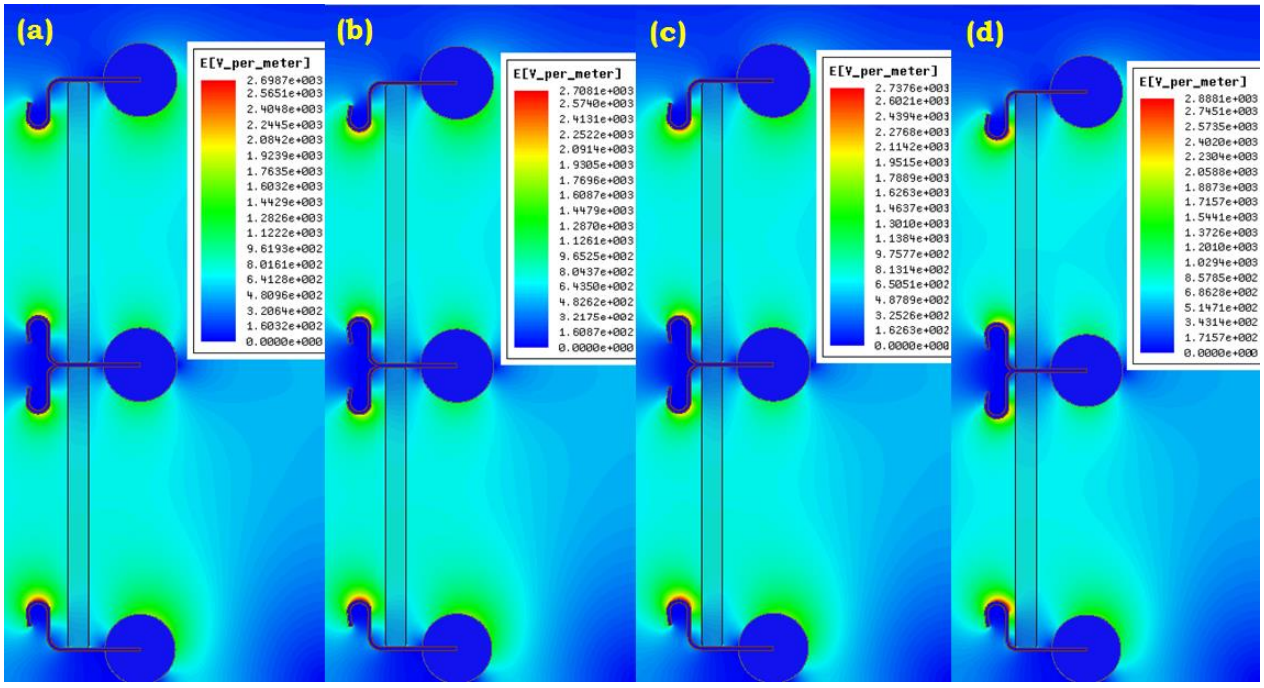


**Figure 5.27** Electric field values across the surface of the insulator with different distances between the metal shield and the insulator

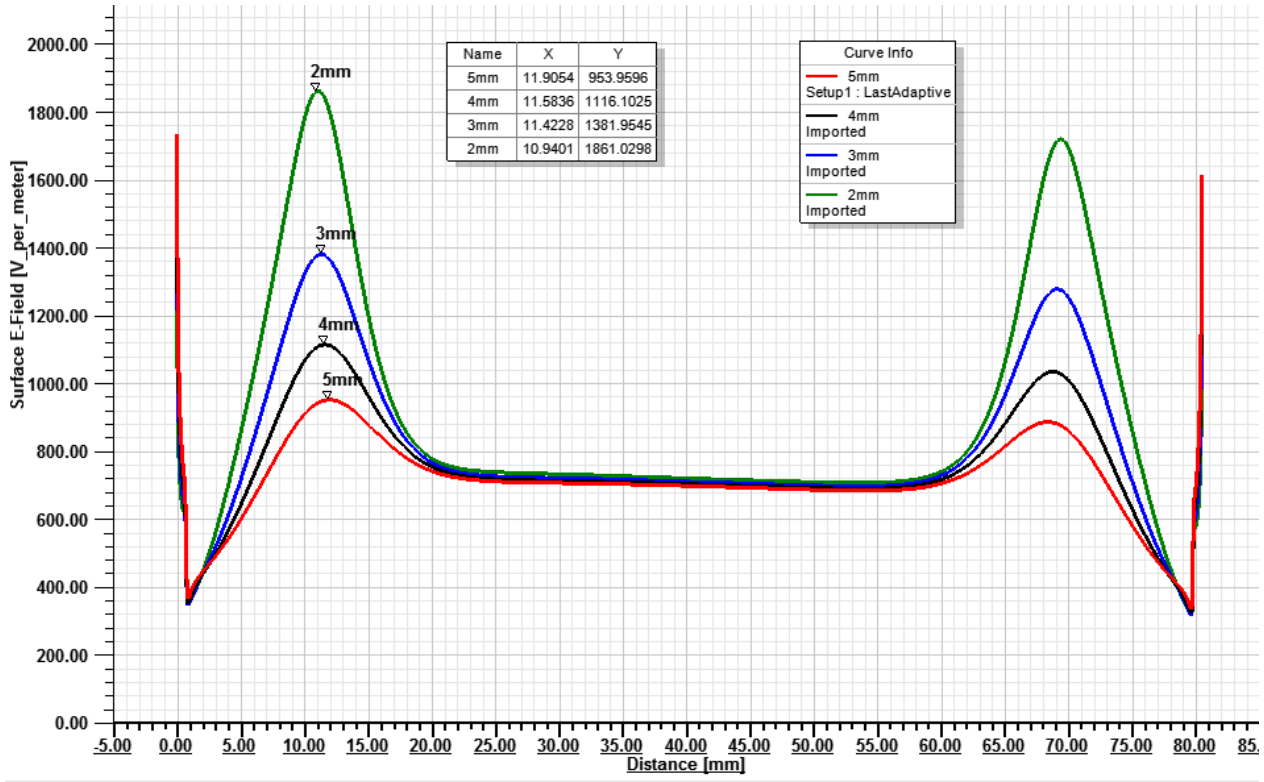


**Figure 5.28** Electric field values across the surface of the insulator with different distances between the metal shield and the insulator

The maximum field stress on the insulator surface and the overall field strength of the each model is shown in table 5.3.

| **Distance between the metal shield and Insulator** | **Maximum field stress (on the shield curvature)** | **Maximum field stress on the insulator surface** |
|---|---|---|
| 5mm | 2.69kV/m | 0.95kV/m |
| 4mm | 2.71kV/m | 1.12kV/m |
| 3mm | 2.74kV/m | 1.38kV/m |
| 2mm | 2.88kV/m | 1.86kV/m |

**Table 5.3** Dependence of surface field stress and maximum field stress in the model on the distance between the metal shield and the insulator

From all the above parameters and their simulation results, it is evident that these parameters influence the field stress at the critical zones. In the following chapter, simulations were done with the conditions close to the real interrupter model and the optimized dimensions of the interrupter tube are suggested.

# Chapter 6

# SIMULATIONS WITH CONDITIONS CLOSE TO A REAL INTERRUPTER TUBE

Various parameters that influence the withstand voltage of the interrupter tube are explained in chapter 5. But those simulations are carried out to observe the influence of variation in those parameters, but the realistic conditions such as the effect of contact rod, the effect of potential distribution over the metal shields, threshold limit of electric field stress values for different dielectric mediums and the diameter of the interrupter tube are not considered. In the current chapter, the simulations are done by taking these conditions into account.

The effects of contact rod and the potential distribution over the metal shields are considered by designing two different models namely Model A and Model B in Ansys Maxwell as shown in the figure 6.1. In Model A, the contact rod is applied with 0V, upper metal shield is applied with 0V and the bottom metal shield is applied with 81.25kV. For Model B, the contact rod is applied with 0V, upper metal shield is applied with 81.25kV and the bottom metal shield is applied with 162.5kV. The above values were derived based on the situation that the rated lightning impulse withstand voltage is applied across the 72.5kV rated interrupter which is in open state and it is assumed that the movable contact is at ground potential, i.e. 0V, and the fixed contact is at high potential i.e. 325kV. Since the interrupter is in the open state, the potential distribution across each metal shield varies. Each variation of Model A and Model B is simulated by taking the effect of fixed contact rod (diameter of 40mm) and movable contact rod with bellows (diameter of 70mm) separately.

The basic idea behind the consideration of the two models A and B was that the optimum geometries for the two cases will be different especially in the situation of optimizing the tube´s diameter. In the case of model A, it is possible to get a more compact optimum design than in the case of model B. If the both models A and B are combined, that is similar to the geometry in chapter 5, one will have an interface between two ceramic blocks with different diameter which makes it impossible to apply grading rings and the inner shield at the interface. This problem can be avoided by using the same diameter for ceramics of model A and B. But then the field stress will be lower in the model A, and that makes the optimization solely dependent on model B. So to overcome these problems, model A and model B are simulated independently in order to determine the individual optimization potential and to reduce the computation time.

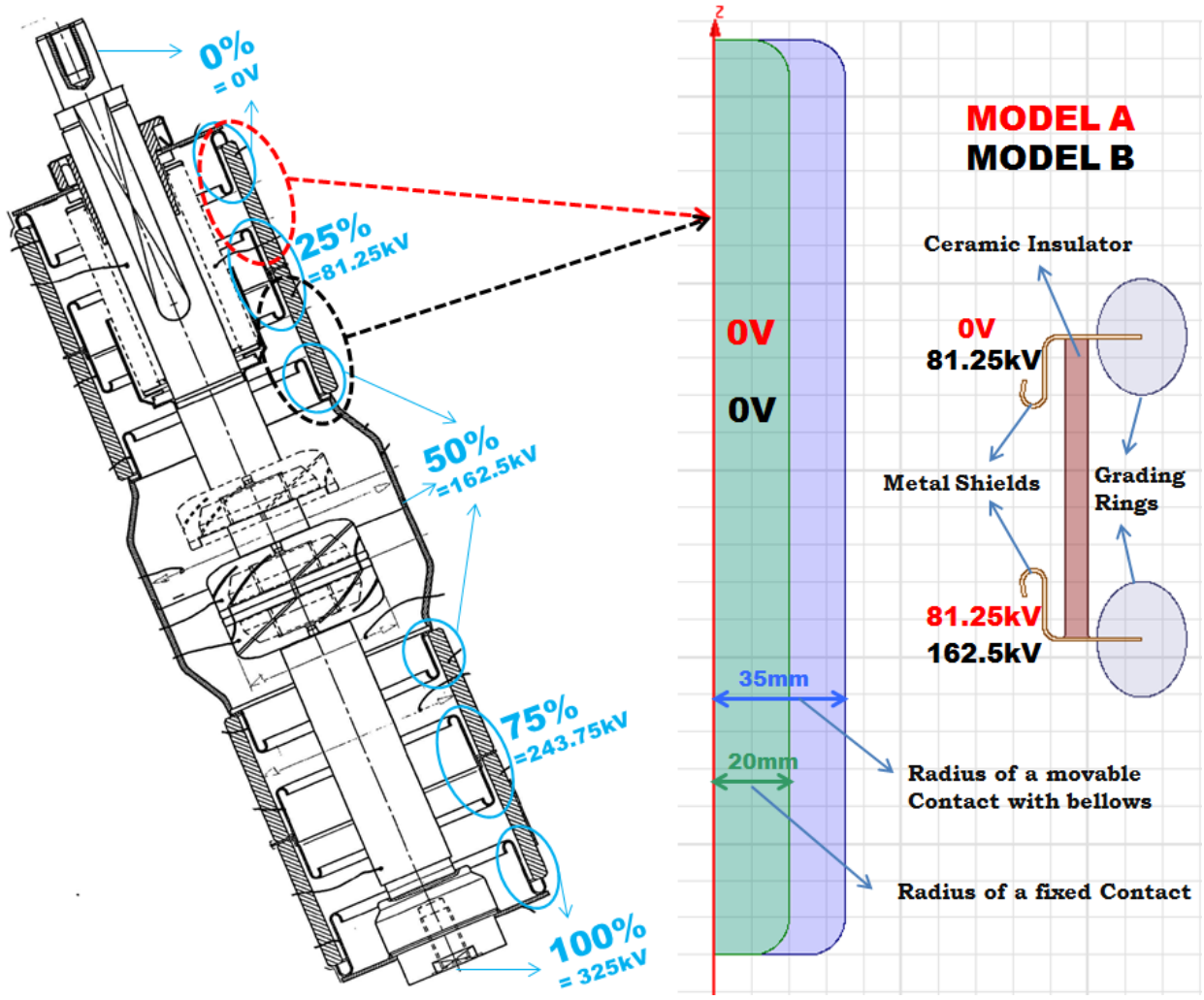


**Figure 6.1** Prototype of a simulation arrangement of two models with different excitation voltages [45]

Using this new arrangement, the parameters like insulator shape, metal inserts, shape of the grading rings, distance between the insulator and the contact rod and the shape of metal shield curvature are simulated. Table 6.1 explains all the variations that are simulated with different parameters in context of model A and model B. The designs of 45° insulator and 135° insulator are same as the ones that are showed in figure 5.15

| Parameters/ Insulator Shape/ Radius of contact rod | Model A | | | | Model B | | | |
|---|---|---|---|---|---|---|---|---|
| | 45° Insulator | | 135° Insulator | | 45° Insulator | | 135° Insulator | |
| | 35mm | 20mm | 35mm | 20mm | 35mm | 20mm | 35mm | 20mm |
| Metal inserts | ☑ | ☑ | ☑ | ☑ | ☑ | ☑ | ☑ | ☑ |
| Grading rings | ☑ | ☑ | ☑ | ☑ | ☑ | ☑ | ☑ | ☑ |
| Tube inner radius | ☑ | ☑ | ☑ | ☑ | ☑ | ☑ | ☑ | ☑ |
| Shape of metal Shield | | | | | | | ☑ | |

**Table 6.1** Different parameters that are simulated with Model A and Model B

## 6.1 Threshold Values of the Influencing Parameters

Once the two models are designed, the following threshold values of the electric field at different areas in the vacuum interrupter are assigned. All these values are assumed based on the literature survey and from the discussions with engineers at Siemens AG.

### 6.1.1 Nitrogen Gas (Outside)

Generally the gap between the interrupter tube and the outer insulator is filled with dielectric gas as showed in figure 3.2 (b). The length of the interrupter tube is generally smaller than the length of the outer insulator which means the gap between the metal enclosures of the interrupter tube is smaller than the gap between the metal enclosures of the outer insulator. In order to withstand the voltage level outside the interrupter tube, an insulating gas of certain pressure is used. One of the frequently used pressurized gases is sulfur hexafluoride ($SF_6$) because of its high dielectric properties. But in the context of global warming effect, the SF6 is considered as one of the most aggressive gas. So the gases like dry air, nitrogen ($N_2$), carbon dioxide ($CO_2$) are considered as a possible substitute. The relative breakdown voltages of these insulating gases are compared with each other to select the gas dielectric in the gap between the interrupter and the outer housing and given in table 6.2.

| Gas | Formula | Breakdown voltage relative to air | Global Warming Potential (GWP) |
|---|---|---|---|
| Sulfur hexafluoride | $SF_6$ | 3.0 | 22800 |
| Nitrogen | $N_2$ | 1.15 | - |
| Air | - | 1 | - |
| Carbon dioxide | $CO_2$ | 0.95 | 1 |

**Table 6.2** Relative breakdown voltages of insulating gases at 1atm [53]

Based on the breakdown voltage, nitrogen gas is considered as the dielectric medium between interrupter tube and outer housing.
Further, the dielectric strength of the nitrogen gas is calculated in order to get the threshold value. From table 6.2 and reference [54], it is derived that the dielectric strength of $SF_6$ is 2.4-2.7 times the dielectric strength of $N_2$. Table 6.3 shows the breakdown voltages of $N_2$ gas relative to $SF_6$

| Pressure (bar) | BDV* of $SF_6$ | Relative BDV of $N_2$ ($SF_6$/2.7) |
|---|---|---|
| 1 | 8.6kV/mm | 3.18kV/mm |
| 2 | 16.1kV/mm | 5.96kV/mm |
| 3 | 21.8kV/mm | 8.07kV/mm |
| 4 | 26.8kV/mm | 9.92kV/mm |

*Breakdown Voltage

**Table 6.3 Break down voltages of N2 in relation with SF6 at different pressure levels (10mm gap)**

A pressure of 4 bars is considered as an optimum pressure because at this pressure the bellows can function effectively without having high mechanical stress on them. So the breakdown voltage of 9.92kV/mm is considered as a threshold value outside the interrupter tube. By keeping this value as reference, the shapes of the field grading rings are changed in order to achieve a compact design of the circuit breaker.
From section 5.1, it is observed that grading rings of elliptical shape with less distance from the ceramic insulators had reduced the field stress at the triple junction. Keeping this elliptical shape as a reference, the vertical radius and horizontal radius of the grading rings are changed and simulated. Figure 6.2 shows the different variations of the grading rings.

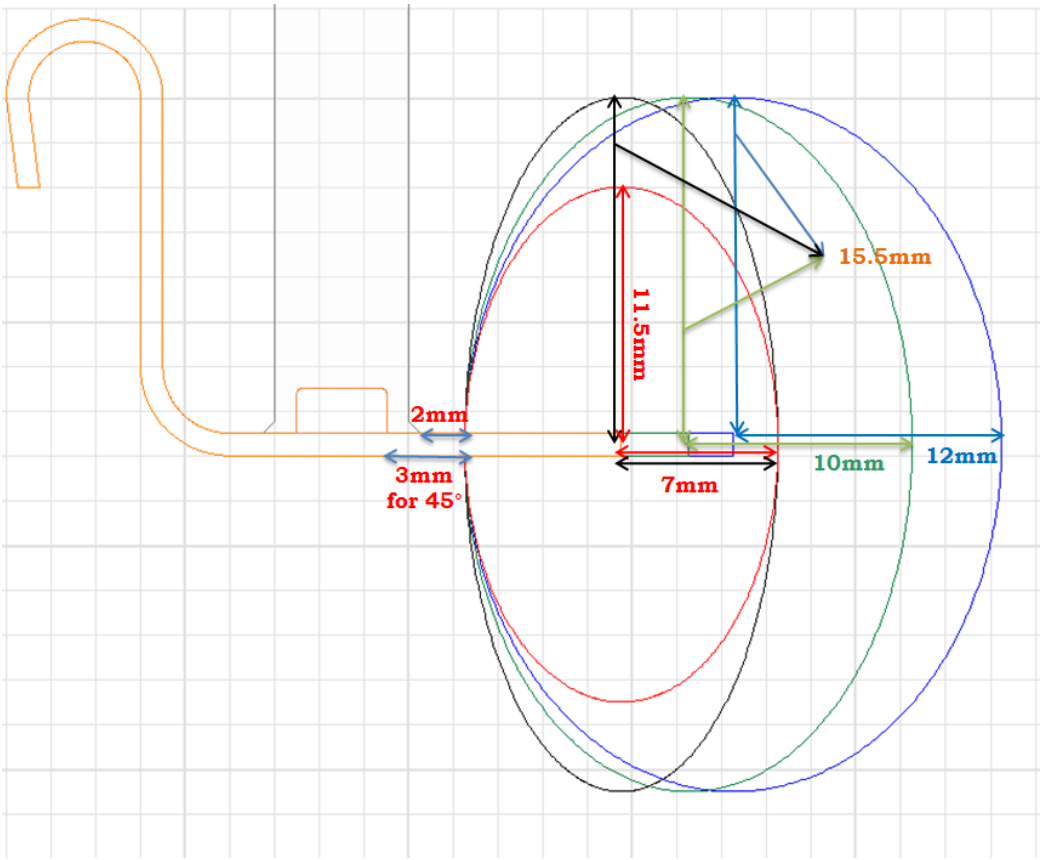


**Figure 6.2** Field grading rings of elliptical shape with different vertical and horizontal radius

All the above variations are simulated with the arrangement of Model A and Model B with metal inserts of 2mm at both ends of the insulator, contact rod of different radius and with the insulators with contact angles of 45°and 135° (figure 5.15). The field values at the cathode triple junction as well as around the grading rings are given in table 6.4.

By observing these field values of all the variations from the table 6.4, the maximum field stress around the ring was 4.57kV/mm which is below the threshold value of N2 i.e. 9.95kV/mm. Based on the dimensions of the rings, the grading ring of 7mm horizontal radius and 11.5mm vertical

radius is selected as an optimum shape. The above dimensions reduce the material cost as well as the outer diameter of the interrupter tube and still have the field stress below the threshold value.

| **Parameter - Field Grading Ring** | **Model A** | | | | **Model B** | | | |
|---|---|---|---|---|---|---|---|---|
| | **45° Insulator** | | **135°Insulator** | | **45° Insulator** | | **135°Insulator** | |
| | **20mm** | **35mm** | **20mm** | **35mm** | **20mm** | **35mm** | **20mm** | **35mm** |
| **E-Field at the CTJ (Outside) kV/mm** | | | | | | | | |
| H-12mmV-15.5mm | 0.137 | 0.134 | 0.040 | 0-040 | 0.130 | 0.120 | 0.037 | 0.035 |
| H-10mmV-15.5mm | 0.134 | 0.132 | 0.039 | 0.038 | 0.126 | 0.118 | 0.037 | 0.036 |
| H-7mmV-15.5mm | 0.127 | 0.124 | 0.038 | 0.036 | 0.120 | 0.113 | 0.033 | 0.032 |
| H-7mmV-11.5mm | 0.145 | 0.142 | 0.044 | 0.043 | 0.137 | 0.127 | 0.039 | 0.037 |
| **$E_{max}$ around the ring (kV/mm)** | | | | | | | | |
| H-12mm V-15.5mm | 2.76 | 2.81 | 2.76 | 2.81 | 2.94 | 3.08 | 2.94 | 3.08 |
| H-10mmV-15.5mm | 3.07 | 3.13 | 3.07 | 3.13 | 3.29 | 3.46 | 3.29 | 3.46 |
| H-7mmV-15.5mm | 3.86 | 3.95 | 3.86 | 3.95 | 4.18 | **4.57** | 4.18 | **4.57** |
| H-7mmV-11.5mm | 3.17 | 3.26 | 3.17 | 3.26 | 3.51 | 4.21 | 3.51 | 4.21 |

CTJ- Cathode Triple Junction, H-Horizontal radius, V-Vertical radius, $E_{max}$-Maximum E field

**Table 6.4** E-field at CTJ and around the grading ring with different elliptical shapes

## 6.1.2 Triple junctions & Ceramic Insulator

As explained before, triple junction is one of the most critical areas in the interrupter where the initiation of the surface flashover takes place. So the design suggestions like the shape of the insulator and metal inserts were suggested. Before simulating these design parameters with new models, the threshold value for the electric field at the triple junction should be known in order to compare the improvement of field stress at these areas. Based on the literature by Latham [19], Miller [23] and Slade [55], the maximum allowable electric field at the triple junction varies from 1kV/mm to 2kV/mm. For the simulations in this section, the value of 1kV/mm is considered as the threshold limit. Insulator shape and the metal inserts were used to reduce the electric field at the triple junction to a value below the mentioned threshold value.

### *6.1.2.1 Insulator Shape:*

Insulators with 45° and 135° angle of contact with metal shields are simulated with an arrangement that is shown in figure 6.1. Each model is simulated separately with 35mm radius contact rod and 20mm radius contact rod. Field stress at the triple junction for all the models

were calculated and compared. But the field stress at the exact point of triple junction is unreal and the values obtained at this point are not true values. So in order to get the true values, the mesh at the region of triple junction is intensified. The following figures 6.3 and 6.4 will explain the influence of the mesh on the field stress at the triple junction and the point where the stress values can be considered as true values.

Figure 6.3 shows the normal default mesh for a 45° insulator of Model A near the vicinity of the cathode triple junction. The zoomed version shows three points where the field stress is measured. The point m1 is very close to the triple junction and the field stress at this point is 2.302kV/mm. The point m2 is just 0.003mm away from point m1 and the field stress at this point is 2.252kV/mm. The point m3 is 0.015mm away from m2 and the field stress is 1.996kV/mm. To obtain realistic field values, there should be at least 10 mesh cells between the measuring point and the actual triple junction and 3 to 4 cells between the measuring point and the ceramic surface. But in this case all these three points are just inside one mesh cell.

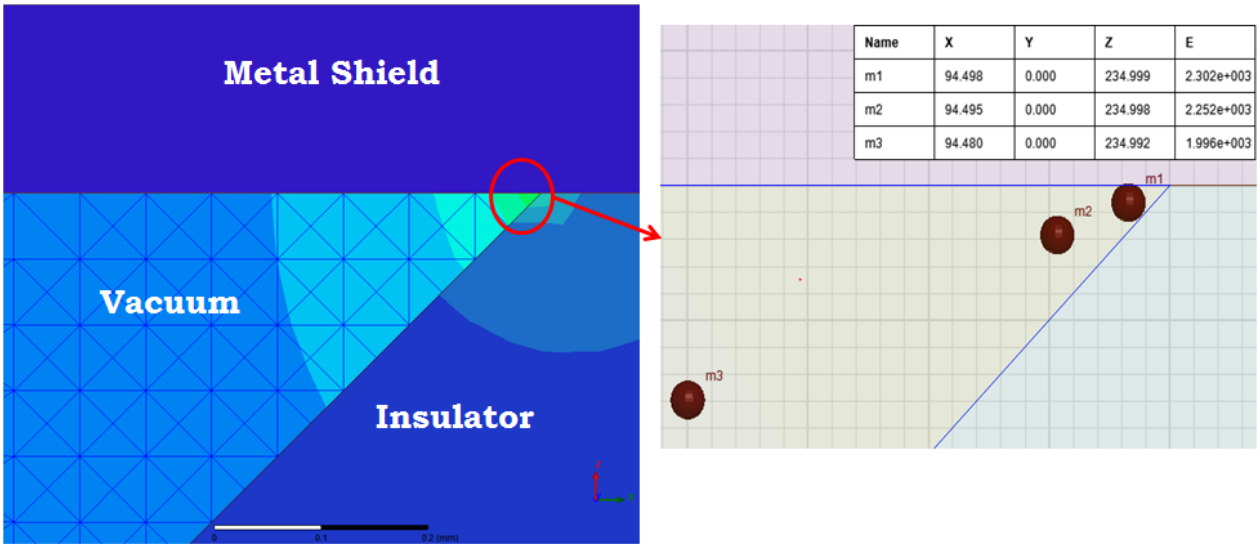


| Name | X | Y | Z | E |
|---|---|---|---|---|
| m1 | 94.498 | 0.000 | 234.999 | 2.302e+003 |
| m2 | 94.495 | 0.000 | 234.998 | 2.252e+003 |
| m3 | 94.480 | 0.000 | 234.992 | 1.996e+003 |

**Figure 6.3** Field stresses near the cathode triple junction with a default mesh

On the other hand figure 6.4 shows the intensified mesh for the same 45°insulator of Model A near the cathode triple junction. It is clearly visible that the number of mesh cells near the triple junction is more when compared to figure 6.3. The zoomed version shows the same three points as of figure 6.3 and the field stress is measured at these points. The field stress at m1 is 3.904kV/mm, m2 is 3.008kV/mm and at m3 it is 2.049kv/mm. Since there are more than 10 mesh cells between point m3 and the triple junction, the value at m3 is considered as realistic.

In the current section, any values that are mentioned as the field stress at the triple junction are measured at a point where there are at least 10 mesh cells between the measuring point and the triple junction. Similarly the field stress along the ceramic surface is measured along a line that is drawn with at least 4 cells away from the surface.

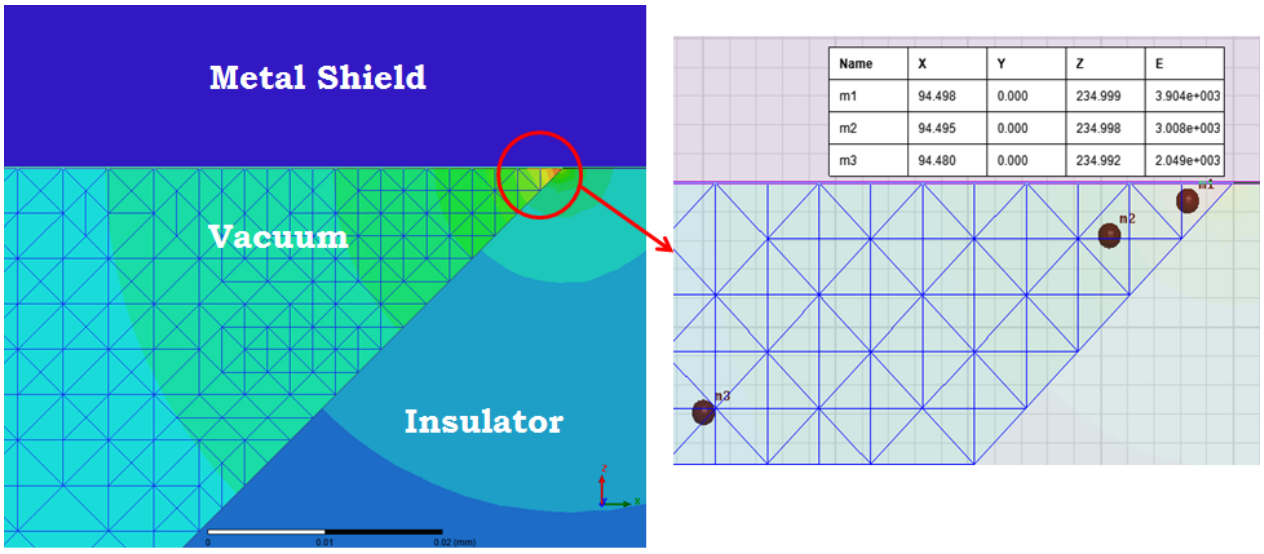


**Figure 6.4** Field stresses near the cathode triple junction with a refined mesh

Table 6.5 gives the values of field stress near the cathode triple junctions of both insulator shapes with the contact rods of different radius and different excitation voltages.

| **Insulator Shape** | **Model A** | | **Model B** | |
|---|---|---|---|---|
| | **20mm** | **35mm** | **20mm** | **35mm** |
| 45° Insulator | **2.08kV/mm** | **2.05kV/mm** | **1.95kV/mm** | **1.83kV/mm** |
| 135° Insulator | 0.22kV/mm | 0.22kV/mm | 0.21kV/mm | 0.19kV/mm |

**Table 6.5** Electric field stress near cathode triple junctions of two insulator shapes

The electric field plots of 45° Insulator and 135° insulator in Model B with a contact rod of 35mm radius are shown as an example in figure 6.5. In addition the electric field values across the surface of the insulator starting from cathode triple junction (CTJ) to anode triple junction (ATJ) are also shown in the figure 6.6.

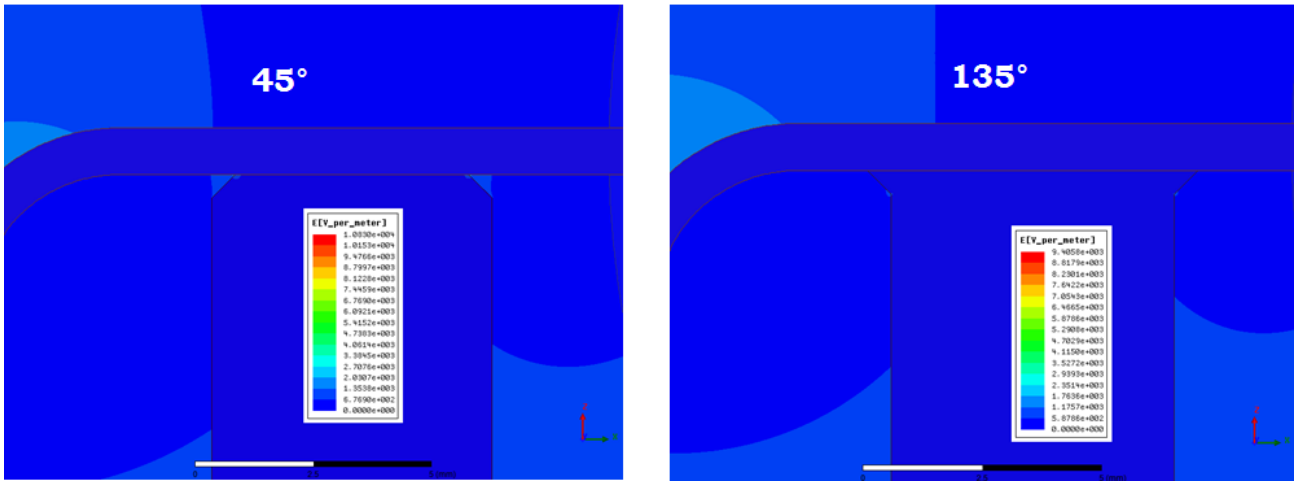


**Figure 6.5** Electric field plots of the insulators with 45° and 135° angles of contact with shields

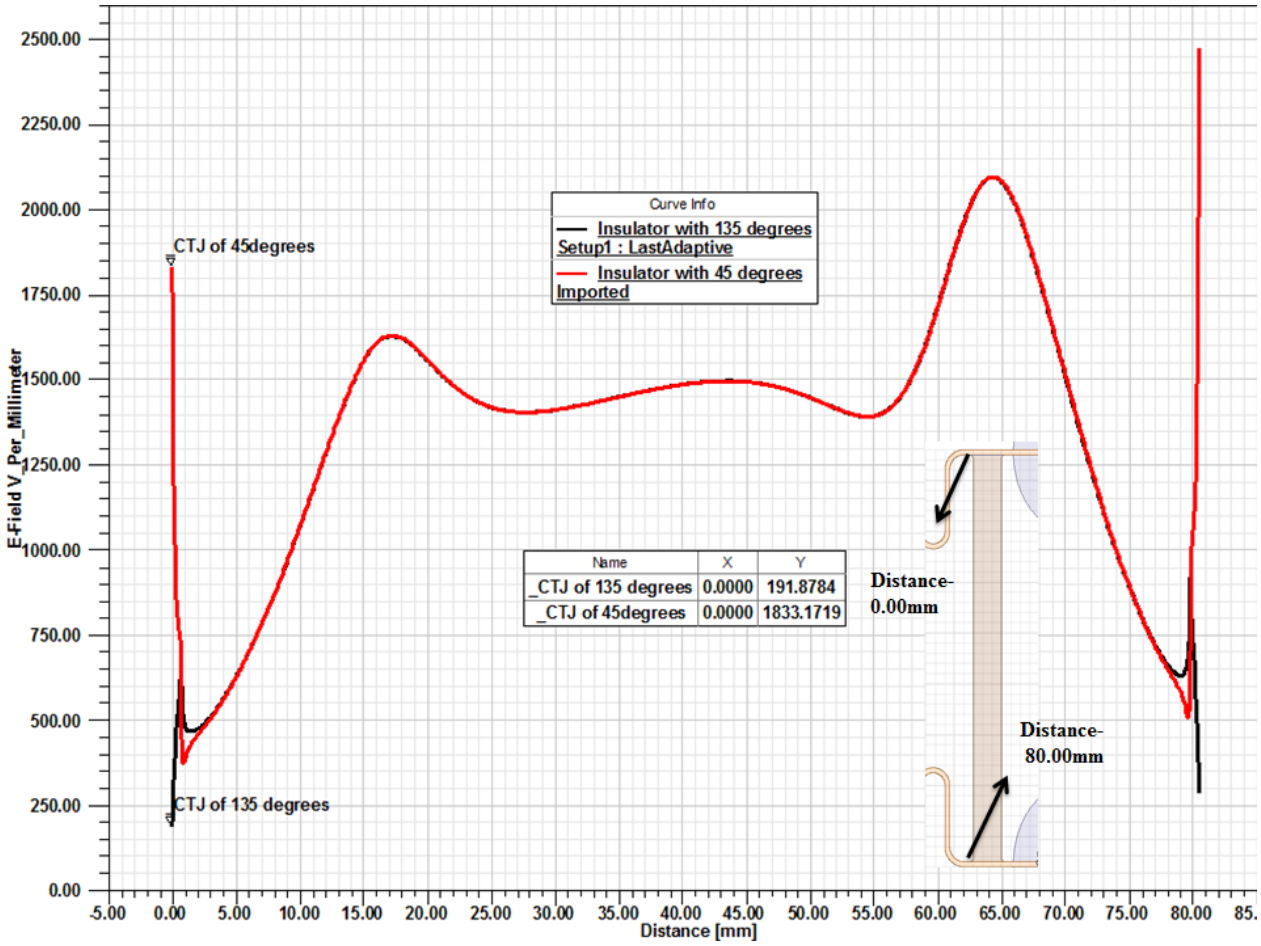


**Figure 6.6** Electric field values along the surface of the insulator from CTJ to ATJ

The field values from the table 6.5 and from figure 6.6 show that the field stress values near the triple junction of 45° insulator are higher than the threshold value of 1kV/mm stress at triple junction. For the 135° insulator, the field values are below the threshold value.

### *6.1.2.2 Metal Inserts:*

In addition to the insulator shape, metal inserts are used to further reduce the field near the triple junctions. Metal parts are inserted at the both ends of the insulator to a certain depth, and that results in the field reduction at the triple junctions. As the metal parts are inserted into the insulator, a higher field stress at the corners of metal parts inside the insulator can lead to volume breakdown. So before inserting the metal parts, the volume breakdown strength of $Al_2O_3$ ceramics must be determined. After referring to the data sheets of possible ceramic suppliers [56] [57], the average volume dielectric strength of the ceramic insulator ranges from 8.5kV/mm to 10kV/mm. The electric field at the corners of the metal inserts are calculated and presented in table 6.6 and it is made sure that the values are less than the range of volume dielectric strength of ceramics. In addition, some of the experiments done at CERN and by another scientists [58]

[59] [60] [61] have suggested that the maximum electric field for the discharge inception on the surface of the alumina ceramics is in the range of 7kV/mm to 13kV/mm (parallel field). In the following simulations an average value of 10kV/mm is considered as a threshold value for the electric field on the surface of the ceramic insulators.

The arrangement of the insulators with metal inserts as shown in figures 5.18 and 5.19 are simulated and their respective electric field distributions were observed. Figure 6.7 and 6.8 show the electric field values across the insulator surfaces starting from the cathode triple junction to the anode triple junction with the depths of metal inserts varying from 0.5mm to 2mm. These graphs are plotted for the insulator shapes of 45° and 135° of model B with 35mm radius contact rod.

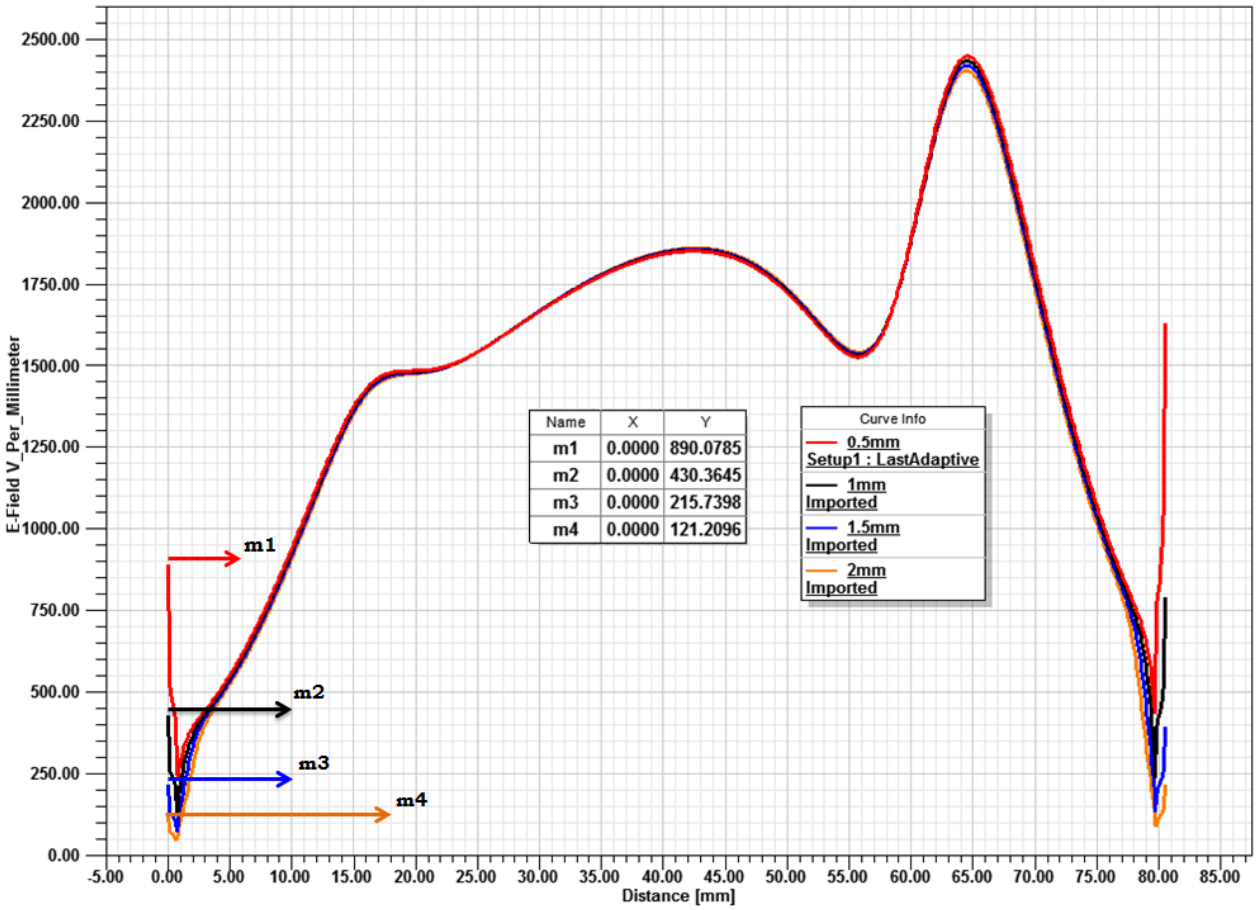


**Figure 6.7** Electric field values across the surface of the insulator of 45° shape with metal inserts of different depths

In figure 6.7, the electric field stress at the cathode triple junction can be seen as 0.89kV/mm for 0.5mm deep metal insert (a), 0.43kV/mm for 1mm deep metal insert (b), 0.22kV/mm for 1.5mm deep metal insert (c) and finally 0.12kV/mm for 2mm deep insert (d). If we compare these results with the 45°insulator without metal inserts, the field stress has been reduced from 2.47kV/mm to 0.12kV/mm.

Similarly in figure 6.8, the electric field at the cathode triple junction of a 135° insulator with metal insert of 0.5mm is 0.179kV/mm, with metal insert of 1mm deep is 0.125kV/mm, with

metal insert of 1.5mm deep is 0.084kV/mm and with 2mm metal insert is 0.057kV/mm. Now it can be said that the electric field at the triple junction without metal insert i.e. 0.29kV/mm is reduced to 0.057kV/mm by the presence of a metal insert of 2mm deep.

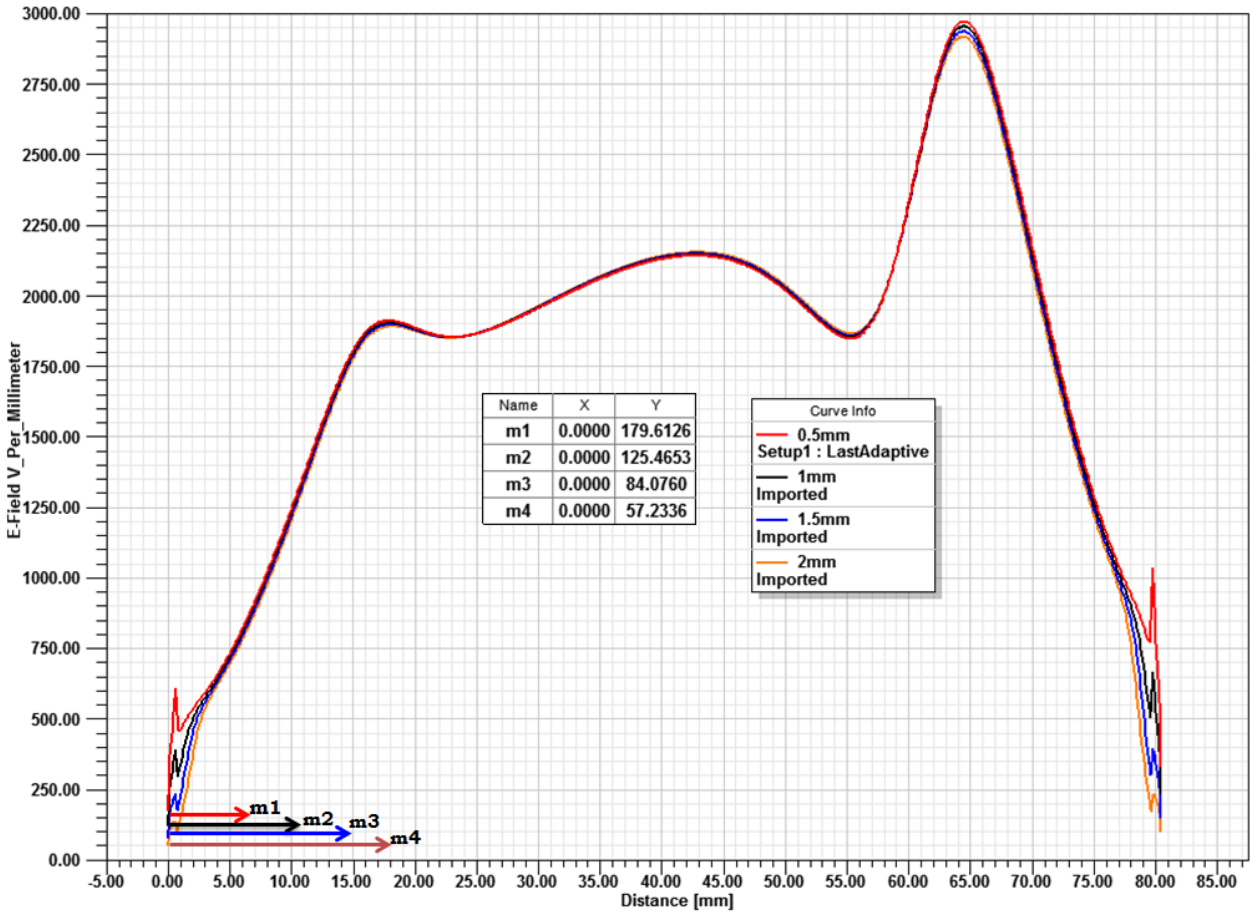


**Figure 6.8** Electric field values across the surface of the insulator of 135° shape with metal inserts of different depths

Further, both the insulators are simulated with the arrangement of model A and model B with a 2mm deep metal insert and the contact rods of different radius. The field stress at the triple junctions as well as the field stress near the corner of the metal insert inside the insulator are calculated for the models and tabulated in table 6.6.

| Parameter- Metal Insert (2mm deep) | Model A | | | | Model B | | | |
|---|---|---|---|---|---|---|---|---|
| | 45° Insulator | | 135°Insulator | | 45° Insulator | | 135°Insulator | |
| | 20mm | 35mm | 20mm | 35mm | 20mm | 35mm | 20mm | 35mm |
| E-Field at the Cathode Triple Junction | 0.144 kV/mm | 0.142 kV/mm | 0.054 kV/mm | 0.053 kV/mm | 0.134 kV/mm | 0.127 kV/mm | 0.049 kV/mm | 0.049 kV/mm |
| Maximum E-field at the corner of the metal insert | 1.077 kV/mm | 0.798 kV/mm | 0.975 kV/mm | 0.846 kV/mm | 1.140 kV/mm | 1.163 kV/mm | 0.869 kV/mm | 1.039 kV/mm |

**Table 6.6** E-field values at cathode triple junction and at the corner of metal insert.

When comparing the average volume dielectric strength of ceramic, the field stress values at the corner of metal inserts for all the models are less and cannot lead to a breakdown inside the insulator.

So from the tables 6.5 and 6.6, it is evident that the insulator of 135° angle of contact with a 2mm deep metal inserts can completely avoid the field emission from the triple junctions.

### 6.1.3 Copper/ Stainless Steel Shields

As explained in chapter 2, the vacuum interrupter is equipped with metal shields in order to avoid the metal vapor deposition on the ceramic surface inside the interrupter tube. These metal shields also help in uniform potential distribution inside the interrupter. Coming to the type of material to be used for these metal shields, Copper (Cu) and Stainless Steel (St-St) are ideal materials. But based on the experiments from the reference [62], the usage of Stainless Steel shield showed an improvement of breakdown voltage in the range of 15 to 40% when compared with Copper. So theoretically Stainless steel is a better choice for the shields. But when it comes to production process, especially during brazing, Stainless Steel has problems when compared with copper. During the brazing process, the shields are backed up to 800°C and the cooled down. After cooling down, it is observed that the stainless steel shield that is in contact with insulator is strained and becomes brittle. On the other hand, copper is soft and get glued to the insulator perfectly. Also, by looking into the statement from the reference [63] "The surfaces of the both rings electrodes are cleaned with emery cloth (grade 1000) before the tests are conducted. After the surfaces have been prepared with the emery cloth the copper rings are etched in a bath for 90 s to remove any micro-protrusions. The surfaces of the stainless steel ring electrodes are electro polished with a current density of 1kA/m2. Preconditioning of the electrodes through the application of a power frequency voltage before ascertaining the dielectric strength by means of lightning impulse voltages is not employed." which clearly suggests that the Cu shield and St-St shields are preconditioned with different methods which might have the effect on breakdown voltages especially on St-St shields which are treated in a much better way. In addition the emission voltage of Cu and St-St is in the same order of magnitude which again suggests that the improvement in breakdown voltages of St-St is mainly due to the better preconditioning process than Cu. So by considering the above statements Cu shields are considered as optimized metal shields inside the vacuum interrupter.

Based on the statements and results from the literature [63] [64] [62], the maximum electric field strength on surface of the copper that leads to an electron emission varies from 17 to 22kV/mm depending up on the type of preconditioning. Keeping this range as threshold, the diameter of the interrupter tube as well as the changes to the shield curvatures are suggested as following.

### *6.1.3.1 Diameter of the interrupter tube:*

In order to reduce the cost and size of the interrupter tube, the dimensions of the interrupter tube should be as small as possible. Of all the dimensions, the diameter of the interrupter tube is one of the parameters that can be reduced and result in a small sized interrupter. The only way to reduce the diameter of the tube is by reducing the distance between the center rod and the ceramic insulator. Figure 6.9 shows the possible variations in the distance between the center rod and the ceramic insulator by taking the both contact rods of 20mm and 35mm radius into account.

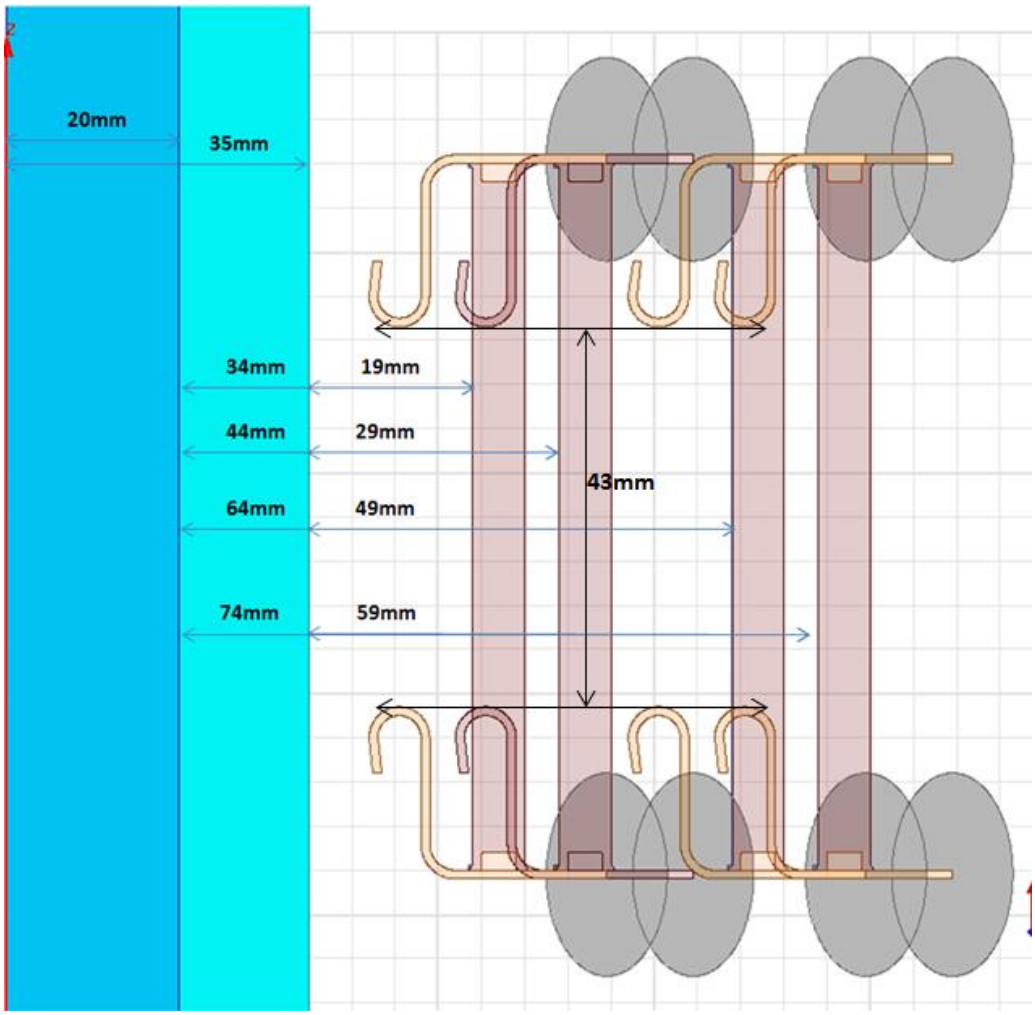


**Figure 6.9** Different distances from the insulator to the contact rod

From the figure it can be seen that the distance of 74mm between the insulator and the contact rod of 20mm radius is the longest. The distance of 19mm between the insulator and the contact rod of 35mm is the shortest. The distance between the shields is kept as 43mm. All those arrangements were simulated and the results were presented in the table 6.9. The values from the table suggest that as the distance between the insulator and the contact rod decreases, the field stress on the surface of the Cu shield increase especially for the designs of Model B with 29mm and 19mm distance. The values that are given in red are the values that are more than the

threshold field value of Cu surface. In order to have a compact design, the distance between the insulator and the contact rod should be as small as possible which is19mm in this case. The figure 6.10 shows the field plots of the Model A and Model B with 19mm distance and 135° shaped insulator to give an idea about the field distribution inside the interrupter.

| **Distance between the insulator and the contact rod** | **Model A** | | **Model B** | |
|---|---|---|---|---|
| | **45° Insulator** | **135°Insulator** | **45° Insulator** | **135°Insulator** |
| | **$E_{max}$ on the Cu Shield** | **$E_{max}$ on the Cu Shield** | **$E_{max}$ on the Cu Shield** | **$E_{max}$ on the Cu Shield** |
| **With the contact rod of 20mm radius** | | | | |
| 74mm | 5.11 kV/mm | 5.11 kV/mm | 7.78 kV/mm | 7.78 kV/mm |
| 64mm | 5.30 kV/mm | 5.30 kV/mm | 7.80 kV/mm | 7.80 kV/mm |
| 44mm | 5.80 KV/mm | 5.80 kV/mm | 9.46 kV/mm | 9.46 kV/mm |
| 34mm | 7.98 kV/mm | 7.98 kV/mm | 17.48 kV/mm | 17.48 kV/mm |
| **With the contact rod of 35mm radius** | | | | |
| 59mm | 5.49 kV/mm | 5.49 kV/mm | 9.23 kV/mm | 9.45 kV/mm |
| 49mm | 5.83 kV/mm | 5.83 kV/mm | 10.58 kV/mm | 10.52 kV/mm |
| 29mm | 10.97 kV/mm | 10.97 kV/mm | **21.66 kV/mm** | **21.66 kV/mm** |
| 19mm | **26.88 kV/mm** | **26.88 kV/mm** | **53.72 kV/mm** | **53.72 kV/mm** |

**Table 6.7** E-field on the surface of the Cu shield and contact rod with respect to the changes in distance between the insulator and the contact rod.

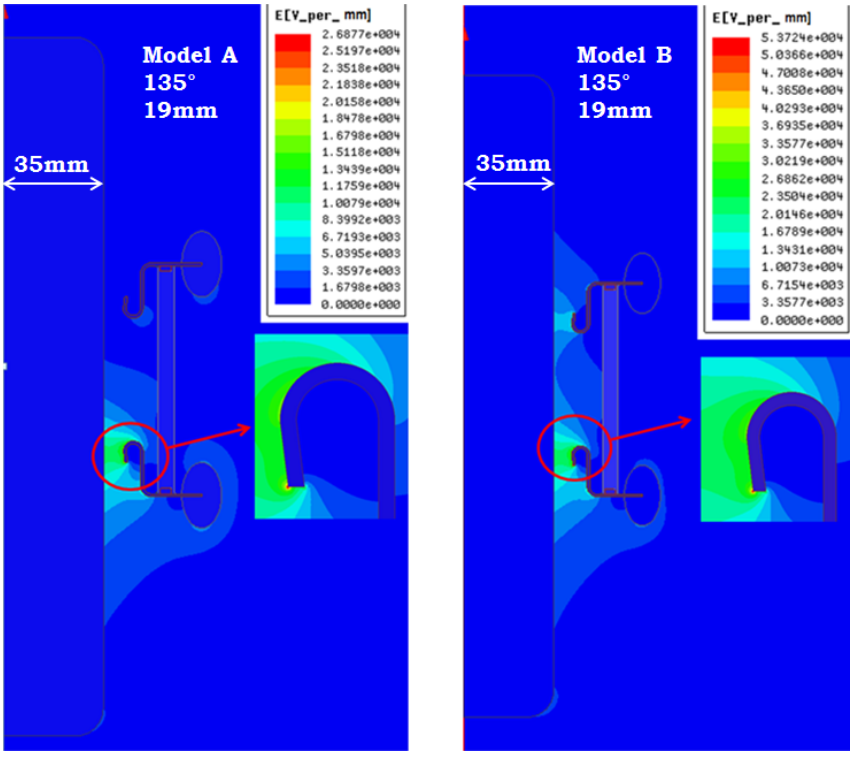


**Figure 6.10** Electric field distribution near the surface of the Cu shield for Model A and B with 19mm distance

The field plots of figure 6.10 shows that the high field stress is concentrated on the curvature of the Cu shield especially at the tip of the shield. For the both model A and Model B of figure 6.10, the stress is higher on the shields with higher potential i.e. 81.25kV for Model A and 162.5kV for model B. So in order to reduce the high field stress on these shield curvatures, geometrical modifications have to be made to these curvatures and the field stress has to be maintained in the range of the threshold values by keeping the 19mm distance.

### *6.1.3.2 Metal shield curvatures:*

Making appropriate geometrical variations can reduce the high field stress at the curvatures. In this research, various geometrical shapes of the Cu shields of Model B (135° insulator and the contact rod of radius 35mm) with 19mm distance between insulator and contact rod are proposed and simulated. From the figure 6.10, it is clear that the bottom metal shield which was applied with higher potential (162.5kV for Model B) is highly stressed when compared with the upper metal shield with lower potential (81.25kV for Model B). So in the following sections, changes are made to the bottom metal shield to reduce the higher field stress on its surface and the same changes can be applied to the upper metal shield later.

#### 6.1.3.2.1 Original Structure:

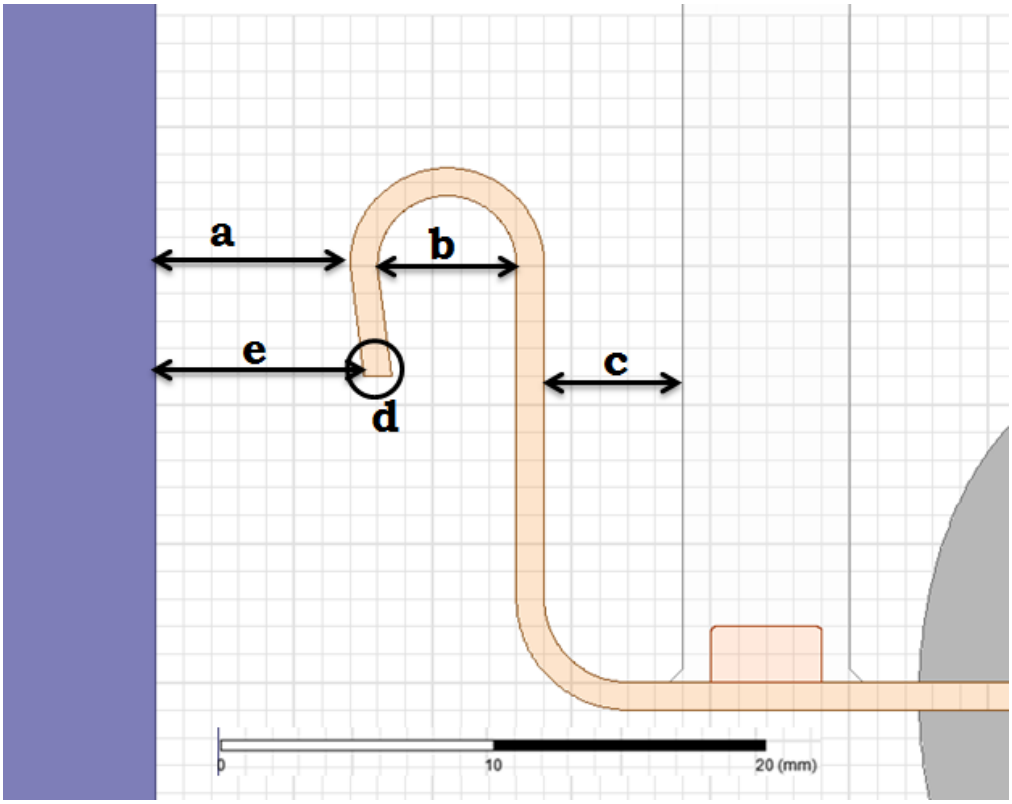


**Figure 6.11** Geometrical arrangement of original shield structure with changeable parameters a, b, c, d and e

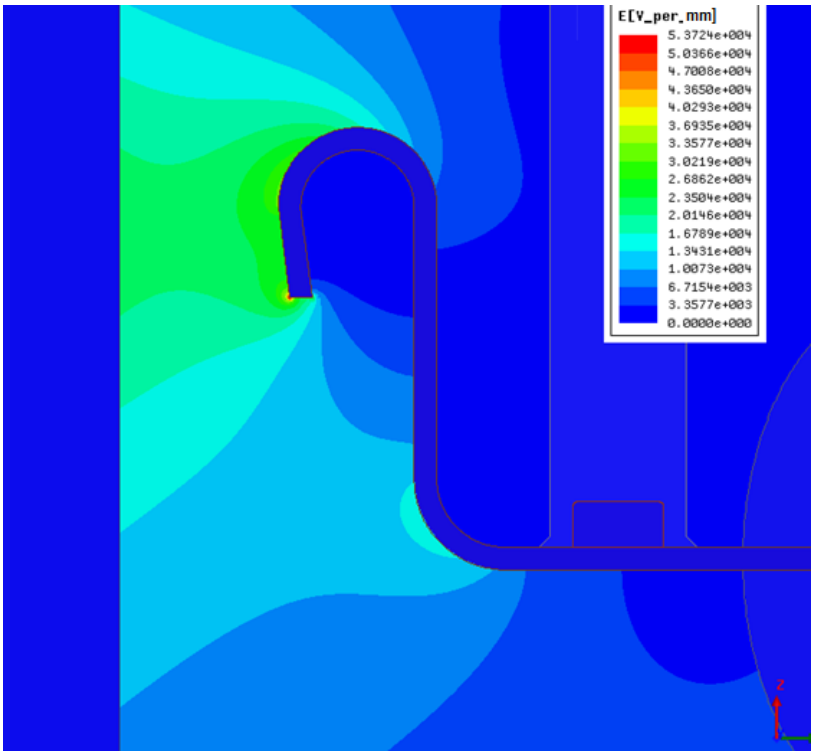


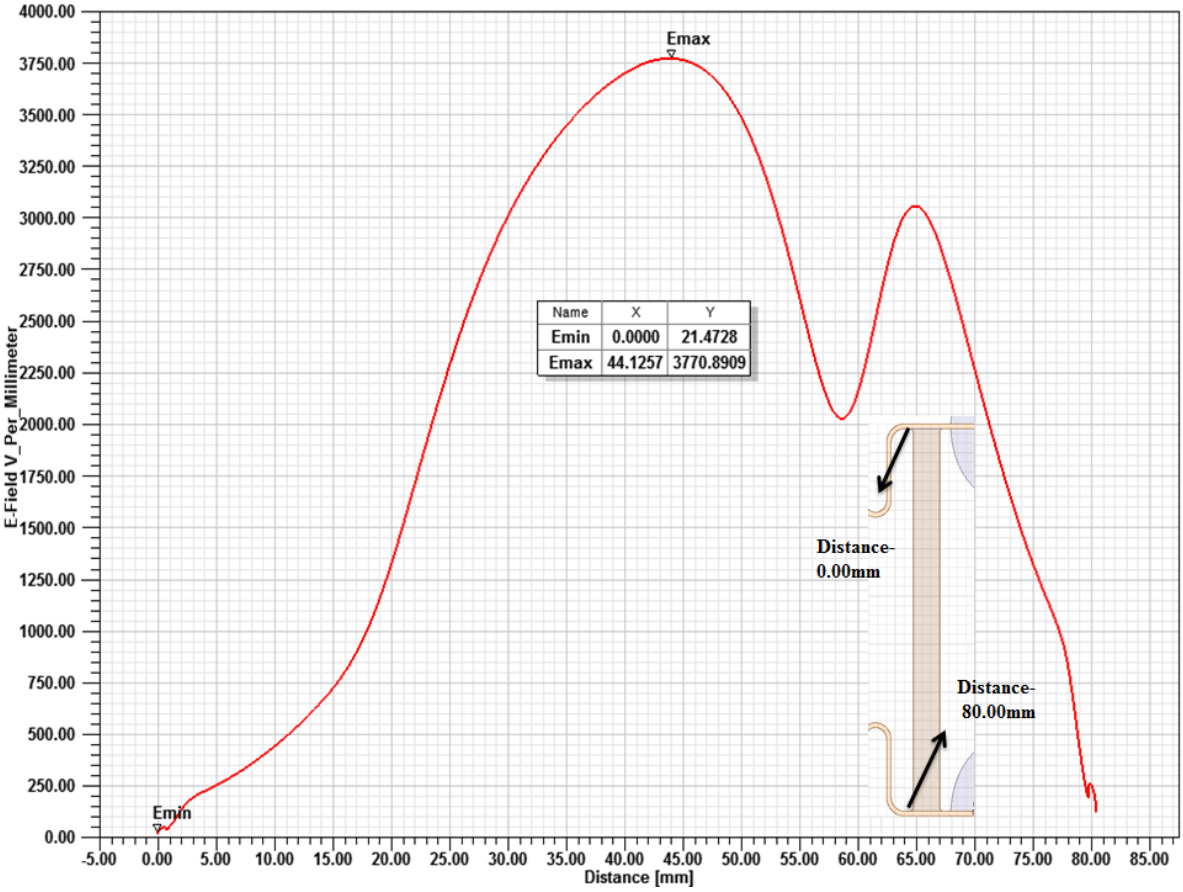


**Figure 6.12** Electric field plot and electric field values across the insulator starting from cathode triple junction to anode triple junction

Figure 6.11 shows the possible parameters that can be changed in order to reduce the high field stress on the shield. Parameter (a) is the smallest distance between the metal shield and the contact rod i.e.7mm, parameter (b) is the diameter of the shield curvature which is 5mm, parameter (c) is the distance between metal shield and the insulator which is also 5mm, parameter (d) is the shape of the tip of the shield and the parameter (e) is the distance between the tip of the shield and the contact rod which is 7.5mm. Figure 6.12 shows the electric field plot which suggest that the shield´s tip is highly stressed than any other part i.e. 53.72kV/mm. The field values across the insulator show that the maximum electric field on the surface of the insulator is around 3.8kV/mm.

#### 6.1.3.2.2 Variation 1:

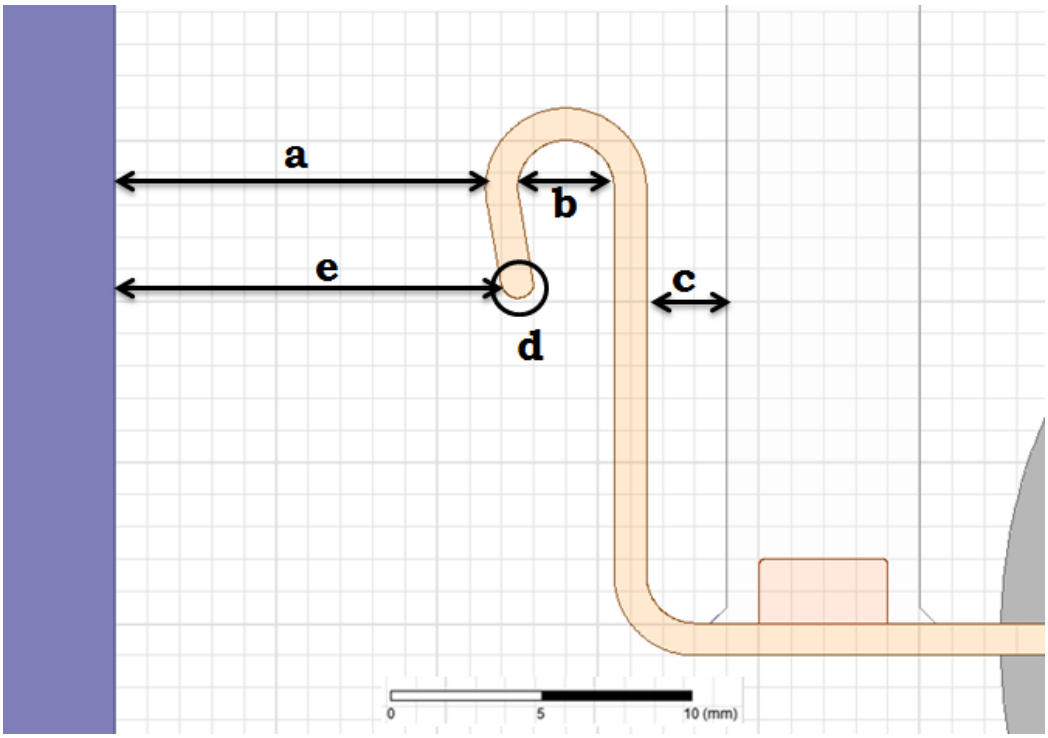


**Figure 6.13** Geometrical arrangement of variation 1 with taking the parameters a, b, c, d and e into consideration

The following discusses the changes made to the parameters in variation 1 as shown in figure 6.13. The smallest distance between the metal shield and contact rod which is considered as parameter (a) has been increased from 7mm to 11.5mm, the diameter of the shield curvature which is parameter (b) has been reduced from 5mm to 3mm, the distance between metal shield and the insulator i.e. parameter (c) has been reduced from 5mm to 2.5mm, the tip of the shield which is the parameter (d) is changed from the sharp edge to a curved edge with the curvature radius of 0.4mm, and finally the distance between the contact rod and the tip of the metal shield (e) is increased from 7.5mm to 12mm.

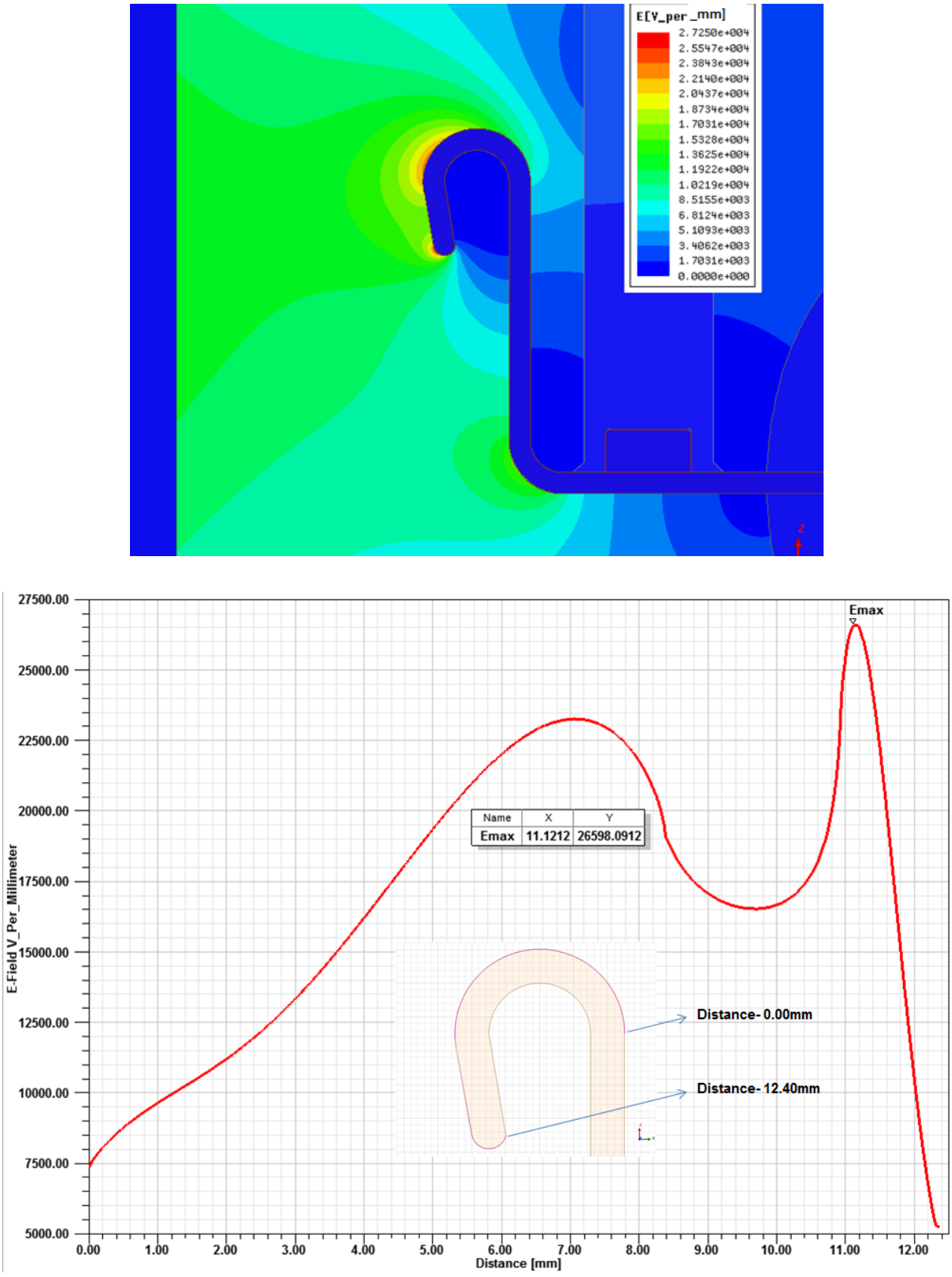


**Figure 6.14** Electric field plot and electric field values on the surface of the shield curvature

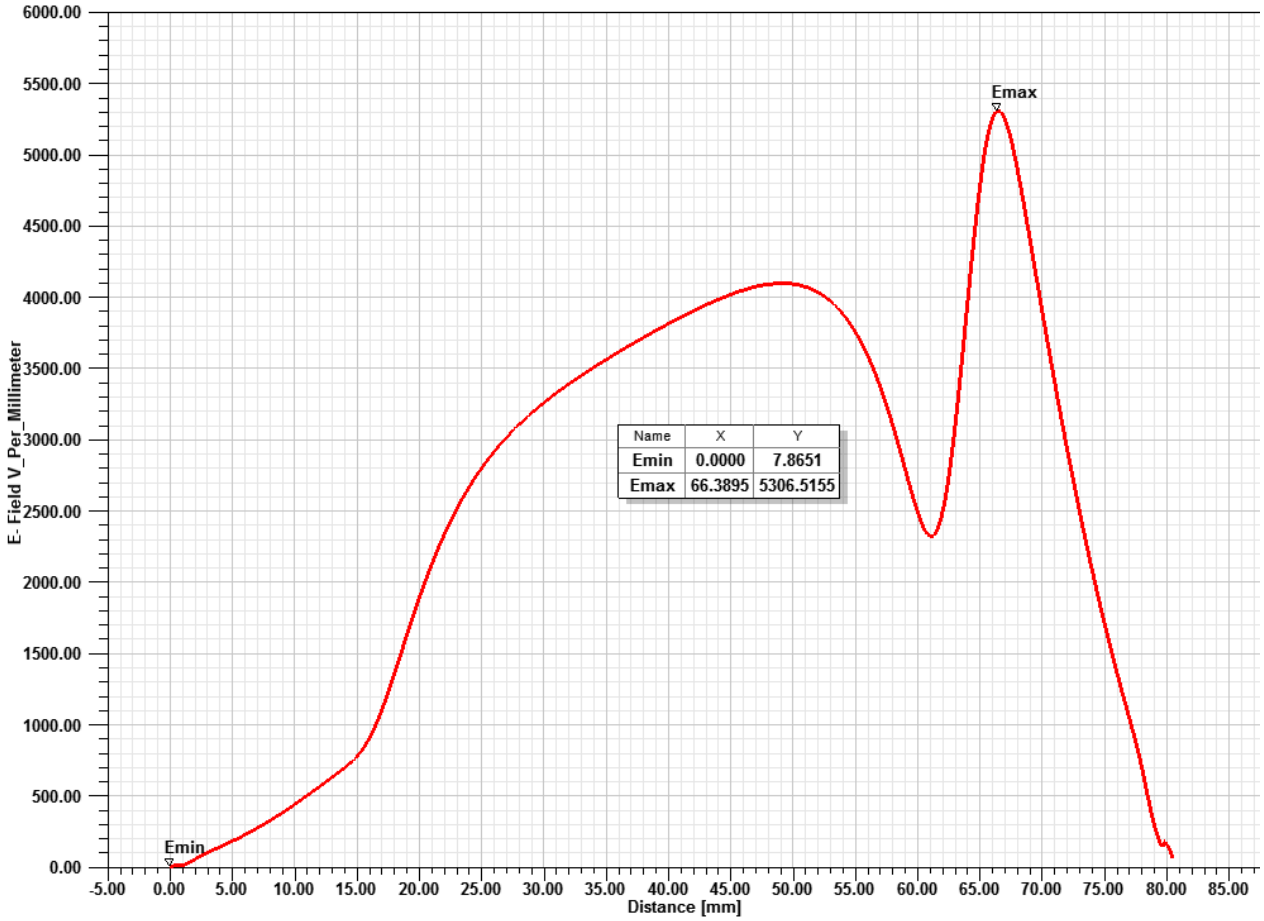


**Figure 6.15** Electric field values across the insulator starting from cathode triple junction to anode triple junction for variation 1

The electric field plot from figure 6.14 shows that the field stress on the surface of the shield has been reduced comparatively. To determine the values of the field stress on the shield curvature, a line has been drawn with 0.01mm away from the shield surface with stat and end points as shown in the figure 6.15. The curved end of the shield is highly stressed with a value of 26.59kV/mm (figure 6.14) but almost 50% less than the original shield. On the other hand the maximum field stress on the insulator surface has been increased from 3.7kV/mm to 5.3kV/mm (figure 6.15).

**6.1.3.2.3 Variation 2:**

Since the curved end of the shield is highly stressed in the variation 1, in this variation 2 the parameters (a), (b), (c), (d) are kept constant and parameter (e) is changed as shown in the figure 6.16. The distance between the curved end of the shield and the contact rod has been increased from 12mm to 13.2mm. The electric field plot from figure 6.16 suggest that after increasing the distance between the contact rod and curved end of the shield the maximum electric field stress is considerably reduced and has been shifted from the curved tip to the shield curvature that is near to the contact rod. The electric field values along the surface of the metal shield as shown in the figure 6.17 suggest that the maximum field stress value was reduced to 24 kV/mm from 26.59kV/mm of variation 1. Since the distance between the insulator and the metal shield is not changed, the maximum field stress on the insulator surface remains the same i.e. 5.3kV/mm.

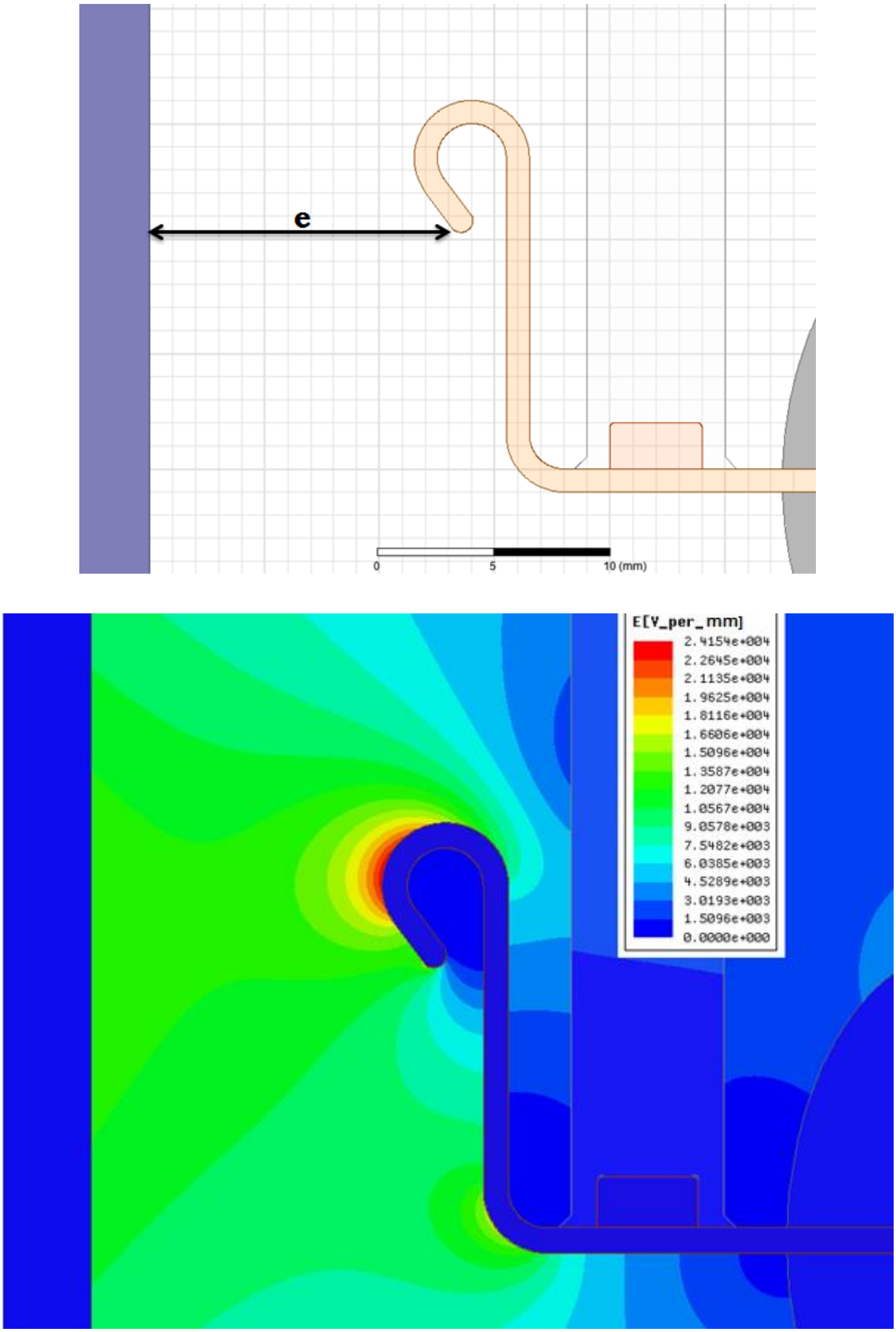


**Figure 6.16** Change in parameter (e) and the electric field plot of variation 2

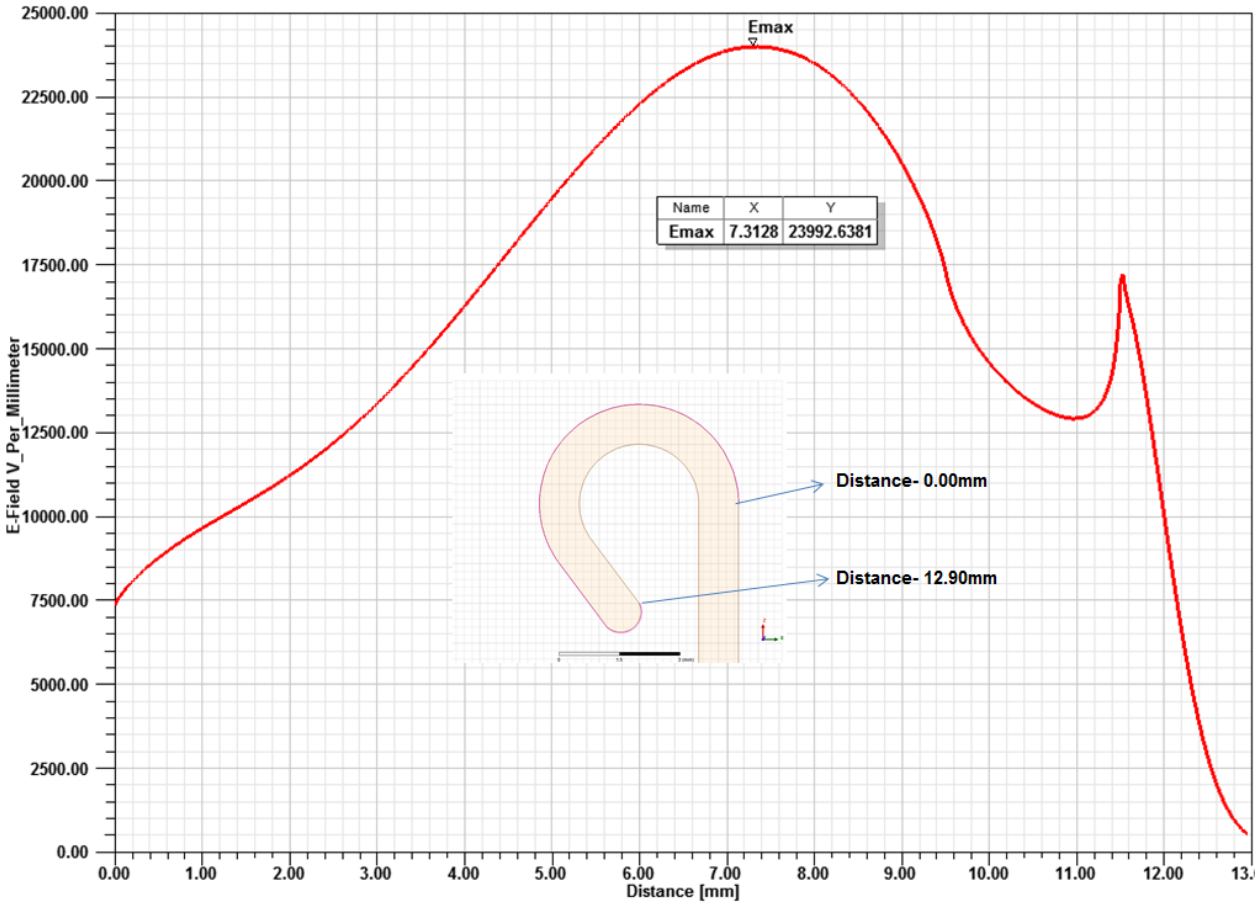


**Figure 6.17** Electric field values on the surface of the shield curvature

#### 6.1.3.2.4 Variation 3:

Since in variation 2 the maximum field stress is shifted from the shield edge to the shield curvature that is closer to the contact rod a new design is proposed and simulated in variation 3 as shown in the figure 6.18. This design is inspired from the optimized shape of the center shield from Kojima et.al [65]. The parameter (a) i.e. the shortest distance between the shield curvature and the contact rod is increased from 11.5mm to 13.5mm. The width of the bulb shaped end of the shield is considered as (f) which is 3mm. The electric field plot shows the area of the shield that is highly stressed. Figure 6.19 (1) shows the field values plotted along the shield curvature. The values suggest that the highest field stress value is 22.6kV/mm is less when compared to variation 2 i.e. 24kV/mm. The distance between the insulator and the metal shield remains unchanged and is the same as in the previous variations i.e. 2.5mm. But, the field values along the surface of the insulator which are showed in figure 6.19 (2) suggest that the highest field stress value on the surface is increased to 6.3kV/mm from 5.3kV/mm of variation 1 and variation 2. But when it comes to manufacturing processes, this design of this shield is not so reliable and not so easy to achieve.

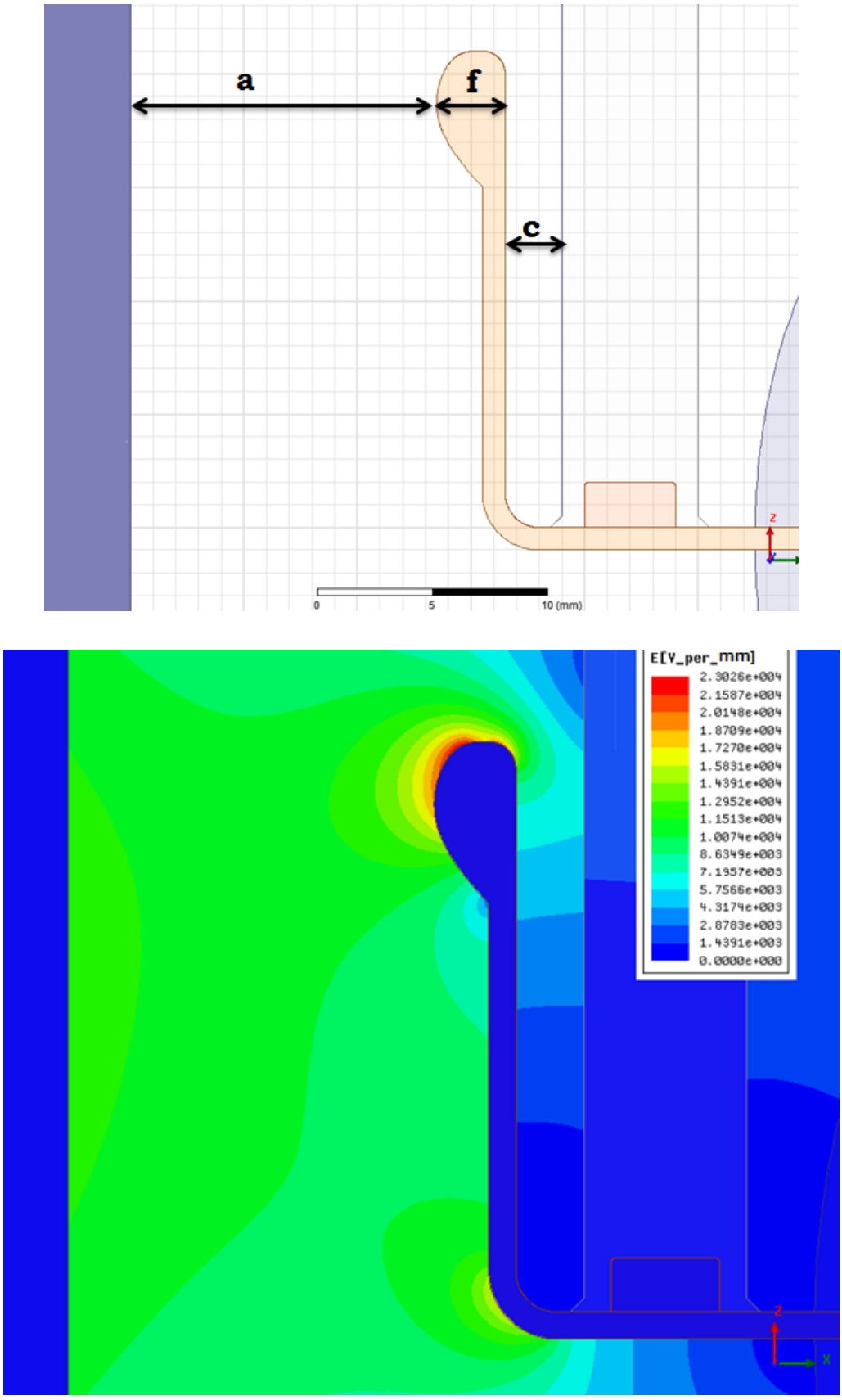


**Figure 6.18** Geometry of design variation 3 and its electric field plot

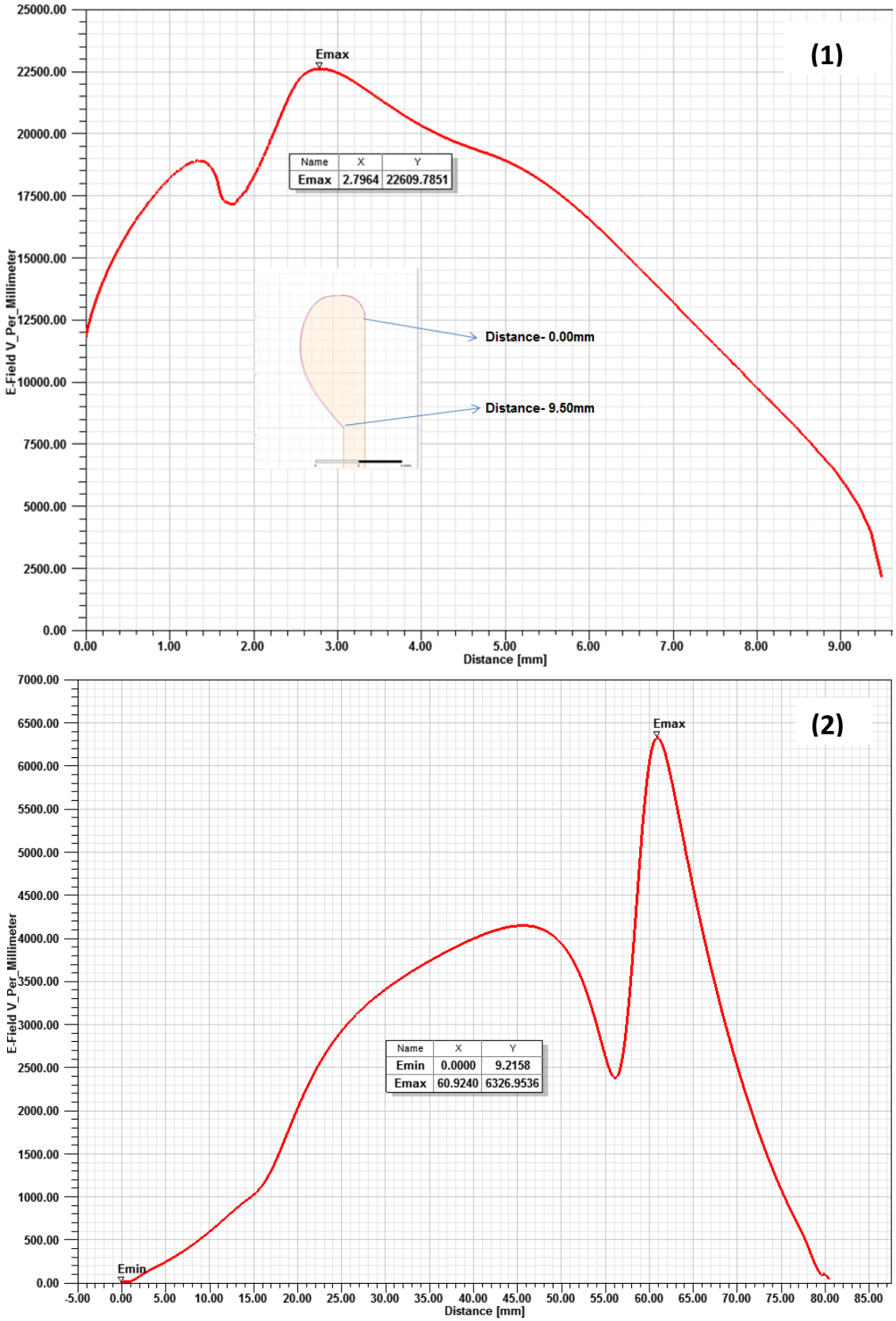


**Figure 6.19** Electric field values (1) across the shield curvature and (2) along the surface of the ceramic insulator

#### 6.1.3.2.5 Variation 4:

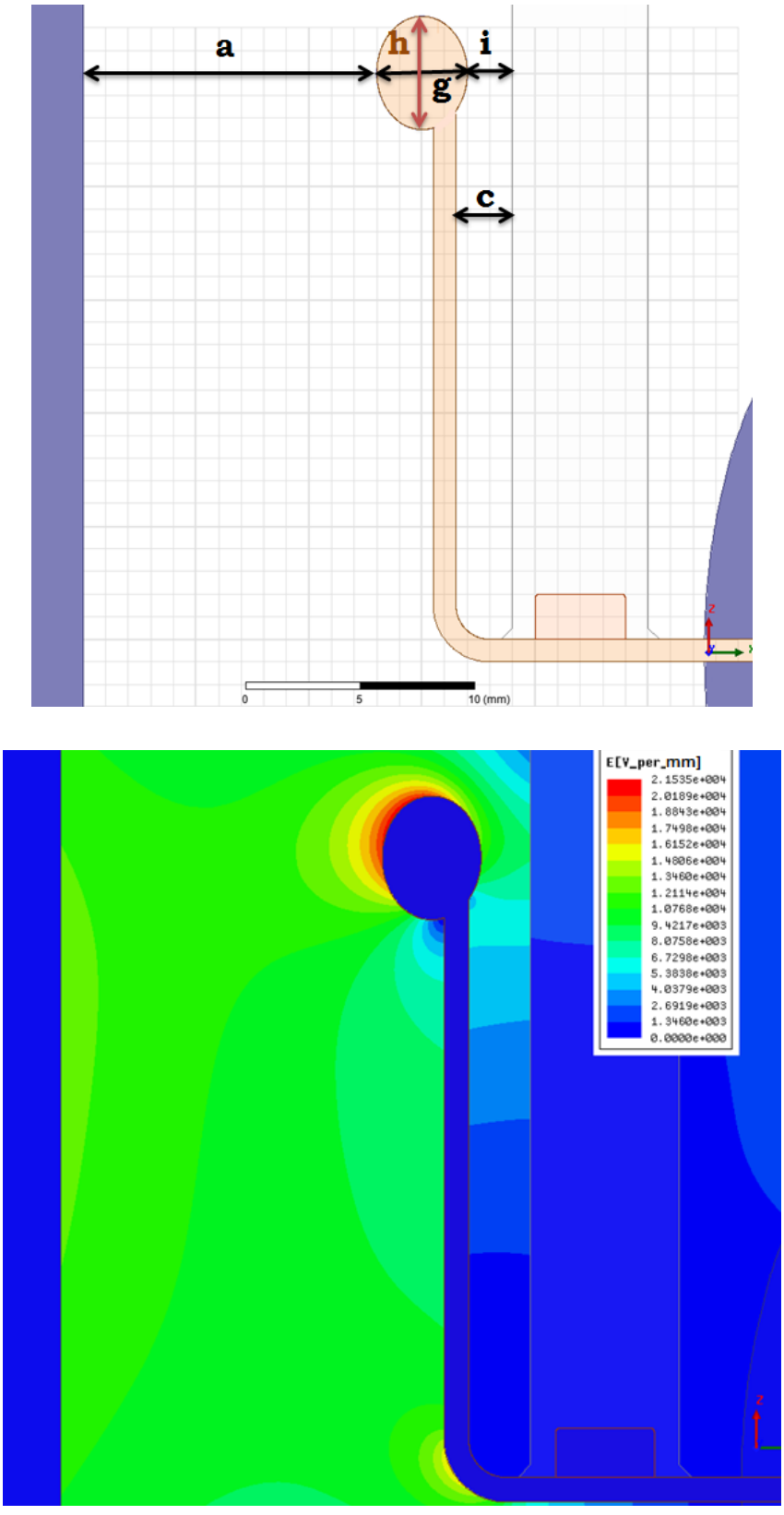


**Figure 6.20** Design variations of parameters (a), (b), (c) and electric field plot of variation 5

Figure 6.20 shows the design variations and the electric field plot of variation 4. The minimum distance between the contact rod and the metal shield i.e. parameter (a) is decreased from 13.5mm to 13mm. The distance between the insulator and the metal shield i.e. parameter (c) is kept constant which is 2.5mm. Since the shape of the shield curvature is elliptical, it has both a vertical diameter and a horizontal diameter. The horizontal diameter which is considered as the parameter (g) is 4mm and the vertical diameter which is considered as parameter (h) is 5mm. Because of this elliptical shape, there is a minimum distance between the insulator and metal shield which is parameter (i) of value 2mm. The electric field plot shows the electric field distribution around the shield curvature. Figure 6.21 shows the electric field values plotted along the surface of the shield. The field values are plotted in the clockwise direction on the shield surface as shown in zoomed image in the figure 6.21. The zero field values represent the field inside the shield. The maximum field stress on the surface of the shield is 21.3kV/mm.

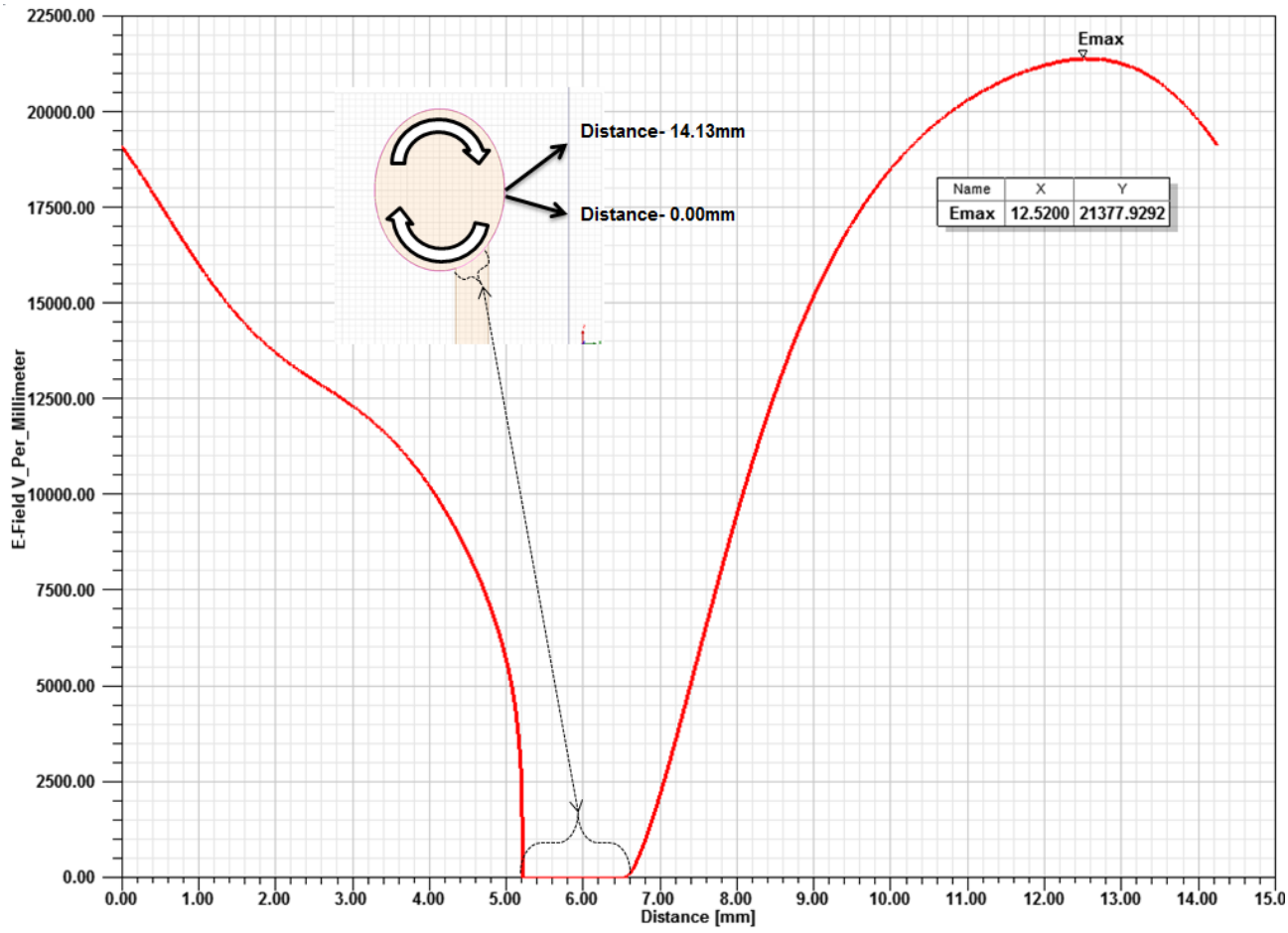


**Figure 6.21** Electric field values along the surface of the curvature of the shield

Similarly the electric field values along the surface of the insulator are also plotted in figure 6.22. The maximum field stress along the surface of the insulator is 8.2kV/mm.

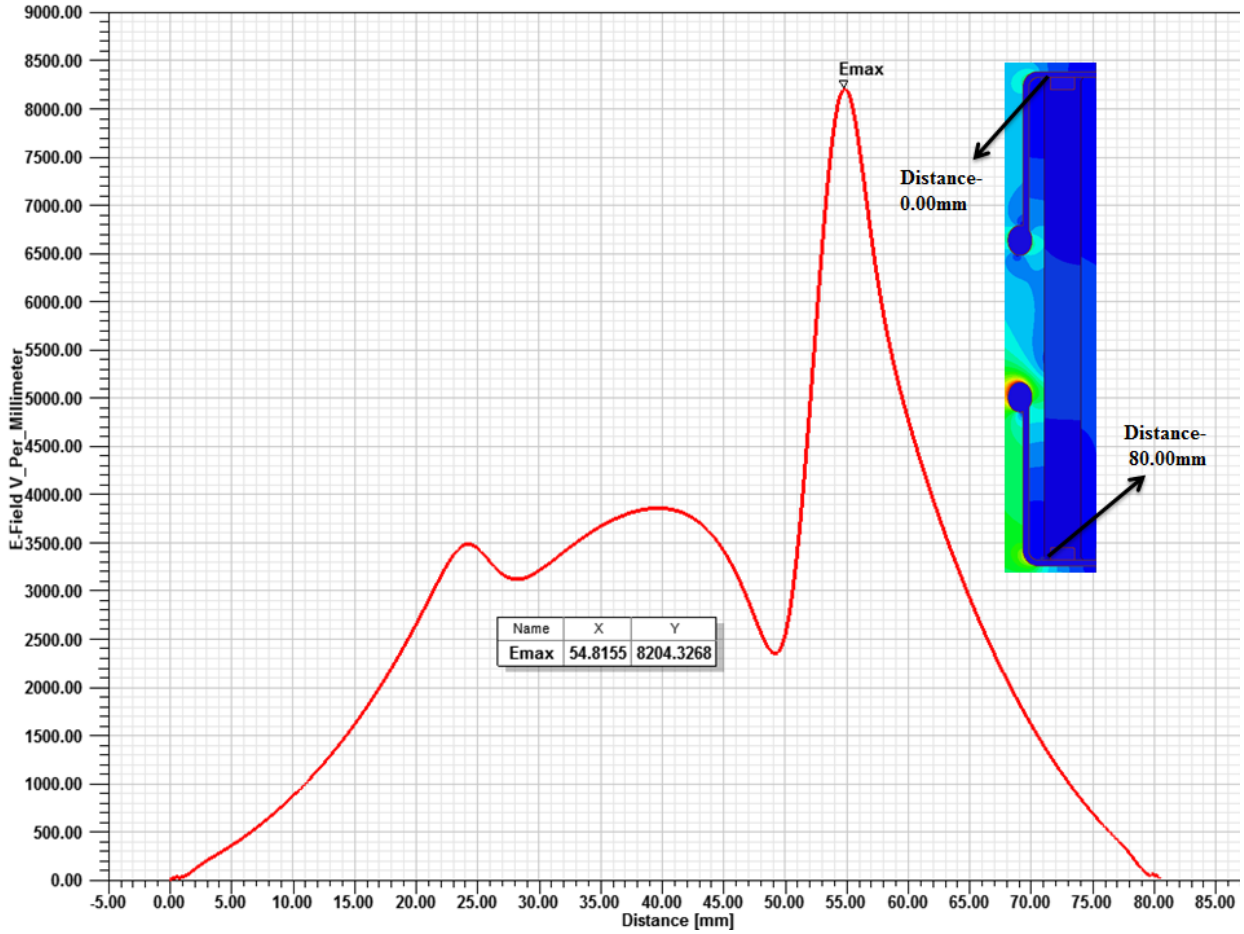


**Figure 6.22** Electric field values along the surface of the insulator

#### 6.1.3.2.6 Variation 5:

The variation 5 is very similar to variation 4 with the only difference of shield curvature is facing the insulator instead of the contact rod as shown in figure 6.23. To achieve this arrangement the distance between the insulator and metal shield, i.e. parameter (c), is increased from 2.5 to 4.5mm and the parameters (i) and (a) are kept constant, i.e. 2mm and 13mm respectively. The main reason behind this arrangement is to have a uniform structure facing the contact rod. The electric field plot is also shown in figure 6.23. The electric field values along the surface of the shield curvature are plotted similar to variation 4 are shown in figure 6.24 (1). The field plot suggests that the maximum field stress on the shield surface is 20.9kV/mm which is lower than the field value of 21.3kV/mm for variation 4. Figure 6.24(2) shows the field values along the surface of the insulator, and the maximum field stress value is 8.5kV/mm.

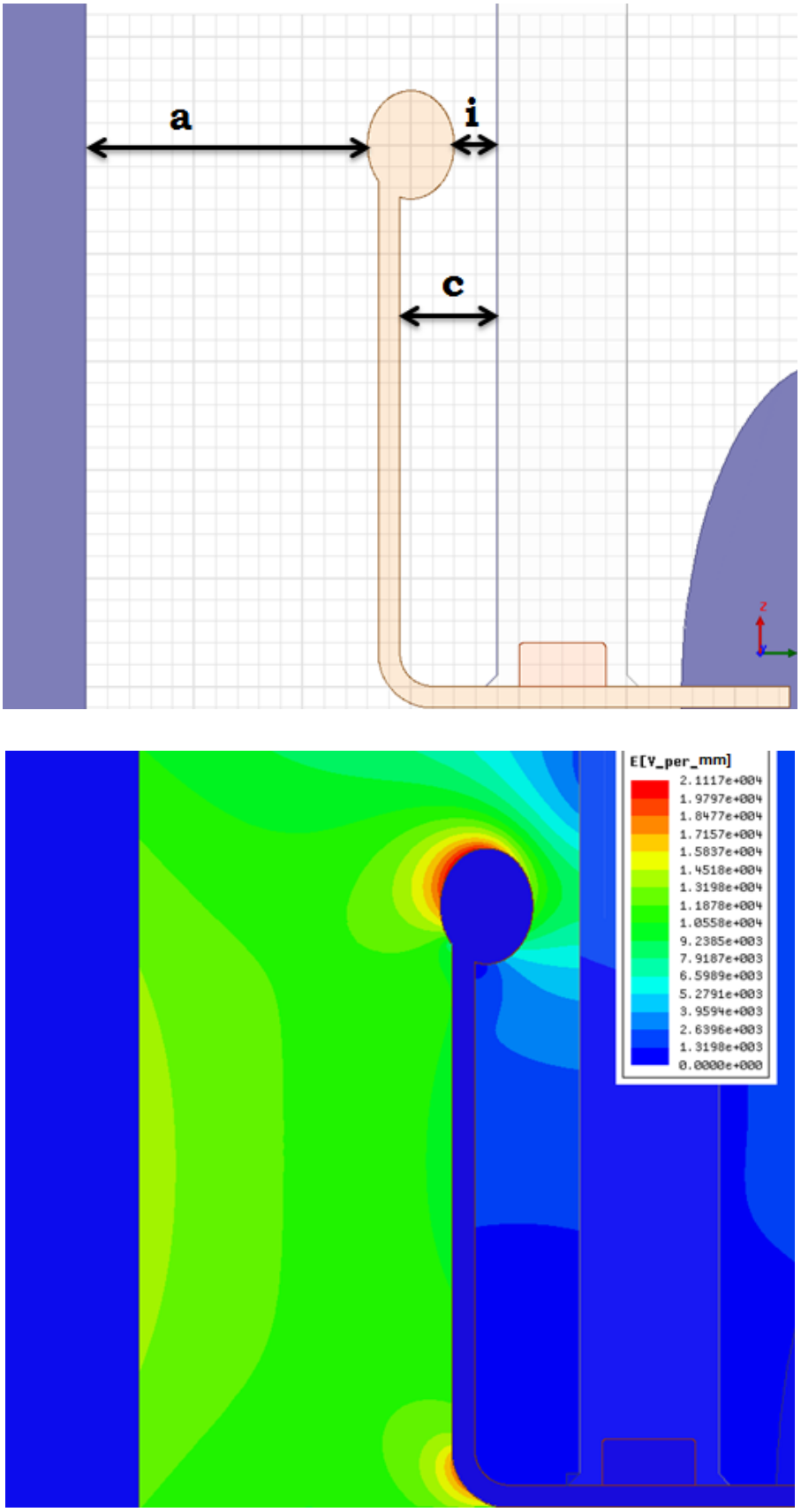


**Figure 6.23** Design variations of parameters (a), (b), (c) and electric field plot of variation 5

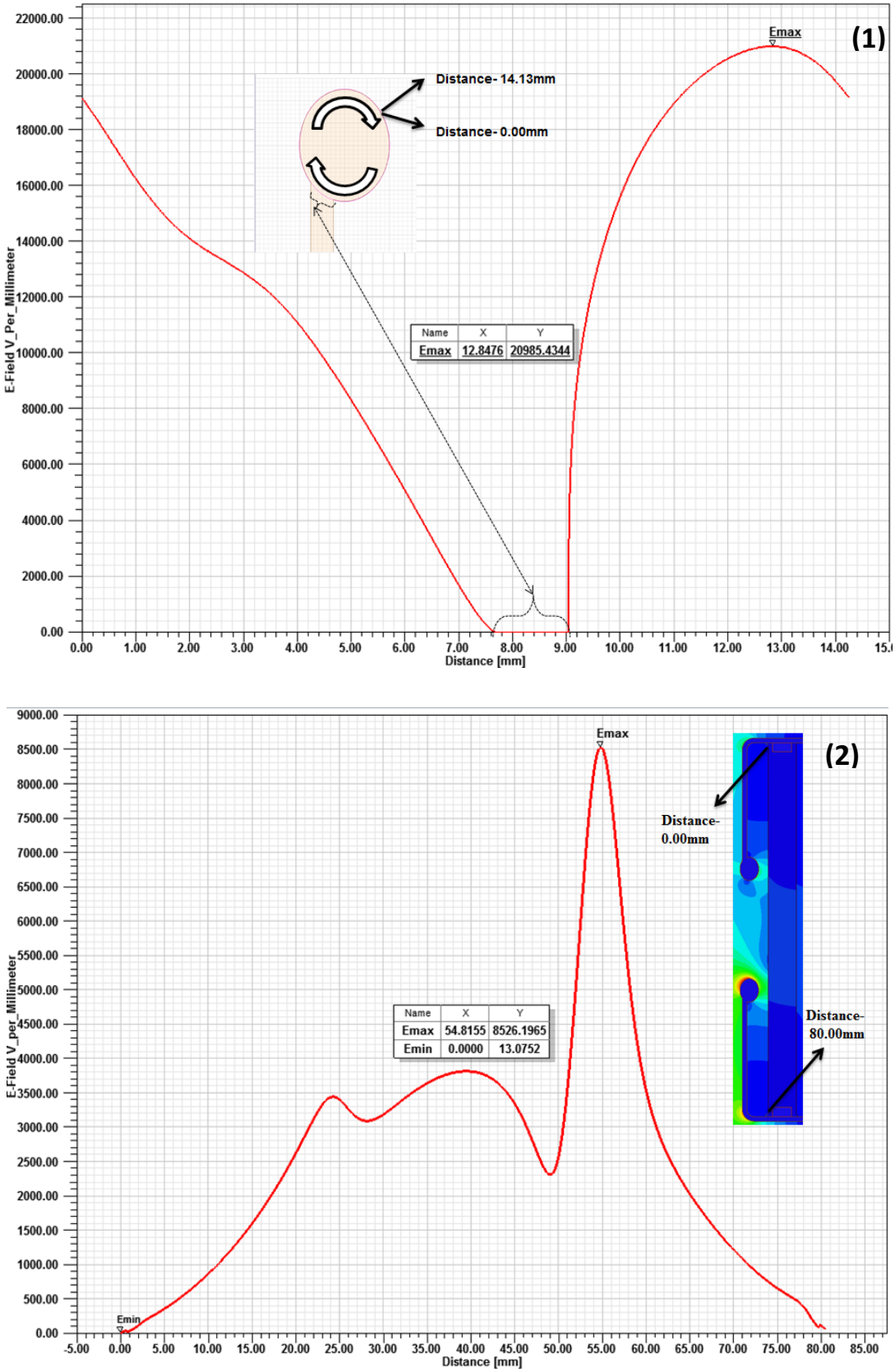


**Figure 6.24** Electric field values (1) along the surface of the shield curvature, (2) along the surface of the insulator

As mentioned before these Cu shields are not only used to achieve a uniform field distribution inside the interrupter but also to avoid the metal vapor deposition on the insulator surface during the arc interruption. So in order to improve the dielectric strength of the insulator surface, a major part of the insulator should be covered by these Cu shields which demands the smallest possible distance between the shields. As mentioned in the figure 6.9, the distance used in all the above simulations is 43mm. Now, by using the shield designs of variation 4 and variation 5, simulations are done to the geometries with the distance between the shields reducing to 21mm. Figure 6.25 shows the geometrical arrangement with both upper metal shield and the lower metal shield being similar and having the distance of 21mm between them.

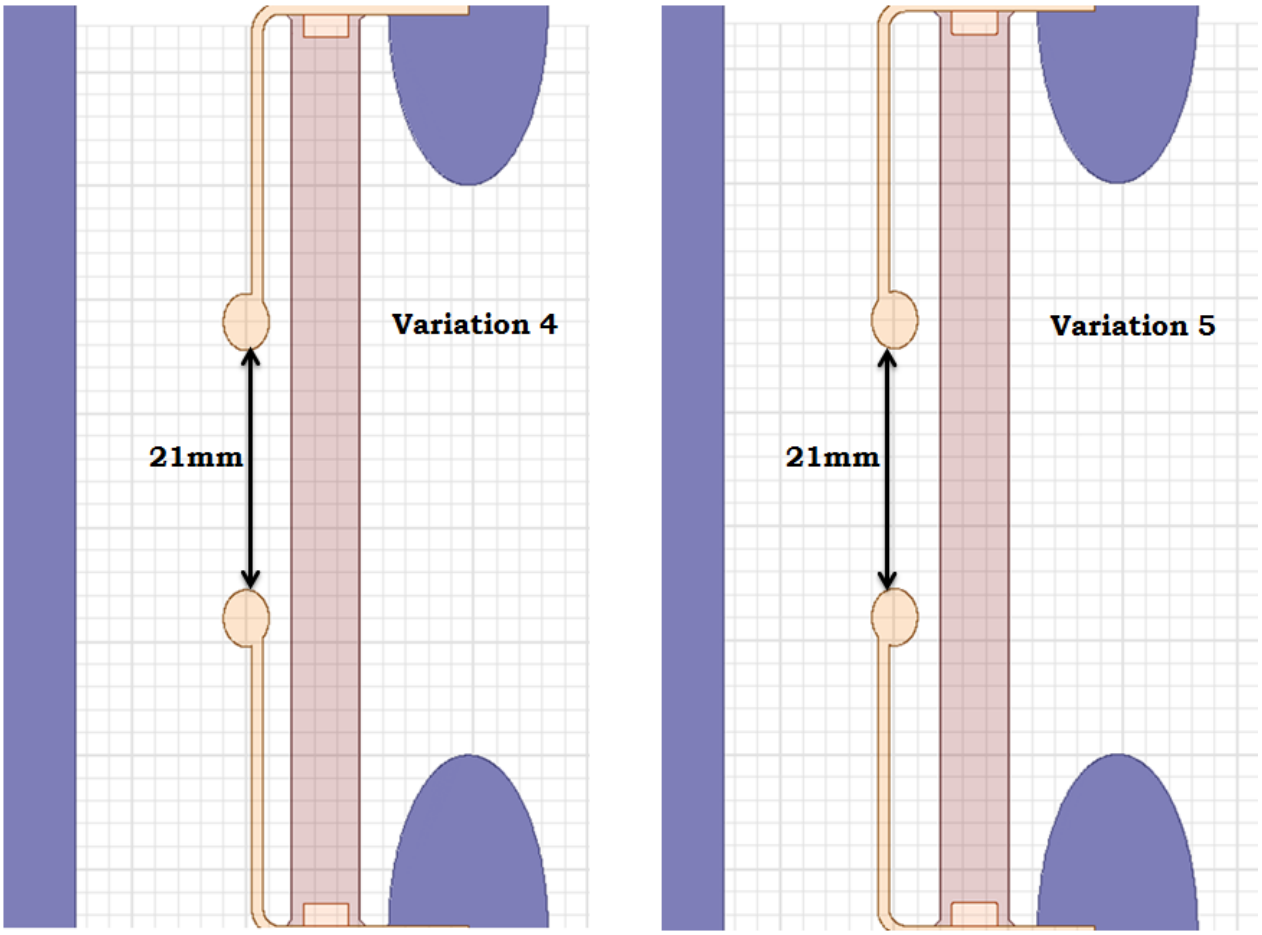


**Figure 6.25** Geometrical arrangement showing 21mm distance between the two metal shield with variation 4 and variation 5

The electric field plot and the field values along the surface of the shield curvatures of both variations are shown in figure 6.26. Based on the electric field values the maximum electric field on the surface of the shield of variation 4 is 21.6kV/mm whereas for the shield of variation 5 is 21.2kV/mm. The electric field values across the insulator surface are also plotted in figure 6.27 which suggests that the arrangement with variation 4 has the maximum field value of 8.7kV/mm and the arrangement with variation 5 has the maximum field value of 9kV/mm.

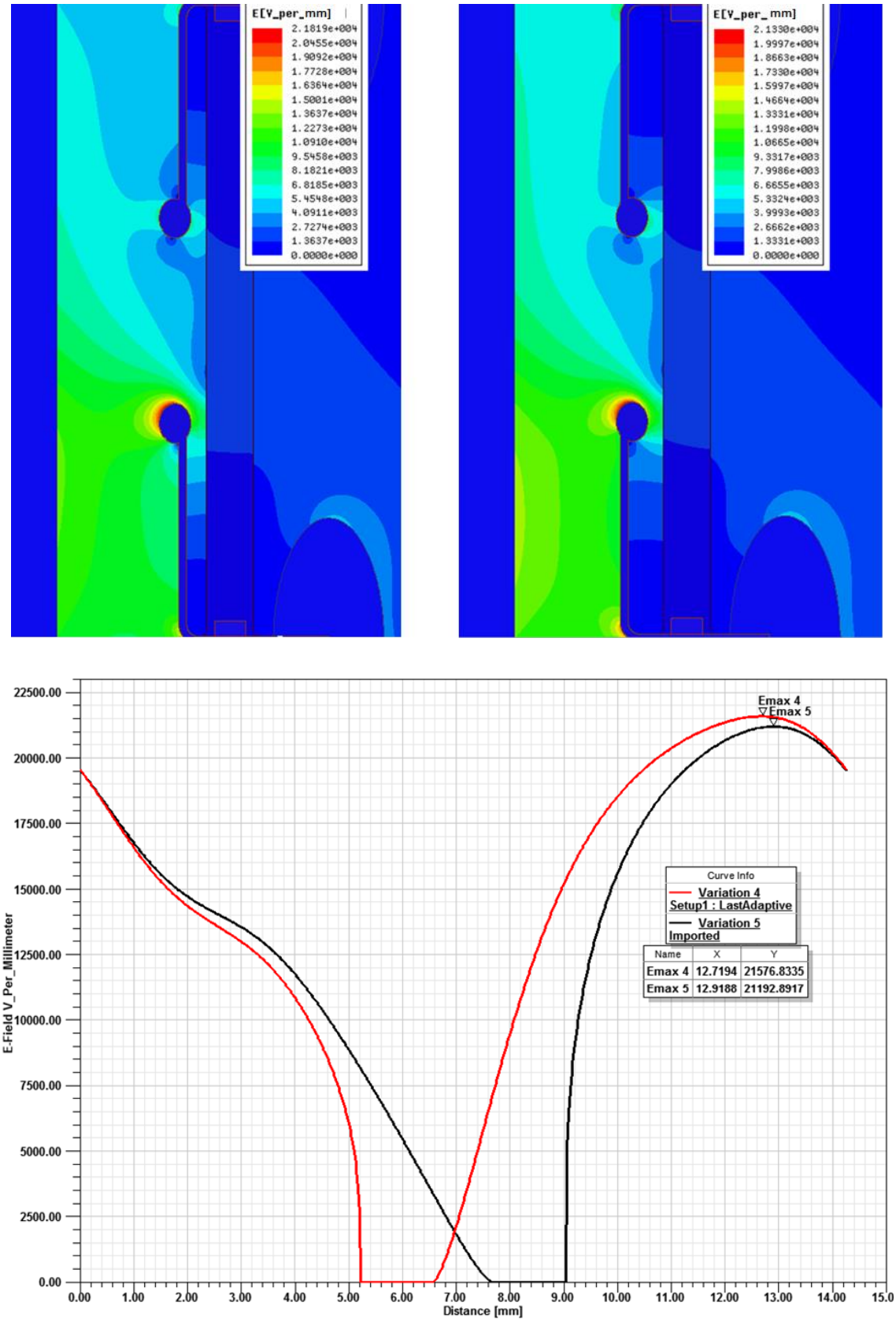


**Figure 6.26** Electric field plot and the field values across the surface of the shield curvatures of variations 4 and 5 with 21mm distance between them

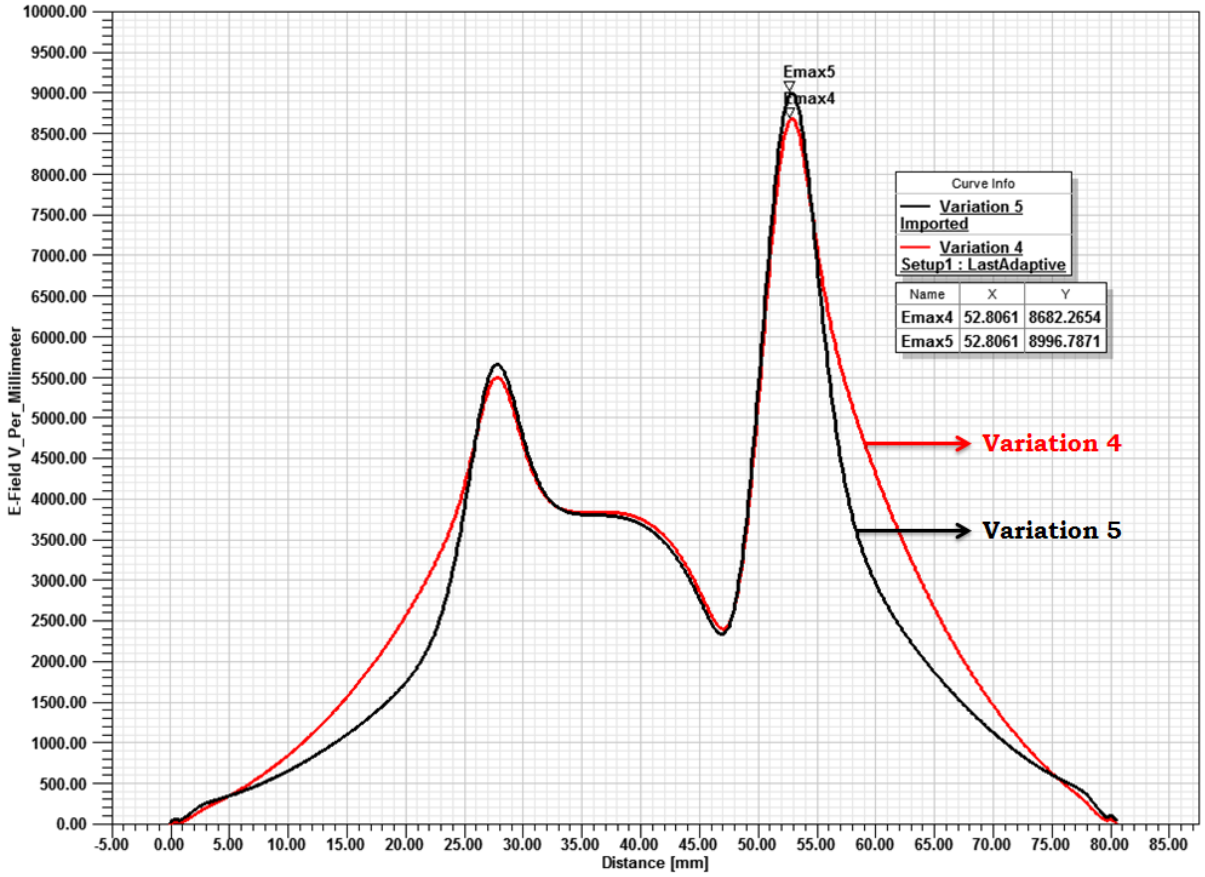


**Figure 6.27** Field values across the surface of the insulator with 21mm distance between the shields

### *6.1.3.3 Summary*

| Type of the design | $E_{max}$ of the shield surface | $E_{max}$ on the insulator surface |
|---|---|---|
| Original shield structure | **53.7 kV/mm** | 3.8 kV/mm |
| Variation 1 | **26.6 kV/mm** | 5.3 kV/mm |
| Variation 2 | **24.0 kV/mm** | 5.3 kV/mm |
| Variation 3 | **22.6 kV/mm** | 6.3 kV/mm |
| Variation4/ With 21mm distance | 21.3 kV/mm / 21.6kV/mm | 8.2 kV/mm / 8.7kV/mm |
| Variation5/ With 21 mm distance | 20.9 kV/mm / 21.2kV/mm | 8.5 kV/mm / 9kV/mm |

**Table 6.8** Summary of the design variations with maximum electric field on the shield and the insulator surface

Based on the values from the above table, the variation 4 or variation 5 have the maximum electric field values on their shield surfaces that are less than the threshold range of the Cu and the maximum electric field values on their insulator surfaces that are less than the threshold range of the alumina surface which makes both of them as a good substitute for existing shield structures. Using the variation 4 or 5, the distance between the insulator and the contact rod can be reduced to 19mm and that reduces the diameter of the tube.

# Chapter 7

# CONCLUSIONS & FUTURE WORK

The development of vacuum circuit breakers and their applications has overcome many expectations from their early supporters in 1960s. They are ascertained to be exceptionally reliable. Some of its advantages like sealed for life, environmental friendly, maintenance free and the long mechanical life have pushed the vacuum circuit breakers to a dominant position at the distribution levels. Implementing this same vacuum interrupter technology for transmission levels was quite an argument since many years and raises the question of withstand capacity of vacuum circuit breakers at these levels of voltages.

## 7.1 Conclusions

The objective of this research is to identify some of the critical areas inside the interrupter that can hamper the withstand capacity of the breaker and suggesting the possible solutions to strengthen the dielectric strength in these areas which in turn improve the overall withstand voltage of the breaker for high voltage levels, especially for 72.5kV. The critical areas that are considered in this research are triple junctions (Vacuum-Ceramic insulator-Metal shield), surface insulation, outer insulation (between the insulator and outer housing) and the gap between the contact rod and metal shield. Also a brief theoretical explanation of different mechanisms of discharges that take place in the above mentioned critical areas is given. The geometrical design variations to various parts at these areas are suggested and verified the field behavior with 2D electrostatic simulations using ANSYS Maxwell.

The following are the conclusions that are derived from the current research.

- High field intensity at the cathode triple junctions results in an electron emission from this junction which is assumed to be the primary initiating event of the surface flashover along the insulator in the vacuum and in the outer insulating medium, which is in our case $N_2$.

    - ✓ In order to overcome the above initiating event by reducing the high field stress at the triple junction, the geometrical arrangement of the triple junction has to be changed. To examine this, different angle of contacts between the insulator and metal shield like 45°, 90°, 135° and hemispheric contact are simulated.

- ✓ Based on the results from the simulations, the insulator with a contact angle of 135° with the metal shield is considered as the best option as the field stress at the triple junction is drastically reduced by this arrangement.
- ✓ In addition to the angle of contact, inserting metal inserts at both the ends of the insulators is also assumed to be a solution to reduce the high field stress at the triple junctions. To examine this, metal inserts of different depths, i.e. 0.5mm, 1mm, 1.5mm and 2mm are simulated.
- ✓ The simulation results showed that the metal inserts with the depth of 2mm has reduced the field stress effectively at the triple junctions which is assumed to avoid the surface flashover along the insulator.

- The metal shields which are sandwiched between the ceramic blocks leave undefined edges outside the interrupter. Since the thickness of these metal shields is 1mm, these edges are considered as sharp edges and can result in an intensified electric field around them. This high field stress can be the reason for discharges occurring in the gap between the insulator and outer housing.

  - ✓ To avoid such a high field stress at the edges, the metal shields are extended out of the ceramic blocks and covered by field grading rings around the metal shield edges.
  - ✓ In additions different shapes of these grading rings are simulated in order to observe the influence of the shape of the grading ring on the field stress at the triple junction outside the interrupter.
  - ✓ Based on the results of the simulations, grading rings of elliptical shape are proved to have a positive influence on reducing the stress at the triple junctions.
  - ✓ After simulating various elliptical shapes, a grading ring with 7mm horizontal radius and 11.5mm vertical radius with a distance of 2mm between the ring and the triple junction is proved to be an optimum solution.

- Finally simulations are done in order to get optimized shield structures inside the interrupter. Because, having an optimized shield structure can help in reducing the overall diameter of the tube by reducing the distance between the insulator and the contact rod with bellows.

  - ✓ To realize this, metal shield structures of 5 different variations with different parameters are simulated. Based on the results of the simulations, a shield structure of variation 5 with a distance of 21mm between the two shields is considered as an optimized structure.

- ✓ Using this variation helps to reduce the distance between the insulator and contact rod with bellows from 54mm to 19mm and thus reducing the overall diameter of the interrupter tube.

- Figure 7.1 shows the 2D arrangement of a possible 72.5kV vacuum interrupter tube by implementing all the above mentioned optimum solutions followed by its 3D diagram.

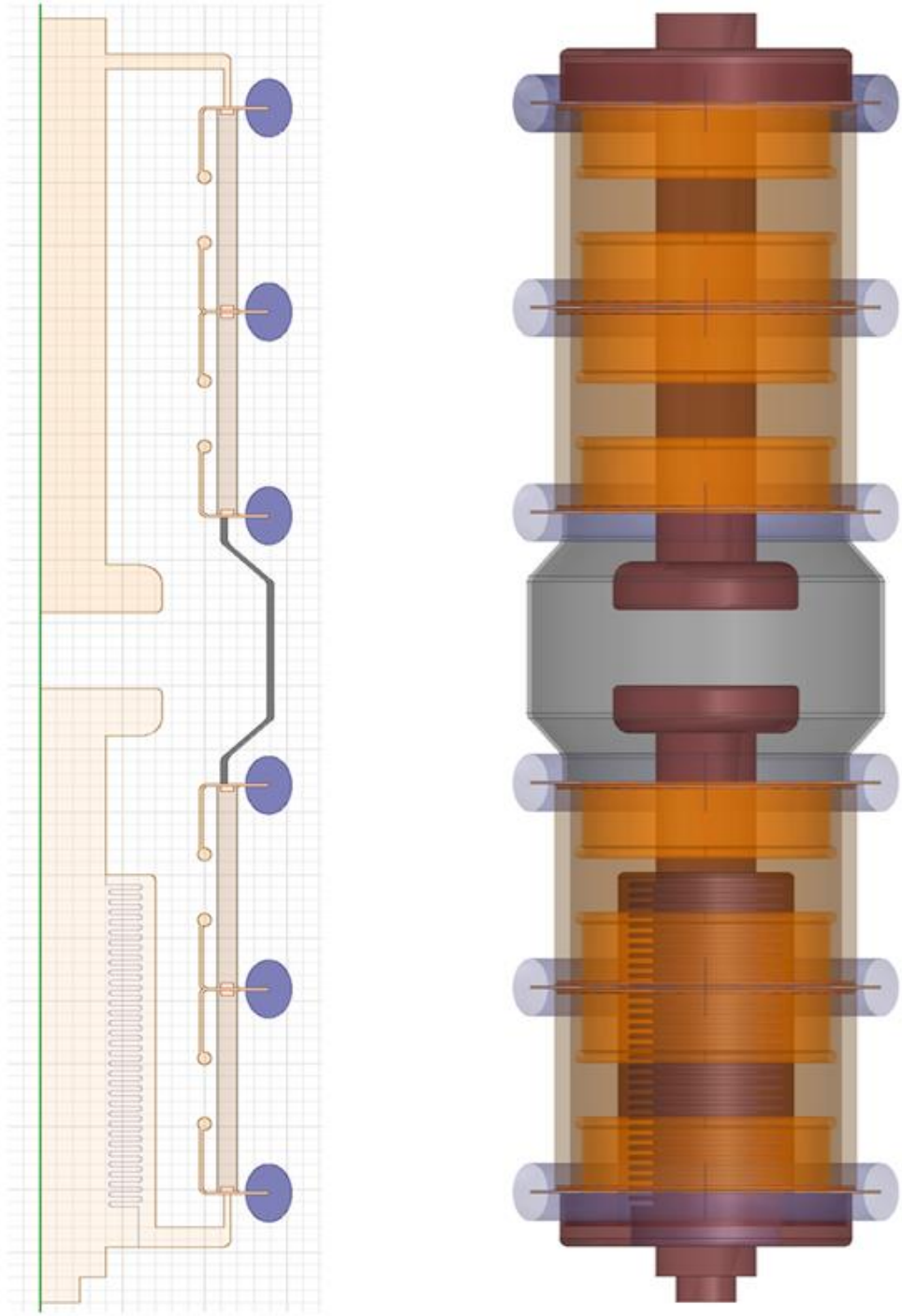

**Figure 7.1** A possible design of an optimized 72.5kV vacuum interrupter in both 2D and 3D models

- Similarly when a 145kV vacuum interrupter is considered, the 135° angle of contact between the insulator and the metal shield, metal insert of 2mm deep at the both ends of the insulator and the grading rings of elliptical shape can be still considered as the solutions for their respective problems. But when it comes to metal shield structures, the distance between the insulator and the contact rod with the bellows should be more than the existing 19mm.

## 7.2 Future Work

The following are the tasks that should be carried out in future

- Finding the maximum electric field on surface of the $Al_2O_3$ insulator and Cu shield that can initiate a discharge by conducting the required experiments on the specific model. In this way, a fixed threshold value can be used rather than using a wide range of it.
- A simple study about the thermal properties of metal inserts as well as of the $Al_2O_3$ insulators is necessary in order to avoid the problems of thermal expansion during the brazing process of the interrupter.
- And finally designing a vacuum interrupter with the proposed geometry changes and conduct high voltage tests to study its performance.

# REFERENCES

[1] Commission Regulation No 305/2008 of 2 April 2008 establishing, pursuant to Regulation (EC) No 842/2006 of the European Parliament and of the Council, *"Minimum requirements and the conditions for mutual recognition for the certification of personnel recovering certain fluorinated greenhouse gases from high-voltage switchgear"*, Official Journal of the European Union, L92/17, 2008

[2] Duan Xiong-ying *et al "Dielectric strength and statistical property of single and triple-break vacuum interrupters in series"* IEEE Dielec. Elect. Insul. Vol-14, 2007

[3] A.Iturregi, E. Torres, I. Zamora, O. Abarrategui, "*High Voltage Circuit Breakers: SF6vs. Vacuum International conference on Renewable Energies and Power Quality"* Int. Conf. Renew. Ener. Pow. Qual. Valencia 2009

[4] M. Schlaug *et al*., "*Electrical Life of Vacuum Interrupters",* XXIInd Int. Symp. on Disch. and Electr. Insul. in Vac., Matsue, Japan, 2006

[5] A. Müller *"Mittelspannungstechnik, Schaltgeräte und Schaltanlagen"* Siemens AG, Ausgabe 19D2 2009-11

[6] http://www.csanyigroup.com/comparison-between-vacuum-and-sf6-circuit-breaker

[7] L. Falkingham, M. Waldron, *"Vacuum for HV applications - Perhaps not so new? - Thirty Years' Service Experience of 132kV vacuum Circuit breaker",* XIInd Int. Symp. On Disch. and Electr. Insul. In Vacuum, Matsue, 2006

[8] R.B. Shores, V.E. Philips, *"High Voltage Vacuum Circuit Breakers",* IEEE Trans. Power App. Syst., Vol. PAS-94, no. 5, pp. 1821-1830, Sept/Oct 1975

[9] E. Umeya, H. Yanagisawa, *"Vacuum Interrupters"*, Meiden Review, series 45, pp. 3-11, 1975

[10] Y. Matsui *et al. "Development and Technology of High Voltage VCBs; Brief History and State of Art"*, XXIInd Int. Symp. on Disch. and Electr. Insul. in Vac. Matsue, Japan, 2006

[11] S.Yanabu, *et al. "Ten Years' Experience in Axial Magnetic Field Type Vacuum Interrupters",* IEEE PES, 1986 Winter Meeting, 86 WM 140-8, Feb 2-7, 1986

[12] M. Homma *et al., "History of Vacuum Circuit Breakers and Recent Developments in Japan"*, IEEE Trans. Dielectr. Electr. Insul., Vol.13, No.1, pp. 85 - 92, 2006

[13] J. Wang, *et al., "Development of High Voltage Vacuum Circuit Breakers in China",* XXIInd Int. Symp. Disch. and Electr. Insul. in Vac., Matsue, 2006

[14] S. Giere, H. Knobloch and J. Sedlacek, *"Double and Single-Break Vacuum Interrupters for High Voltage Application: Experiences on Real High-Voltage Demonstration-Tubes"*, CIGRE, Paris, 2002

[15] H. Schellekens, G. Gaudart, *"Compact High-voltage Vacuum Circuit Breaker, a Feasibility Study"*, IEEE Trans. Dielectr. Electr. Insul., Vol. 14, no. 3, pp. 613 – 619, June 2007

[16] X. Godechot, *et al*. *"Vacuum Interrupters in High Voltage Applications",* XXIIIrd Int. Symp. Disch. Electr. Insul. Vac., Bucharest, 2008

[17] H. Boersch, H. Harmish, and W. Ehrlich: *"Surface discharge across insulators in vacuum"*, Z. Angew Phys.,Vol. 15, pp. 518-525, 1963

[18] C. H. De Tourreil, K. D. Srivastava, *"Mechanism of Surface Charging of High-Voltage Insulators in Vacuum"*. IEEE Trans. Electr. Insul., Vo. 8, No. 1, pp.17-21, 1973.

[19] H. C. Miller, *"Flashover of insulators in vacuum: review of the phenomena and techniques to improve hold off voltage",* IEEE Trans. Electr. Insul.,Vol. 28, pp. 512-527,1993.

[20] M. Kurrat, S. Giere, U. Schumann *"Electric field design of high voltage vacuum tubes",* XIIIrd Int. Symp. on Discharges and Electr. Insul. in Vac., Netherlands, 2003

[21] Leslie FALKINGHAM, "*The evolution of vacuum interrupter arc control systems"* XVIII Int. Conf. Electr. Distrib Turin, 6-9 June 2005.

[22] R.E. Voshall, *et al. "Experiments On Vacuum Interrupters In High Voltage 72kV Circuits"* IEEE Trans. Power App. and Sys., Vol. PAS-99, No.2; March/April 1980.

[23] R.V.Latham, "*High Voltage Vacuum Insulation: The Physical Basis"*, Academic Press, UK 1981.

[24] Dr. Harald Fink, Dr. Markus Heimbach, Dr. Wenkai Shang "*Vacuum interrupters with axial magnetic field contacts Technology Review*", ABB; 1/2000.

[25]Metwally, I.A. "*New Technological trends in high voltage power circuit breakers"*, Potentials IEEE Vol 25, 2006.

[26] Satoru Yanabu, *et al. "Recent Technical Developments in High-Voltage and High-Power Vacuum Circuit Breakers"* IEEE Trans. Plasma Sci., Vol. 17. No.5; October 1989.

[27] Zhiyuan Liu, *et al. "Development of High-Voltage Vacuum Circuit Breakers in China"* IEEE Trans. Plasma Sci., vol. 35, No. 4, august 2007.

[28] IEC 62271-1, "*High voltage switchgear and control gear-Part 1: Common Specifications"*

[29] K. Kato, *et al. "Optimization Technique for Electrical Insulation Design of Vacuum Interrupters"*, IEEE Trans. Dielectr. Electr. Insul., Vol. 15, No.5; October 2008.

[30] Ravindra Arora; Wolfgang Mosch "*High Voltage and Electrical Insulation Engineering*" John Wiley & Sons ISBN 978-1-118-00896-6. Retrieved 9 January 2012.

[31] Trichel , G. W. *"The mechanism of the positive point - to - plane corona in air at atmospheric pressure"* , Physical Review , 55 ( 1939 ), pp. 382 – 390 .

[32] M. Naidu, V. Kamaraju *"High Voltage Engineering"* 2nd edition- McGraw-Hill, 1996.

[33] John G. Trump, R. J. Van De Graff, *"The Insulation of High Voltages in Vacuum",* Journal Appl. Phys. Vol-18, 327 (1947)

[34] Lawrence Cranberg, *"The Initiation of Electrical Breakdown in Vacuum",* Journal Appl. Phys. Vol- 23, 518 (1952)

[35] H. C. Miller, Surface Flashover of Insulators, IEEE Trans. Elect. Insul, Vol 24, No.5, October 1989.

[36] O.Yamamoto *et al. "Factors affecting the charging characteristics of solid insulators in vacuum"* XXIIIrd Int. Symp Disch. Electr. Insul. Vac. Bucharest, 2008

[37] E. W. Gray, *"Vacuum Surface Flashover: A High pressure Phenomenon"*, J. Appl. Phys. Vol. 58, 1985

[38] Caroline Watier, *et al. "72.5 Kv Vacuum Switchgear For Electrical Power Transmission Networks- An Application Study With Pilot Customers"*

[39] Tipler, Paul, *"Physics for Scientists and Engineers: Electricity, Magnetism, Light, and Elementary Modern Physics (5th ed.)"*, W. H. Freeman (2004)

[40] Purcell, Edward M., *"Electricity and Magnetism"*, McGraw-Hill (1985)

[41] U. van Rienen, *"Numerical Methods in Computational Electrodynamics - Linear Systems in Practical Applications",* Springer, Lecture Notes in Computational Science and Engineering, Vol. 12 (2001).

[42] Behrooz Fateh., *"Modeling, Simulation and Optimization of a Microcoil for MRI-Cell Imaging"*, Master thesis, University of Rostock, Germany, Nov 2006

[43] ANSYS® Introduction to ANSYS Maxwell 2014, Release 15.9, ANSYS, Inc.

[44] ANSYS® Maxwell 16.0, Release 15.0 Help system, ANSYS, Inc.

[45] R. Renz, *"Vakuumschaltröhe",* DE Patent 100 29 763 B4, January 15, 2009

[46] Thomas Christen, Lise Donzel, and Felix Greuter *"Nonlinear Resistive Electric Field Grading Part 1: Theory and Simulation"* DEIS November/December - Vol. 26, No. 6

[47] Y.L. Cheng, et al *"Single-pulsed Surface Flashover Voltage of the Electrode Geometry in Vacuum"*, XXIV Int. Symp. Disch. Electr. Insul. Vac., Braunschweig, 2010

[48] R. A. Anderson, *"Study of Surface Flashover of Conical Insulators Using 3 Ns Risetime Pulses"*, VII Int. Symp. Disch. Electr. Insul. Vac., Novosibirsk, 1976.

[49] O. Milton, "Pulsed Flashover of Insulators in Vacuum",IEEE Trans. Electr. Insul., Vol. 7, pp. 9-15, 1972.

[50] Yasushi Yamano et al., *"Influence of Electric Field Distribution on Charging Mechanism on Alumina Dielectrics by Triple Junction in Vacuum"*, XIX Int. Symposium on Discharges and Electrical Insulation in Vacuum, Xi´an, 2000.

[51] C.M. Cooke, John G. Trump, *"Post-type support spacers for compressed gas-insulated cables"*, IEEE Trans. Power. App. Syst., Vol. 92, pp. 1441-1447, 1973.

[52] T. Nitta, *et al.* "*Factors controlling surface flashover in SF6 gas insulated systems"*, IEEE Trans. Power. App. Syst., Vol. 97, pp. 959-968, 1978.

[53] http://en.wikipedia.org/wiki/Dielectric_gas

[54] Kirk-Othmer Encyclopedia of Chemical Technology, Volume 10, Third edition, P: 799-805

[55] Paul. G. Slade, *"The Vacuum Interrupter: Theory, Design and Application"*, CRC Press, 2008

[56] http://www.coorstek.com/resource-library/library/8510-1170_Advanced_Metallized_Ceramics.pdf

[57] http://www.theeestory.com/files/Complete_Alumina_Parametrics__rated_by_purity__in_bulk_.pdf

[58]M.J. Barnes et.al *"Reduction of surface flashover of the beam screen of the LHC injection kickers"*, CERN, Geneva Switzerland

[59] Faitha Talbi, Fadila Lalam and David Malec, *"DC conduction of $Al_2O_3$ under high electric field"*, J. Phys. D: Appl. Phys. 40 (2007) 3803-3806

[60] M.J. Barnes et.al *"Surface flashover of high purity alumina during a pulsed electric field",* CERN, Geneva, Switzerland, 2013

[61]J. Dickens et.al *"Surface flashover across ceramic disks in vacuum at cryogenic temperatures"*, Power modulator symposium, 2002

[62] S. Giere, M. Kurrat and U. Schuemann *"HV Dielectric strength of shielding electrodes in vacuum circuit breakers"*, 20th Int. Sym. Disch. Electr. Insul.Vac, Tours, France, pp. 119-122, 2002.

[63] Liu Zhiyuan et.al *"Development of high voltage VCBs in China",* International symposium of discharges and electrical insulation in vacuum 2006

[64]M. Okawa et.al. *"Area effect on electric breakdown of copper and stainless steel electrodes in vacuum"*, IEEE Trans. Elec. Insul Vol.23 No.1 1988

[65]H. Kojima et.al. *"Electric field optimization of floating electrode configuration in vacuum interrupter"*, Int. Conf. High voltage Engineering and Application, USA, 2010

# List of Publications

The following publications have been made during this project

1. Factors affecting the electron emission at the triple points in high voltage vacuum interrupters

   Proceedings of 16th International Workshop on High Voltage Engineering, Wroclaw, Poland- 2012

   Author: Karthik Reddy Venna

2. Methods to reduce the electron emission at the triple junctions in high voltage vacuum interrupters

   Proceedings of 18th International Symposium on High Voltage Engineering (ISH), OD3-02, Seoul, Aug. 2013

   Authors: *Karthik Reddy Venna*, Heinz. H. Schramm, Stefan. Giere

3. Simulation analysis on reducing the electric field stress at the triple junctions & on the insulator surface of the high voltage vacuum interrupters.

   Proceedings of XXVI International Symposium on Discharges and Electrical Insulation in Vacuum (ISDEIV), Mumbai, India Sept – 2014

   Authors: *Karthik Reddy Venna*, Heinz. H. Schramm